VOLKER DREWELLO

TUNNELING SPECTROSCOPY OF MAGNETIC TUNNEL JUNCTIONS

UNIVERSITÄT BIELEFELD
FAKULTÄT FÜR PHYSIK

UNIVERSITÄT BIELEFELD
FAKULTÄT FÜR PHYSIK

Dissertation zur Erlangung des Doktorgrades

Diese Dissertation wurde von mir persönlich verfasst. Einige Textpassagen sind in veränderter Form aus Publikationen, deren Autor ich war, übernommen. Ich versichere weiterhin, dass ich, abgesehen von den ausdrücklich bezeichneten Hilfsmitteln, die Dissertation selbständig und ohne unerlaubte Hilfe angefertigt habe.

Gutachter:
PD Dr. Andy Thomas
Prof. Dr. Armin Gölzhäuser

August 2010

Contents

1 Introduction

Chapter 1
(this chapter)

From its beginning to the present day, information processing technology has relied on solely charge-based devices. These conventional electronic devices—ranging from the now quaint vacuum tube to today's million-transistor microchips—move electric charges around. The spin that tags along for the ride on each electron is ignored.

The use of the spin as an additional degree of freedom is the basis of spintronics, a new field in condensed matter physics. Spintronic devices can be easily manipulated by magnetic fields. It is no surprise that the first commercial spintronic products were read heads and other magnetic sensors. More sophisticated technologies based on spintronics, such as MRAM and reconfigurable magnetic logics, have also been proven to work in principle. The information (or configuration) is stored magnetically like in a hard disk drive and, therefore, non-volatilely. This makes the devices draw little energy. With switching times in the range of nanoseconds, such devices can be comparably fast as current electronics.

MRAM: magnetic random access memory

The basic element of many spintronic devices is a magnetic tunnel junction (MTJ). There, two layers of magnetic materials (also called electrodes) are separated by an insulator. The insulator forms an energy barrier, which hinders electrons from directly moving from one electrode into the other. If the insulator is sufficiently thin (only a few nanometers), electrons can cross this tunnel barrier, due to the quantum-mechanical tunnel effect. Thus, if a bias voltage is applied across the junction, a finite current can be measured (illustrated in Figure 1).

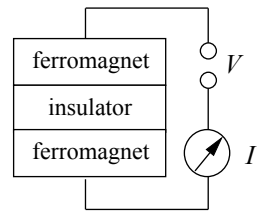

Figure 1: Schematic illustration of a magnetic tunnel junction.

The resistance of the magnetic tunnel junction depends on the relative orientation of the magnetization of the ferromagnetic elec-

trodes. In the common case, the resistance is minimized for a parallel alignment and maximized for an antiparallel alignment. This is called the tunneling magneto resistance, or in short TMR effect. To quantify this effect, the TMR ratio is used. It is defined as the relative change of the resistance in the antiparallel compared to the parallel state. A straightforward method to get an antiparallel alignment of the magnetizations is to use two materials with different coercive fields. If an external magnetic field is applied to the junction both magnets can be saturated parallel to each other. If the field is now reduced and reversed, the softer magnetic material switches first and the MTJ is in the antiparallel state. Further increase of the field brings the junction back to the parallel state. The resistance of an MTJ in dependence of the magnetic field is illustrated in Figure 2.

$$TMR = \frac{R_{AP} - R_P}{R_P}$$
(TMR ratio)

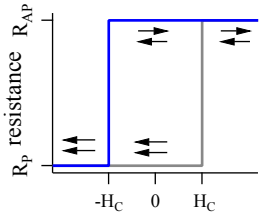

Figure 2: Minor loop: the resistance of an MTJ for field sweeps from − to + and from + to − (arrows indicate the orientation of the ferromagnets' magnetizations, H_C is the coercive field of the soft ferromagnet).

A high TMR ratio is favorable to increase the efficiency of MTJ based spintronic devices. Generally, spintronic devices are in need of high spin polarization. This is the quantity that describes the relative excess of one spin-state (*up*) over the other (*down*). For magnetic tunnel junctions Jullière found as an approximation that the TMR ratio is linked to the spin polarization of the ferromagnets.[1]

$$P = \frac{n_\uparrow - n_\downarrow}{n_\uparrow + n_\downarrow}$$
(spin polarization)

$$TMR = \frac{2P_1P_2}{1 - P_1P_2}$$
(Jullière's formula)

The first generation of magnetic tunnel junctions was based on amorphous alumina barriers. They reached up to 80 % TMR ratio at room temperature. In 2001, two groups independently predicted[2] very high TMR ratios of more than 1000 % for fully crystalline junctions of Fe, MgO, and Fe. The crystallinity in such a system lets the wave-functions of some electronic bands decay slower than others. This results in different transmission rates for electrons in the different bands. This effect is known as *symmetry filtering*. For electrodes made of Fe, Co, or Co-Fe this is equivalent to a *spin filtering*, as the different bands are filled with electrons of different spin. The result is an increased effective spin polarization of the tunneling current and, thus, a higher TMR ratio.

TMR ratios much higher than for alumina based MTJs were indeed shown in 2004. With a magnetron sputtered MgO barrier and Co-Fe-B electrodes Parkin reached over 200 % TMR ratio at room temperature.[3] At the same time, Yuasa showed TMR ratios of up to 180 % for MTJs grown with molecular beam epitaxy.[4] Up

[1] M. Julliere, Phys. Lett. **54**, 225 (1975)

[2] W. H. Butler et al., Phys. Rev. B **63**, 054416 (2001); and J. Mathon et al., Phys. Rev. B **63**, 220403 (2001)

[3] S. S. P. Parkin et al., Nat. Mater. **3**, 862 (2004)

[4] S. Yuasa et al., Nat. Mater. **3**, 868 (2004)

to now, these values have been increased to over 600 % at room temperature.[5] For these MTJs the use of Co-Fe-B has been shown to be crucial. After sputtering it is amorphous and gives a very smooth interface with the MgO barrier. Post-deposition annealing at high temperatures induces the crystallization of the MgO barrier. Also, the boron diffuses out of the Co-Fe-B electrodes and crystalline interfaces are formed with the MgO barrier.

[5] S. Ikeda et al., Appl. Phys. Lett. **93**, 082508 (2008)

Aside from the symmetry filtering barriers, there are other possibilities to increase the TMR ratio. One is the use of electrodes with higher spin polarization, such as half-metallic ferromagnets. In these materials only electrons of one spin-state are present at the Fermi level, which is equivalent to a spin polarization of 100 %. It is difficult, however, to incorporate these materials in MTJs. Promising candidates in these category are the Heusler compounds.[6] Full Heusler compounds are of the composition X_2YZ with X and Y being transition elements and Z an element of the 3rd to 5th main group with an existing $L2_1$ phase. This gives many possibilities for designing a material with certain desired properties. For example, Heusler compounds may be magnetic, even if the constituting elements are not. For spintronics, it is interesting that some Heusler compounds are predicted to have a gap in the minority density of states. If this gap can be positioned at the fermi level the desired spin polarization of 100 % is achieved. The variety of possible Heusler compound constituents enables the tuning of the fermi level.

[6] Recent reviews on this wide topic:

K. Inomata et al., Sci. Technol. Adv. Mater. **9**, 014101 (2008); and B. Balke et al., Sci. Technol. Adv. Mater. **9**, 014102 (2008)

Optimizing magnetic tunnel junctions is crucial to make them applicable. One wants to increase the TMR ratio, tune the area resistance over a wide range, and control the magnetic switching behavior, just to mention a few aspects. This may seem a materials science or engineering problem at first. It is certainly true that a huge amount of work goes into designing better production processes and optimizing the involved parameters for fabrication of the magnetic tunnel junctions. After all, these are nanostructured systems, a creation of which might always require lots of fine tuning with macroscopic machines. An example might be IBM's 'rapid turnaround' strategy,[7] specifically developed to speed up the optimization cycles of magnetic tunnel junctions for

[7] D. W. Abraham et al., IBM J. Res. & Dev. **50**, 55 (2006)

MRAM. They concentrated on several fast methods and also developed new ones. For example, the current in-plane tunneling technique (CIPT)[8] can determine the resistance and TMR ratio of layer stacks without need for lithography. Such an approach creates much data, and relationships of preparation parameters and sample properties can be explored. Physics comes into play, when one tries to understand the results of the parameters change. Here, appropriate models have to connect the measured properties and microscopic, physical effects in an logical, coherent way. Predictions made on the basis of those models give the direction on what to focus next.

[8] D. C. Worledge et al., Appl. Phys. Lett. **83**, 84 (2003)

Chapter 2

Large TMR ratios of more than 1000 % have been predicted[9] for magnetic tunnel junctions that use MgO as a crystalline barrier in 2001. In 2004, Parkin et al. and Yuasa et al. showed TMR ratios much higher than before. For some years, the reported experimentally achieved TMR ratios increased steadily. The predicted high values were realized at low temperatures in 2008. TMR ratios larger than 1100 % have been shown by Ikeda et al.[10] But the TMR ratio still decreases by roughly a factor of two, if higher temperatures or voltages are applied.[11] It it obvious that decreasing this temperature dependence is a way to increase the TMR ratio at room temperature. Also the bias voltage might be fixed in a specific application scenario. Therefore, a strong variation of the TMR ratio with the voltage is unwanted. This constantly discussed behavior of the TMR ratio has to be understood.

[9] W. H. Butler et al., Phys. Rev. B **63**, 054416 (2001); and J. Mathon et al., Phys. Rev. B **63**, 220403 (2001)

[10] S. Ikeda et al., Appl. Phys. Lett. **93**, 082508 (2008)

[11] The room temperature TMR ratio in the work mentioned before is about 600 %. The decrease of the TMR ratio with rising temperature can be even higher, depending on the materials that are used.

The temperature dependence of the TMR ratio was a challenge from the beginning. When Jullière had found the TMR effect in 1975 it was at low temperatures. It was no less than two decades later that the effect was shown at room temperature by Moodera et. al.[12] and Miyazaki et al.[13] Following this discovery the interest in the TMR effect increased and several models for the temperature dependence emerged. In 1997, Zhang et al. described the excitation of spinwaves ('magnons') by tunneling electrons as the reason for the temperature dependence.[14] This model could also explain the voltage dependence of the TMR to some degree. The model by Shang et al.[15] from 1998 only ex-

[12] J. S. Moodera et al., Phys. Rev. Lett. **74**, 3273 (1995)

[13] T. Miyazaki et al., J. Magn. Magn. Mater. **139**, L231 (1995)

[14] S. Zhang et al., Phys. Rev. Lett. **79**, 3744 (1997)

[15] C. H. Shang et al., Phys. Rev. B **58**, R2917 (1998)

plains the temperature dependence. It is also based on spinwaves, but these are only seen as the reason for the decreasing magnetization and therefore decreasing spin polarization. There are other models such as work by Bratkovsky et al.[16] or Dimopoulos et al.,[17] but most people consent to the former ones.

In alumina based magnetic tunnel junctions the change of the TMR ratio with temperature goes along with comparable conductance changes in both magnetic states.[18] It is difficult to say which model is more appropriate for alumina based magnetic tunnel junctions. Both models can—with some reasonable assumptions—be fitted to the experimental data.

In chapter 2 'Temperature dependence' of this thesis it will be shown that this is not the case in newer junctions with MgO barriers and high TMR ratios. For these the decrease of the TMR ratio with rising temperature is mostly carried by a change in the antiparallel conductance. The parallel conductance often changes so little that it seems roughly constant, if compared to the antiparallel conductance. This cannot be appropriately described by Shang's model. The model by Zhang gives a better physical explanation, but the description of the conductance in the parallel state is unsuitable. We show that the inclusion of the thermal smearing of the electrons' energy leads to an improved correspondence of the experimental data and the model. This is visible in the improved fits and can be seen as a confirmation that the thermal smearing is the missing link.

Our according publication[19] has been cited 13 times by 2010 and the model was applied to the direct tunneling process by other groups as well.[20] The success of our model shows that the excitation of spinwaves is an important effect in the electronic transport mechanism of magnetic tunnel junctions. So, how can the intrinsic inelastic excitations be studied in detail?

[16] A. M. Bratkovsky, Appl. Phys. Lett. **72**, 2334 (1998)

[17] T. Dimopoulos et al., Europhys. Lett. **68**, 706 (2004)

[18] See e.g. the original work of Zhang or Shang

S. Zhang et al., Phys. Rev. Lett. **79**, 3744 (1997); and C. H. Shang et al., Phys. Rev. B **58**, R2917 (1998)

[19] V. Drewello et al., Phys. Rev. B **77**, 014440 (2008)

[20] J. M. Teixeira et al., Appl. Phys. Lett. **96**, 262506 (2010)

Chapter 3

Tunneling spectroscopy is a method for the analysis of tunneling processes, in which small changes of the current in dependence of the applied voltage are investigated.[21] An electron which crosses the barrier and excites a localized state must have an energy that is higher or equal to that of the excited state. If such an excitation takes place an additional conductance channel

[21] E. Wolf, *Principles of Electron Tunneling Spectroscopy*, Int. Ser. Monogr. Phys. No. 71 (Oxford University Press, New York, 1989)

is available and the current increases. This happens at the threshold where the applied bias voltage corresponds to the energy of the excited state.

The change of the current is usually small, so it is easier to see in the derivatives of the current, especially in the second one. Furthermore, the elastic background is linear in the second derivative. This is called inelastic electron tunneling spectroscopy (IETS). In general, we use 'tunneling spectroscopy' as a generic term for both the first and the second derivative of the current.

The method IETS goes back to the characterization of (non magnetic) tunnel junctions.[22] It can in principle reveal all inelastic processes in which electrons take part in the tunneling process. Especially, it was shown that it is possible to excite and identify phonons of the barrier[23] and the electrodes,[24] as well as magnons in magnetic materials.[25]

Shortly after Moodera et. al. found the TMR effect at room temperature[26] they also applied the IET spectroscopy to magnetic tunnel junctions.[27] They already noticed large peaks and concluded that this was the excitation of magnons. However, magnetic tunnel junctions have been vastly improved since then, bringing higher TMR ratios with them. In newer studies, much finer structures have been found in the spectra. Especially, the spectra of MgO based magnetic tunnel junctions show differences[28] compared to the spectra of the older alumina based junctions.

Now, it is imperative to understand the details of these spectra. While quantitative explanations are still absent, several attempts have been made to qualitatively explain the tunneling processes. In chapter 3 'Co-Fe-B electrodes and MgO barriers', we try to identify different contributions such as the excitation of barrier phonons and electrodes magnons, as well as the zero bias anomaly. Therefore, we will discuss the spectra of several designs of MgO magnetic tunnel junctions. All have been optimized for high TMR ratios at room temperature. By comparing the spectra, we conclude the origin of the excitations. We focus on the relation of annealing temperature and zero bias anomaly and assess the limiting factors of each design. The analysis of the IET spectra displays itself as a useful method to investigate magnetic tunnel junctions, besides the mere determination of the TMR ratio.

[22] R. C. Jaklevic et al., Phys. Rev. Lett. **17**, 1139 (1966); and A. L. Geiger et al., Phys. Rev. **188**, 1130 (1969)

[23] J. G. Adler, Solid State Commun. **7**, 1635 (1969)

[24] T. T. Chen et al., Solid State Commun. **8**, 1965 (1970)

[25] D. C. Tsui et al., Phys. Rev. Lett. **27**, 1729 (1971)

[26] J. S. Moodera et al., Phys. Rev. Lett. **74**, 3273 (1995)

[27] J. S. Moodera et al., Phys. Rev. Lett. **80**, 294 (1998)

[28] G.-X. Miao et al., J. Appl. Phys. **99**, 08T305 (2006); and M. Mizuguchi et al., J. Appl. Phys. **99**, 08T309 (2006)

Chapter 4

The situation is more complex if Heusler electrodes are investigated.[29] Up to now, the predicted higher TMR ratios for Heusler compounds have not been found. Still, a lot of effort has been done and many improvements have been reported for magnetic tunnel junctions with several Heusler compositions. But the currently highest TMR ratios are 217 % for Co_2MnSi, 220 % for $Co_2Fe_{0.5}Al_{0.5}Si$, and 330 % for Co_2FeAl, all at room temperature.[30] They are still smaller than those achieved with Co-Fe-B electrodes, which have a rather low spin-polarization but seem to get a larger benefit from the spin-filtering of the MgO barriers.

If tunneling spectroscopy[31] is applied to Heusler based magnetic tunnel junctions a distinctive gap structure is often found.[32] First shown by Sakuraba et al., it was interpreted as a signature for vanished tunneling in the minority channel, due to the gap in the minority DOS of the Heusler compound.

In the the first part of chapter 4 'Heusler electrodes' tunneling spectroscopy is applied to magnetic tunnel junctions in which the lower electrode is made of the Heusler compound Co_2FeAl. The used barrier material is MgO. We find the same gap structure in the conductance that is described by other groups.

It can be noticed that in all available reports and in our own measurements that the gap ends at (or within a few mV of) zero bias voltage. This cannot be pure coincidence, so we looked for a physical explanation. When comparing the magnon excitation in a rather straightforward model, we find that electrons tunneling *out* of the Heusler *cannot* excite magnons (the electrons are all spin up!). We investigated the IET spectra, which indeed show much less excitation in this situation. On the other hand, electrons tunneling *into* the Heusler *can* excite magnons. This is the reason why the conductance sharply rises at zero bias for the polarity when electrons enter the Heusler electrode.

While the elegance of the model cannot be seen as a prove, another experiment can. After we published the model in Applied Physics Letters,[33] Sakuraba et al.[34] reported on an experiment that gave more insight into the tunneling process. There, a systematically altered composition of the Heusler electrode fills the DOS with electrons and, hence, shifts the fermi level of the material through the gap. For one bias voltage polarity there is always

[29] Recent reviews:
K. Inomata et al., Sci. Technol. Adv. Mater. **9**, 014101 (2008); and B. Balke et al., Sci. Technol. Adv. Mater. **9**, 014102 (2008)

[30] S. Tsunegi et al., Appl. Phys. Lett. **93**, 112506 (2008); K. Inomata et al., Sci. Technol. Adv. Mater. **9**, 014101 (2008); and W. Wang et al., Appl. Phys. Lett. **95**, 182502 (2009)

[31] Usually the first derivative, i.e. the conductance, is used here. Band structure effects are large, so they are already visible.

[32] Y. Sakuraba et al., Appl. Phys. Lett. **89**, 052508 (2006); T. Kubota et al., Appl. Phys. Lett. **94**, 122504 (2009); R. Shan et al., Phys. Rev. Lett. **102**, 246601 (2009); and S. Tsunegi et al., Appl. Phys. Lett. **93**, 112506 (2008)

[33] D. Ebke et al., Appl. Phys. Lett. **95**, 232510 (2009)

[34] Y. Sakuraba et al., Phys. Rev. B **81**, 144422 (2010)

a sharp rise of the conductance at zero bias, just as our model predicts. Sakuraba et al. also conclude that this is due to dominant inelastic excitations. Basically, this proves the model we have suggested.

This finding has some implications. If electrons tunneling into the Heusler can excite magnons, this can give rise to the large temperature dependence that some Heusler based magnetic tunnel junctions show.[35] Also the relatively small TMR that these materials show can be explained by this. With this knowledge one can think about solutions to get rid of this behavior. Not only must the preparation of highly ordered materials be improved, they have to be selected under consideration of their magnetic ('magnonic') behavior.

[35] For exsample, Co_2MnSi:
S. Tsunegi et al., Appl. Phys. Lett. **93**, 112506 (2008)

In the following section 'Further effects in Heusler compounds' of chapter 4, especially of multilayers Heusler electrodes, are discussed. Here we find that in the case of magnon excitation the multilayer structure does have little influence on the tunneling process. Only the interfacial layer seems to explain the behavior. In the (one) case where magnon excitation is suppressed (or very small), an influence of the multilayers is found. Especially, the gap structure seen in the conductance is altered. We would suggest that a highly spin polarized compound, decorated with an interfacial layer of a material with low magnon excitation, allows higher TMR ratios.

Chapter 5

Asymmetric effects in the spectra are expected when tunnel junctions with one magnetic electrode and one non-magnetic electrode are investigated. This can be used to distinguish magnetic from nonmagnetic excitations. Paluskar et al. did this with an alumina barrier in 2007.[36] They find a single peak, which they identify as the magnon excitation.

[36] P. V. Paluskar et al., Appl. Phys. Lett. **91**, 222501 (2007)

In chapter 5 'Pseudo spin valves and non-magnetic electrodes' we prepare such samples with one non-magnetic electrode. In difference to Paluskar's work an MgO barrier is used. This adds coherent tunneling to the effects that can be expected. The spectra are compared to those of magnetic tunnel junctions.[37]

[37] The MTJs are so called pseudo spin-valves with a rather simple layer stack. They can be annealed at high temperatures and yield the highest TMR ratios that have been measured in our laboratory so far. They are only surpassed by H. Ohno's laboratory.
S. Ikeda et al., Appl. Phys. Lett. **93**, 082508 (2008)

Junctions with no ferromagnet are also prepared to give some kind of reference. The spectra of these junctions show less fea-

tures none of which can be spin-dependent. This helps to identify the contributions that are found in the asymmetric spectra of junctions with one magnetic electrode. However, not all contributions in these junctions can be explained. While one of the peaks corresponds to the excitation of magnons, this cannot be concluded for other parts of the spectra. It cannot be decided, if the coherent tunneling, that is present in the MgO based pseudo spin valves, has an equivalent in the junctions with non-magnetic electrodes. However, this should be possible with further work and helps to identify coherent (elastic) from inelastic magnon effects.

Still, we can conclude, that the zero bias anomaly in these samples is not caused by the excitation of magnons in the ferromagnetic electrode. We can use IET spectroscopy to evaluate this undesired contribution to the tunneling current. This allows us to control or even suppress these contributions.

Appendix

The appendix of this thesis includes a list of references, ordered alphabetically by first author, a brief overview on the preparation, optimization, and characterization of pseudo spin valve-type magnetic tunnel junctions, as well as a list of publications and manuscripts which I have (co-)authored.

Acknowledgments

First, I would like to thank Günter Reiss for giving me the opportunity to work in his laboratory on the presented topic and Andy Thomas for supervising my work.

I also like to thank the other supervisors Andreas Hütten and Jan Schmalhorst for support and discussions. Also I thank Karsten Rott for help with a lot of machinery.

I thank all of the colleagues who worked with me, especially: Daniel Ebke, Patryk Krzysteczko, Zoë Kugler, Markus Schäfers, Oliver Schebaum, and Patrick Thomas.

Personally, I would like to thank my family and Zoë in particular.

Bielefeld, August 2010

2 Temperature dependence

This chapter deals with the temperature dependent change of the resistance and the TMR ratio of magnetic tunnel junctions. The discussion is based on the experimental results of the prepared MgO based MTJs. For these the temperature dependent behavior is different compared to alumina based junctions. This gives reason to compare different models, which leads to the selection of a physically reasonable model. This model will be enhanced with another basic physical effect, which was neglected so far. This results in a better fit with the experimental data.

The temperature dependent change of the TMR ratio in alumina based magnetic tunnel junctions goes along with comparable conductance changes in both magnetic states.[38] This is not the case in newer junctions with MgO barriers and high TMR ratios.[39] For these the decrease of the TMR ratio with rising temperature is mostly carried by a change in the antiparallel conductance. This is also the case in systems with two different electrodes, for example Co-Fe and a Heusler compound.[40] The parallel conductance changes so little that it seems roughly constant, if compared to the antiparallel conductance.

There are different models at hand for the mechanism of this temperature dependence. Here, the two most prominent will be discussed. The first one is the model by Shang et al.[41] which combines Jullière's model[42] with a temperature dependent spin polarization of the ferromagnetic electrodes. The other model by Zhang et al.[43] is based on the excitation of spinwaves (magnons) by tunneling electrons. The assumed magnon dispersion relation leads to the temperature dependent behavior. This model and enhanced versions of it will also be referred to as *the magnon model*.

[38] S. Zhang et al., Phys. Rev. Lett. **79**, 3744 (1997); and C. H. Shang et al., Phys. Rev. B **58**, R2917 (1998)

[39] S. S. P. Parkin et al., Nat. Mater. **3**, 862 (2004); and J. Hayakawa et al., Appl. Phys. Lett. **89**, 232510 (2006)

[40] T. Ishikawa et al., Appl. Phys. Lett. **89**, 192505 (2006)

[41] C. H. Shang et al., Phys. Rev. B **58**, R2917 (1998)

[42] M. Julliere, Phys. Lett. **54**, 225 (1975)

[43] S. Zhang et al., Phys. Rev. Lett. **79**, 3744 (1997)

[44] C. H. Shang et al., Phys. Rev. B **58**, R2917 (1998)

The model by Shang[44] starts from the assumption that the spin polarization of a ferromagnet is proportional to its magnetization. This results in a temperature dependence

$$P(T) = P_0 \left(1 - \alpha T^{\frac{3}{2}}\right) . \tag{1}$$

[45] M. Julliere, Phys. Lett. **54**, 225 (1975)

Jullière's formula[45] links the spin polarization and the conductance and TMR ratio of the junction. Combined with equation 1 the temperature dependence of the conductance in the parallel (P) and antiparallel (AP) magnetic state is:

$$G_P^* = G_T \left(1 + P_0^2 \left(1 - \alpha T^{\frac{3}{2}}\right)^2\right) \tag{2}$$

$$G_{AP}^* = G_T \left(1 - P_0^2 \left(1 - \alpha T^{\frac{3}{2}}\right)^2\right) . \tag{3}$$

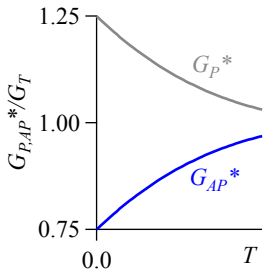

Figure 3: Illustration of the conductance in parallel and antiparallel magnetic state for $P = 50\,\%$.

Here G_T is the coefficient for direct tunneling and is considered to be constant, P_0 is the effective spin polarization at 0 K.

It is easily seen from equation 3 that the antiparallel conductivity increases with rising temperature (Figure 3). In the parallel case the conductivity is falling with temperature. But contrariwise a small increase of the conductivity in parallel state with rising temperature is found in magnetic tunnel junctions.[46] To explain these results an additional spin-independent term G_{SI} is introduced to the model, so that:

$$G_P = G_P^* + G_{SI} , \qquad G_{AP} = G_{AP}^* + G_{SI} .$$

[46] J. Schmalhorst et al., Phys. Rev. B **68**, 224437 (2003); S. S. P. Parkin et al., Nat. Mater. **3**, 862 (2004); T. Dimopoulos et al., Europhys. Lett. **68**, 706 (2004); L. Yuan et al., Phys. Rev. B **73**, 134403 (2006); J. Hayakawa et al., Appl. Phys. Lett. **89**, 232510 (2006); and S. Yuasa et al., Appl. Phys. Lett. **89**, 042505 (2006)

This contribution must have a temperature dependence which shows a strong increase in conductivity in order to compensate the basic $\mathrm{d}G_P/\mathrm{d}T < 0$ behavior. Shang et al. proposed that this contribution could be from electrons hopping through localized states. This would also fit with the observed power law dependence on the temperature.

However, this model cannot hold for junctions with high TMR ratios, typically MgO based junctions. If different junctions with high TMR ratios are investigated, the model gives a larger temperature dependence of the conductivity in both magnetic states. Therefore, the spin-independent term in this model must also be larger to compensate the stronger basic $\mathrm{d}G/\mathrm{d}T < 0$ tendency. One

would assume that a larger TMR ratio is linked to a junction of better quality with regard to barrier structure and magnetism. A spin independent term has the tendency of lowering the TMR and is a sign for a barrier of inferior quality. Then it would be very unlikely that a spin independent term can be higher in a magnetic tunnel junction with higher TMR. Yet, it is unlikely but not impossible.

Additionally, in every single case the two independent contributions to the tunneling current must be 'fine tuned' to exactly cancel each other out. Only then a small dependence with $\mathrm{d}G_P/\mathrm{d}T > 0$ can be found. For a given set of samples this could be possible by incident, but it is physically unreasonable to expect this in general for all MTJs. On the contrary, the size of the dependence is nearly the same in all publications. The chance that the spin-independent and spin-dependent term cancel each other out in every sample prepared by different groups and different methods and with different materials is too small to be a reasonable explanation. Therefore, the spin-independent term is not able to give a physical explanation of the temperature dependence in junctions with high TMR ratios.

IN THE MAGNON MODEL a tunneling electron can excite or absorb a magnon, opening additional conductance channels. The spin of this electron has to be flipped to conserve the angular momentum, and it contributes to another spin-channel. Therefore, the overall conductance for finite temperature is a mixed state of both parallel and antiparallel state. If only incoherent tunneling is considered the starting and final states can simply be described by the density of spin-up and spin-down states. Moreover, if only the states at the Fermi-energy are taken into account the spin polarization of the electrodes can be used.

For zero bias voltage and temperature $TMR(0,0)$, $R_P(0,0)$ and $R_{AP}(0,0)$ are the TMR ratio and the resistance in parallel and antiparallel state, with $TMR = (R_{AP} - R_P)/R_P$. The magnon model then gives the TMR ratio at zero temperature $T = 0$ and low bias voltage V as

$$TMR(0,V) = TMR(0,0) - Q\frac{SeV}{E_m}\frac{R_{AP}(0,0)}{R_P(0,0)}\left(\frac{1}{\xi} - \xi\right), \quad (4)$$

where the parameter Q describes the probability of a magnon to be excited in the tunneling process and is used as a fit parameter. S is the spin, E_m is related to the Curie-temperature $E_m = 3k_BT_C/(S+1)$ of the ferromagnetic electrodes, and ξ is the ratio of the products of density of states ρ in parallel and antiparallel configuration: $\xi = 2\rho_M\rho_m/(\rho_M^2 + \rho_m^2)$. Here ρ_M and ρ_m are the majority and minority DOS at E_F. Then ξ is the same as the ratio of current or resistance in both states $\xi = j_{AP}(0,0)/j_P(0,0)$. The temperature dependence of the resistance in parallel R_P and antiparallel R_{AP} state at zero bias $V = 0$ can be expressed as

$$R_P(T,0) = R_P(0,0)\left[1 + Q\xi\frac{2S}{E_m}k_BT\ln\left(\frac{k_BT}{E_c}\right)\right]^{-1} \quad (5)$$

$$R_{AP}(T,0) = R_{AP}(0,0)\left[1 + Q\frac{1}{\xi}\frac{2S}{E_m}k_BT\ln\left(\frac{k_BT}{E_c}\right)\right]^{-1}. \quad (6)$$

Here, E_c is the magnon energy cutoff energy, which is used as a fit parameter. It describes the minimum energy, which is needed to excite a magnon. Further details can be found elsewhere.[47] The most notable result of the magnon model is the simultaneous modeling of the low temperature dependence of the resistance in the parallel state and the large dependence in the antiparallel state. This describes the situation found for high TMR junctions without introduction of additional contributions to the conductance. Also, it gives a unified treatment of temperature and bias voltage dependence of the TMR effect.[48]

[47] S. Zhang et al., Phys. Rev. Lett. **79**, 3744 (1997); and X.-F. Han et al., Phys. Rev. B **63**, 224404 (2001)

[48] At least this is the case for low bias voltage. At higher bias voltages other excitations come into play, which are more complicated to include. The voltage dependence is in detail discussed in the next chapter.

However, some things should be noted here. First, E_m is calculated assuming the spinwaves are two dimensional and cannot reach energies higher than k_BT_C. It will be discussed later if this is an appropriate assumption. Meanwhile it seems reasonable for the math. Because, second, in both equation 4 and the temperature dependence (equations 5 and 6) the parameter Q is scaled by S/E_m. Therefore, their actual values do not change the temperature dependence but only the numerical value of Q. Theoretically, the proposed magnon assisted tunneling model by ZHANG et. al is also able to describe coherent effects. The barrier Hamiltonian is a function of the annihilation operators for electrons and magnons as well as the transition matrix. The latter depends on the wave vectors $\mathbf{k}$ and $\mathbf{k}'$ of the initial and final state,

respectively. In this situation coherent tunneling can mathematically be described where $\mathbf{k} = \mathbf{k}'$ or $\mathbf{k} = \mathbf{k}' \pm \mathbf{q}$ if magnons are involved. But a Hamiltonian in this form cannot be checked with experimental data. The full band structure and all the energy- and wave-vector-dependent transmission matrix elements would have to be calculated to get an exact description. In the case of incoherent tunneling two simplifications were made, namely the introduction of an effective spin polarization and the non-energy-dependence of the transmission matrix. In the case of MgO based tunnel junctions, two simplifications have also to be made to do a quantitative analysis of the presented data:

The spin polarization P in alumina based MTJs is often interpreted as the difference of the itinerant spin-up and spin-down electrons at the Fermi-energy. This is certainly incorrect for (partially) crystalline MgO barriers. Here, P specifies the difference between the number of spin-up and spin-down electrons tunneling and is an averaged value.

The probability for electrons of different energy and spin tunneling from their initial to their final state (i.e. the transmission matrix elements) is also taken as an averaged value.

ANOTHER FUNDAMENTAL INTRINSIC MECHANISM has been disregarded as very small until now. In a free electron, incoherent tunneling model the thermal smearing of the electron energies decreases the effective barrier height with increasing temperature. This effect can be ignored when the changes in conductivity are substantially higher due to other (extrinsic) effects. But this is not the case for newer systems with higher TMR ratios, especially in the parallel magnetic state where the overall change in conductance is very small.

The magnon-assisted tunneling model can be extended with a contribution of the thermal smearing. This can be successfully applied as a *phenomenological model* to MgO based MTJs. According to STRATTON[49] the influence of the thermal smearing can be expressed as

$$G(T) = G(0)\frac{CT}{\sin(CT)}\,, \tag{7}$$

[49] R. Stratton, J. Phys. Chem. Solids **23**, 1177 (1962)

with the temperature T (in Kelvin) and $C = 1.387 \times 10^{-4} d/\sqrt{\phi}$, where d is the barrier thickness (in Å) and ϕ the barrier height (in eV). To get a better idea of the size of the thermal smearing contribution

$$\alpha = 1 - \frac{\sin(C \times 300\,\mathrm{K})}{C \times 300\,\mathrm{K}} \tag{8}$$

is defined. It is the relative reduction in resistance from 0 to 300 K due to thermal smearing.

As a first order approximation the additional term from equation 7 is multiplied to the resistance from equations 5 and 6 and C is used as an additional fitting parameter:

$$R_\gamma(T,0) = R_\gamma(0,0)\frac{\sin(CT)}{CT}\left[1 + Q\beta_\gamma k_B T \ln\left(\frac{k_B T}{E_c}\right)\right]^{-1}. \tag{9}$$

Here $\gamma = (P, AP)$ denotes parallel and antiparallel state, respectively. The constants are defined as

$$\beta_P = \frac{2S\xi}{E_m}, \qquad \beta_{AP} = \frac{2S}{\xi E_m}.$$

Ru 10
Cu 30
Ta 10
$Co_{40}Fe_{40}B_{20}$ 4
MgO 1.5
$Co_{40}Fe_{40}B_{20}$ 2.5
$Mn_{83}Ir_{17}$ 10
Cu 5
Ta 10
Cu 30
Ta 10
substrate

Table 1: Stack #1. A standard TMR stack with bottom pinning.

THE SAMPLES that are investigated now are MgO based magnetic tunnel junctions. They are prepared in a DC-/RF-magnetron sputter system (LEYBOLD CLUSTERTOOL CLAB 600) with a base pressure of 1×10^{-7} mbar. The working pressure of the argon atmosphere is 5×10^{-3} mbar. The layer stack of the samples is Ta 10/ Cu 30/ Ta 10/ Cu 5/ $Mn_{83}Ir_{17}$ 10/ $Co_{40}Fe_{40}B_{20}$ 2.5/ MgO 1.5/ $Co_{40}Fe_{40}B_{20}$ 4/ Ta 10/ Cu 30/ Ru 10 (all values in nm) on top of a thermally oxidized (50 nm) silicon (001) wafer. To activate the exchange biasing and for the crystallization of the MgO barrier, the layer stack is annealed at 623 K for 60 minutes in a magnetic field of 6500 Oe. The stack is patterned by e-beam lithography and ion beam etching. The resulting patterns are ellipses with an aspect ratio of 1 to 3 and long axes of 6, 1.5 and 0.75 µm. These structures are capped with gold pads. All measurements are done by a standard two probe technique in a closed cycle cryostat (OXFORD CRYODRIVE 1.5) with a temperature range of 13 to 330 K.

The measurement of a typical junction's resistance is shown in Figure 5. The element shows a TMR of 143 % at room temperature, 205 % if cooled to 13 K. This is an increase by a factor of 1.43, while

at the same time the junctions resistance changes 36 % and 8 % in antiparallel and parallel state, respectively. Compared to Co-Fe-B/Al-O/Co-Fe-B junctions[50] this change in resistance in the parallel state is smaller. It suggests that also smaller effects such as thermal smearing become more important here.

Using the barrier thickness of $d = 1.5\,\text{nm}$ and a barrier height of $\phi = 3.5\,\text{eV}$—half of the MgO band gap[51]—the theory gives a theoretical value of $C = 1.112 \times 10^{-3}$. This corresponds to $\alpha = 1.84\%$. It is in the same order as the overall temperature dependence in the parallel case (8 %) and should not be neglected.

[50] J. Schmalhorst et al., Phys. Rev. B **75**, 014403 (2007)

[51] R. C. Whited et al., Solid State Commun. **13**, 1903 (1973)

THE FIRST STEP to apply the model is to get the parameter Q from the $TMR(V)$-curve at 0 K using equation 4, which was

$$TMR(0,V) = TMR(0,0) - Q\frac{SeV}{E_m}\frac{R_{AP}(0,0)}{R_P(0,0)}\left(\frac{1}{\xi} - \xi\right).$$

This is approximated with measurements at 13 K, shown in Figure 4. The used parameters for the MTJ are $R_P(0,0) = 397\,\text{k}\Omega$, $R_{AP}(0,0) = 1203\,\text{k}\Omega$, $TMR(0,0) = 205\,\%$ and $\xi = 3.279$. The other parameters are set to $S = 3/2$, $E_m = 121\,\text{meV}$. The fit results in $Q = 0.0242$.

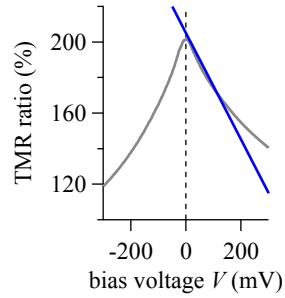

Figure 4: The TMR ratio versus bias voltage of the measured sample and the fit to obtain Q.

With these values, the overall temperature dependence can be fitted with equation 9 . The resulting fit values are $E_c = 0.270\,\text{meV}$ and $C = 1.79 \times 10^{-3}\,\text{K}^{-1}$ or $\alpha = 4.7\,\%$. The fit shows very good agreement with the measured data and is shown in Figure 5. The

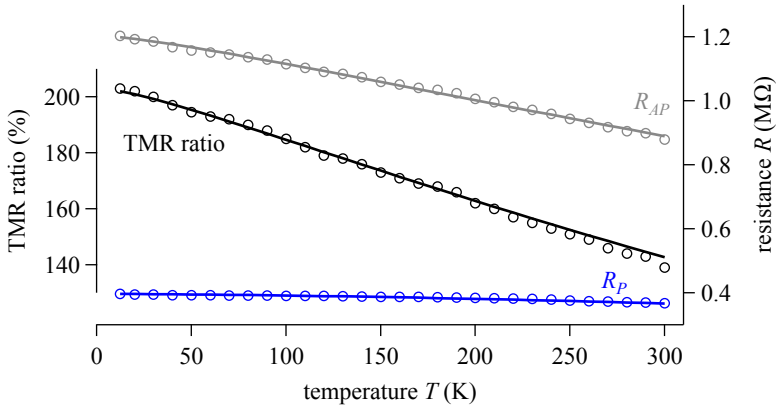

Figure 5: Fit of the resistance in the parallel and the antiparallel state of the MgO based MTJs. The resulting fit of the **TMR ratio** is also shown. The magnon model including thermal smearing is used.

size of the thermal smearing is in agreement with the theoretical expectation. Also, the cutoff energy is comparable to the 0.3 meV found by HAN et al. for alumina based junctions[52].

[52] X.-F. Han et al., Phys. Rev. B **63**, 224404 (2001)

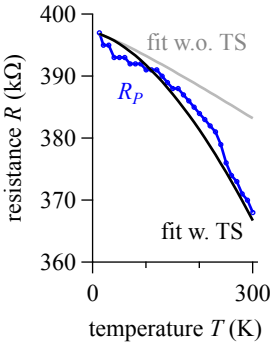

Figure 6: Fit results for the parallel resistance using the magnon model without and **with** thermal smearing for the described junctions.

A comparison between the basic magnon model and the enhanced model is shown in Figure 6. R_P and R_{AP} are fitted together, but only the resistance in parallel state is shown—the improvement is largest there. The basic magnon model clearly underestimates the temperature dependence in the parallel state. Not only does the enhanced model improve the fit quality, it also gives a good agreement of theoretical expectations and the fit value for the thermal smearing. This suggest that thermal smearing is a reasonable explanation. Furthermore, both magnon-excitation and thermal smearing are intrinsic effects which are present in every magnetic tunnel junction. Together a self-consistent explanation for the temperature dependence in MTJs with high TMR ratios can be provided.

DATA BY OTHER GROUPS was also used to test the model. As an example, the work by PARKIN et al.[53] is investigated, here. The barrier has a much higher thickness of 2.9 nm so a stronger temperature dependence of the thermal smearing is expected, as seen from equation 7:

$$G(T) = G(0)\frac{CT}{\sin(CT)}\,.$$

[53] S. S. P. Parkin et al., Nat. Mater. **3**, 862 (2004), The data of figure 4a

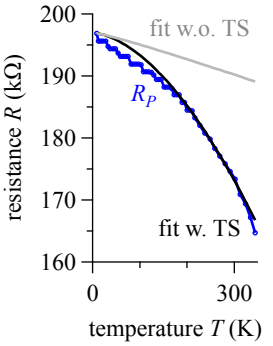

Figure 7: Fit results for the parallel resistance using the magnon model without and **with** thermal smearing for PARKIN's data.

The calculation gives an α of 7 % ($\phi = 3.5$ eV). As no $TMR(V)$-data is available the parameter Q is assumed to have the same value as in the junctions prepared by us. For a general test of the model this seems adequate due to the similar layer stack. The result of the fit is shown in Figure 8.

The cutoff energy of $E_C = 0.116$ meV corresponds to 1.35 K and is in the same range as for our junctions. The thermal smearing has a constant of $C = 0.00256\,\mathrm{K}^{-1}$ or $\alpha = 9.5\,\%$, in very good agreement with the expectation. The parallel conductance change is again almost entirely caused by thermal smearing which is, therefore, even less ignorable. Again, the fit was also done for the basic magnon model and resulted in an underestimation of the change in the parallel resistance (Figure 7).

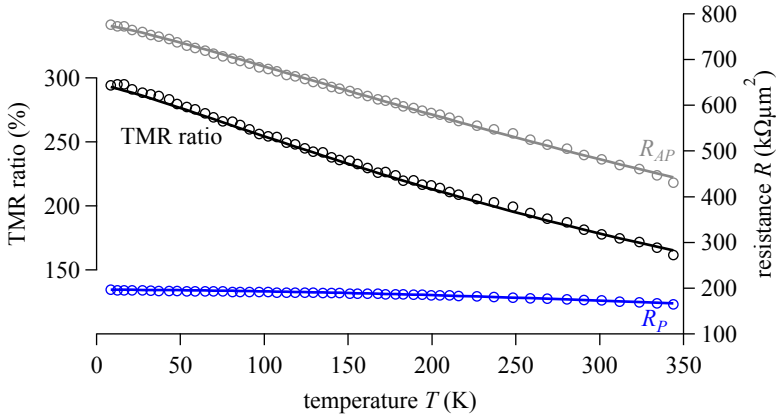

Figure 8: Fit of the resistance in the parallel and the antiparallel state (data of PARKIN et al.). Also shown is the resulting fit of the **TMR ratio**. The model including thermal smearing is used.

SUMMARIZING this chapter, the temperature dependence of the TMR effect has been investigated. The magnon-excitation model by ZHANG has been enhanced to incorporate thermal smearing in a phenomenological model. This way a much better agreement of model and experimental data was achieved. This shows that the effect of thermal smearing cannot be neglected for junctions with high TMR ratios, because of the very small overall change of conductance in the parallel state. The model has also been tested with data from another group for magnetic tunnel junctions with high TMR ratios. The change in the fit-parameters can be attributed to the differences in the junctions, but the agreement of the fits with the experimental data remains very good. The results show that the tailoring of the magnon spectrum is crucial for getting a smaller temperature dependence and, therefore, a higher TMR ratio at room temperature.

The results presented in this chapter have been published[54] *in Physical Review B in 2008.*

[54] V. Drewello et al., Phys. Rev. B **77**, 014440 (2008)

3 MgO barriers and Co-Fe-B electrodes

In the previous chapter the importance of magnons for the TMR effect was demonstrated. In this chapter the goal is to identify magnons—as well as other excitations—via the bias voltage dependence of the electronic transport. More precisely, the tunneling current in parallel and antiparallel state will be measured with very high accuracy by inelastic electron tunneling spectroscopy (IETS). The spectra show the voltage dependence of the tunneling current and give the possibility to identify specific contributions to the current which influence the TMR effect.

Large TMR ratios of more than 1000 % have been predicted for MTJs that use MgO as a crystalline barrier.[55] At low temperatures these predicted values have been experimentally realized. TMR ratios larger than 1100 % have been shown by Ikeda et al.[56] But the TMR ratio still decreases by roughly a factor of 2 to 3, if higher temperatures or voltages are applied. The room temperature TMR ratio in the work mentioned before is about 600 %. The main reason for the decreasing TMR ratios are intrinsic inelastic excitations in the junctions. In Figure 9 an inelastic excitation is illustrated.

[55] W. H. Butler et al., Phys. Rev. B **63**, 054416 (2001); and J. Mathon et al., Phys. Rev. B **63**, 220403 (2001)

[56] S. Ikeda et al., Appl. Phys. Lett. **93**, 082508 (2008)

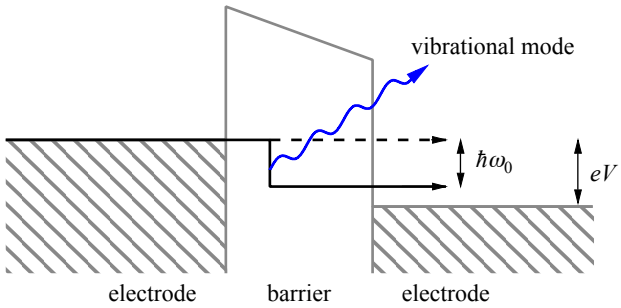

Figure 9: Schematic illustration of inelastic tunneling. In a tunnel junction an electron that crosses the barrier can excite a local vibrational mode, if its energy is high enough.

An electron which crosses the barrier can excite a localized state if its energy eV is higher than or equal to that of the excited state $\hbar\omega_0$. If such an excitation is possible an additional conductance channel is available. Both elastic tunneling and the inelastic tunneling take place, and the current increases. As this change is usually small, it is easier to see in the derivatives of the current. This is illustrated in Figure 10. Usually, the second derivative is of

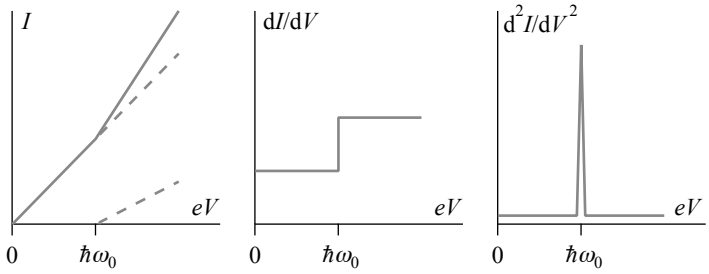

Figure 10: Measuring principle of IETS: the current I and its first and second derivate are shown below and above the threshold for the excitation.

interest as the elastic background is linear here. The technique of measuring the second derivative of the current is called inelastic electron tunneling spectroscopy (IETS).

IETS is a well established method to characterize non magnetic tunnel junctions[57] and was applied to MTJs as well.[58] This technique has a resolution that is limited only by the intrinsic temperature driven energy broadening of the spectra. Additionally, the bias voltage range of the spectra is only limited by the breakdown voltage of the junctions (typically in the range of a few volts[59]). In comparison to laterally resolved methods IETS is much simpler in terms of sample preparation. It is also closer to applications as it provides information about MTJs that could be used as the base for reconfigurable magnetic logic, magnetic sensors, or magnetic random access memory.

IETS can in principle reveal all inelastic processes in which electrons take part in the tunneling process. An overview can be found elsewhere.[60] Here, it shall only be stressed that it is especially possible to excite and identify phonons of the barrier[61] and the electrodes,[62] as well as magnons in magnetic materials.[63] Another prominent feature in IET spectra is the zero bias anomaly (ZB). In the $\mathrm{d}I/\mathrm{d}V$-characteristics a sharp dip at zero bias (up to a

[57] R. C. Jaklevic et al., Phys. Rev. Lett. **17**, 1139 (1966); and A. L. Geiger et al., Phys. Rev. **188**, 1130 (1969)

[58] J. S. Moodera et al., Phys. Rev. Lett. **80**, 294 (1998); and X.-F. Han et al., Phys. Rev. B **63**, 224404 (2001)

[59] A. A. Khan et al., J. Appl. Phys. **103**, 123705 (2008)

[60] C. J. Adkins et al., J. Phys. C **18**, 1313 (1985)

[61] J. G. Adler, Solid State Commun. **7**, 1635 (1969)

[62] T. T. Chen et al., Solid State Commun. **8**, 1965 (1970)

[63] D. C. Tsui et al., Phys. Rev. Lett. **27**, 1729 (1971)

few mV) is usually found which results in large peaks in the IET spectrum. In nonmagnetic tunnel junctions this effect was discovered by Wyatt[64] and has been attributed to single magnetic impurities.[65] A qualitative study of scattering at such impurities, however, has proven to be difficult.[66] In MTJs the zero bias anomaly has always been found since IETS was first applied to MTJs by Moodera et al.[67] Recently, also structures at bias voltages above 200 mV have been discussed.[68] They are of interest because they are presumably connected to the coherent tunneling on which the high TMR ratios of MgO barriers are based.

The technical realization of the measurements is as follows. During the measurements the samples are situated in a closed cycle Helium cryostat (Oxford Cryodrive 1.5) with a temperature range of 13 to 330 K. Electrical contact is established by a conventional two probe technique. Here, the high resistance of the tunneling barrier and the low resistance of the electrodes ensure that neither line resistances nor inhomogeneous current injection[69] influence the measurement. The absolute resistance of lines and electrodes can be estimated from a junction that suffered a dielectric breakdown[70] of the tunneling barrier. Afterwards the resistance is typically smaller than 50 Ohms.

In the following, the bias voltage is always defined with respect to the lower electrode. Thus, negative bias results in electrons tunneling into the upper electrode (Figure 11). A constant voltage source provides the bias voltage V to which a modulation of up to 7 kHz and an amplitude of $\Delta V = 2.83\,\mathrm{mV}$ (2 mV effective voltage) is added. The current $I + \Delta I$ is measured via a current amplifier. A Lock-In technique (Stanford SR830 DSP digital two channel Lock-In) is used to detect the ΔI signal and derive the $\Delta I/\Delta V$-curves. For sufficiently small amplitudes (with respect to the dynamics of the measured current) this can be treated as $\mathrm{d}I/\mathrm{d}V$. The curves are differentiated numerically to get the $\mathrm{d}^2I/\mathrm{d}V^2$-spectra.

The resolution of this method is limited by experimental conditions.[71] The thermal broadening of a sharp peak is $5.4\,k_BT$ (FWHM). More precisely, $\mathrm{d}^2I/\mathrm{d}V^2$ is a convolution product of the spectral weight function with the thermal function $\chi(E)$, shown in Figure 12. Another broadening is induced by the measurement

[64] A. F. G. Wyatt, Phys. Rev. Lett. **13**, 401 (1964)

[65] J. A. Appelbaum, Phys. Rev. **154**, 633 (1967); and J. A. Appelbaum et al., Phys. Rev. B **5**, 544 (1972)

[66] R. H. Wallis et al., J. Phys. C **7**, 1293 (1974); and S. Bermon et al., Phys. Rev. B **17**, 2110 (1978)

[67] J. S. Moodera et al., Phys. Rev. Lett. **80**, 294 (1998)

[68] G.-X. Miao et al., J. Appl. Phys. **99**, 08T305 (2006); and M. Mizuguchi et al., J. Appl. Phys. **99**, 08T309 (2006)

[69] R. J. Pedersen et al., Appl. Phys. Lett. **10**, 29 (1967)

[70] A. Thomas et al., Appl. Phys. Lett. **93**, 152508 (2008)

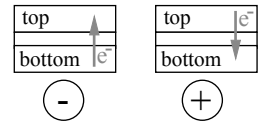

Figure 11: Negative (positive) bias: electrons tunnel from bottom to top (top to bottom)

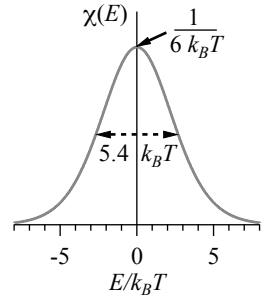

Figure 12: The thermal function: line broadening due to thermal smearing.

[71] J. Klein et al., Phys. Rev. B **7**, 2336 (1973)

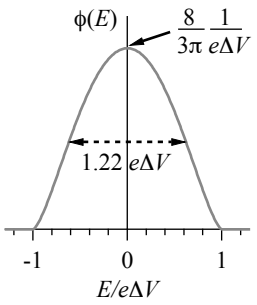

Figure 13: The instrumental function: line broadening due to the finite excitation voltage.

itself. Due to the finite modulation amplitude ΔV a peak is broadened over the range of the modulation ($-\Delta V$ to $+\Delta V$). One can calculate this instrumental broadening function ϕ. It is shown in Figure 13. The half-width of this function is $1.22\,e\Delta V$. As the temperature is given by the setup only the modulation can be modified to get optimum resolution. To get peaks that are limited only by the thermal smearing

$$1.22\,e\Delta V \ll 5.4\,k_B T = 0.28\frac{\text{meV}}{\text{K}} \times T \tag{10}$$

must be satisfied. In the described setup with a temperature of 13 K the line width due to thermal smearing is $5.4\,k_B T = 6.1$ meV. The instrumental broadening is only $1.22 \times e \times 2.83$ mV$= 3.45$ meV, which is sufficient.

Symmetric and asymmetric contributions in the tunneling process can be shown more clearly after some processing. For this, the odd and even spectra[72] are calculated by

$$\text{IETS}^{\text{odd}}_{\text{even}} = \frac{1}{2}\left(\text{IETS}(+V) \pm \text{IETS}(-V)\right) \ . \tag{11}$$

[72] P. V. Paluskar et al., Appl. Phys. Lett. **91**, 222501 (2007)

The even spectrum enhances symmetric features while the odd enhances asymmetric features. By definition the odd spectrum is the difference. It shows additional contributions for one bias direction compared to the other. The even spectrum is an average. It is of meaning if symmetric effects, i.e. excitations that exist for both bias polarities, can be expected.

Different magnetic tunnel junctions are investigated now. Most are based on MgO as the barrier material, one on alumina. Differences and similarities of these systems will be shown, especially with respect to different electrode types in MgO systems and the different barrier materials. The samples are prepared in the same sputter system which was described before (Leybold Clustertool). All are sputtered on top of a thermally oxidized (50 nm SiO_2) silicon (001) wafer. The argon pressure during deposition is 1×10^{-3} mbar for metallic materials. For the deposition of MgO it is increased to 2×10^{-2} mbar to improve the growth of the barrier.[73]

[73] V. Drewello, Diploma thesis, Bielefeld University, 2006

#	lower stack	barrier	upper stack
1	Ta 10/Ru 30/Ta 5/Ru 5/MnIr 10/CoFeB 2.5	MgO 1.8	CoFeB 2.5/Ta 5/Ru 30/
2	Ta 5/Ru 40/Ta 5/CoFeB 2.5	MgO 2.1	CoFeB 2.5/Ru 0.88/CoFe 6/MnIr 9/
3	Ta 5/Ru 30/Ta 10/Ru 5/CoFeB 4	MgO 2.1	CoFeB 1.5/Ta 5/Ru 30/
4	Cu 30/NiFe 4/MnIr 15/CoFe 3	AlO_x 1.4	NiFe 4/Ta 3/Cu 55/

Table 2: The different samples. Layer thicknesses are given in nm. AlO_x t is t nm aluminum + oxidation. Details on this sample are found in: J. Schmalhorst *et al.*, Phys. Rev. B **68**, 224437 (2003)

Different layer stacks are prepared, an overview is given in Table 2. Stack #1 is a typical system for MTJs with MgO barrier and Co-Fe-B electrodes. The bottom electrode is pinned with an antiferromagnet. This is a standard design for a stable antiparallel state. In stack #2 the top electrode is an artificial ferrimagnet (AFi). It is pinned to have a stable unidirectional anisotropy. The lower electrode is the soft one. Stack #3 is a pseudo spin-valve (PSV). The antiparallel state is achieved by hard-soft switching. Sample #4 is a pinned system (such as #1), but alumina based.

After sputtering the layer stacks #1 to #3 are annealed in a magnetic field of 6500 Oe for 60 minutes. This activates the exchange bias and initiates the crystallization of the MgO barrier. The annealing conditions for each sample can be found in Table 3. The different annealing temperatures are chosen with regard to the highest TMR ratios at room temperature and magnetic separation in the antiparallel state of the two electrodes at low temperatures. An exception is sample #1a, which is only annealed at 448 K to get a low TMR ratio comparable to alumina based junctions such as sample #4. The samples are patterned by e-beam lithography and ion beam etching. The resulting patterns are squares of 25 μm^2. These structures are capped with gold contact pads.

#	T_a (°C)	t_a (min.)
1	375	60
1a	175	60
2	350	60
2a	400	60
3	400	60
4	250	5

Table 3: The annealing temperatures T_a and times t_a for the different samples.

Bottom pinned Co-Fe-B spin valve

Sample #1 is a standard MTJ design with a pinned lower electrode. The sample exhibits a TMR ratio of over 200 % at RT and up to 345 % at 13 K. The measured junctions have a typical absolute resistance of 8 kΩ at 13 K.

The spectra for the parallel and the antiparallel magnetic state are shown in Figure 14. At low bias, around $V = 0$ the largest peaks are visible in both states (peaks are marked ZB or M in the Figure). In the parallel state the broader peaks P are next. The ex-

Ru 30
Ta 5
$Co_{40}Fe_{40}B_{20}$ 2.5
MgO 1.8
$Co_{40}Fe_{40}B_{20}$ 2.5
$Mn_{83}Ir_{17}$ 10
Ru 5
Ta 5
Ru 30
Ta 10
substrate

Table 4: Stack #1. A standard TMR spin valve.

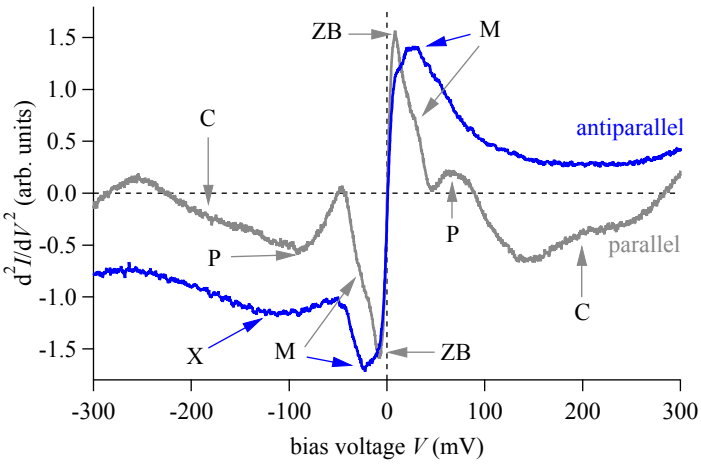

Figure 14: IET spectra of sample #1. In the parallel state the maxima at ±8 mV (ZB), with shoulders (M, about ±25 mV), the Mg-O phonon peaks (P, −86 mV and +68 mV), and the structures C (±200 mV) are marked. In the antiparallel state the maxima (M, −15 mV and +19 mV), and the asymmetric peak X (−130 mV) are marked.

citation of MgO phonons at the barrier-electrode interface—which is typical for tunnel junctions[74]—can be identified as the origin of these peaks. The Mg-O phonon has an energy[75] of 80.7 meV which fit the observed value. A similar behavior is found by other groups.[76] The last significant structures (C) in parallel state are at about ±200 mV. For positive bias this is a peak in a wider dip ($d^2I/dV^2 < 0$), for negative bias only a shoulder is visible. In the antiparallel state the additional structures (C) and the phonon peaks (P) are not visible. Only the low-bias peaks and a peak (X) for negative bias are visible.

In the parallel state the low-bias peaks are sharp with maxima at ±8 mV. In the antiparallel state the peaks are broader with maxima at slightly higher bias of −15 mV and +19 mV. This *shift* to higher energies is commonly observed in other MTJs.[77] With a higher resolved measurements a *substructure* of the low-bias peaks becomes visible (Figure 15). In the parallel state the maxima are at 8 mV (ZB) and shoulders (M) at +30 mV and −25 mV. In the antiparallel state these positions are seemingly switched. The maxima are located (M) at +27 mV and −24 mV while at the other positions (ZB) shoulders appear.

THE ASYMMETRY of the spectra is now investigated with the even and odd spectra. They are shown in Figure 17 for the parallel state. In the even spectrum the phonon peak P becomes more pro-

[74] E. Wolf, *Principles of Electron Tunneling Spectroscopy*, Int. Ser. Monogr. Phys. No. 71 (Oxford University Press, New York, 1989)

[75] P. A. Thiry et al., Phys. Rev. B **29**, 4824 (1984)

[76] K. Ono et al., J. Appl. Phys. **99**, 08A905 (2006); and G.-X. Miao et al., J. Appl. Phys. **99**, 08T305 (2006)

[77] J. Murai et al., Jap. J. Appl. Phys. **38**, L1109 (1999); X.-F. Han et al., Phys. Rev. B **63**, 224404 (2001); and G.-X. Miao et al., J. Appl. Phys. **99**, 08T305 (2006)

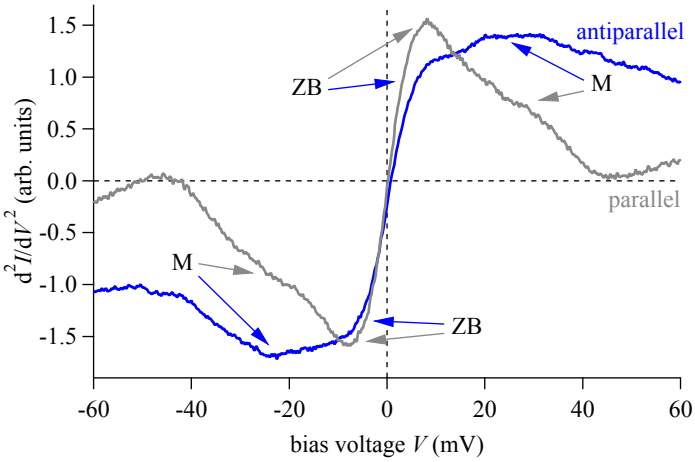

Figure 15: Details of the low-bias peaks. They show a substructure with maxima (ZB for the parallel state, M for the antiparallel state) and shoulders (vice versa).

nounced. The maximum is at 80 mV in very good agreement with the value from literature. The asymmetry of the phonon peaks with respect to bias voltage has its origin in a broad asymmetric contribution (X). Here, more contributions to the tunneling conductance are available for negative bias, i.e. when tunneling into the upper electrode. Remarkably, the same contribution is found in the antiparallel state. This is shown in Figure 16. Also peak C becomes more pronounced in the even spectrum. The reduction of contribution C to a shoulder for negative bias is also caused by the asymmetric contribution (X).

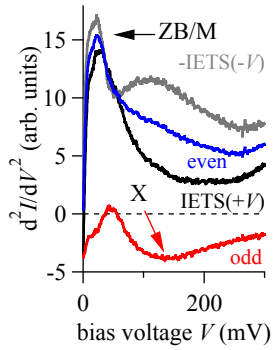

Figure 16: Even and odd IET spectra for sample #1 in the antiparallel state. Despite the low-bias peaks (ZB/M), the same some asymmetric contribution (X) as in the parallel state is found.

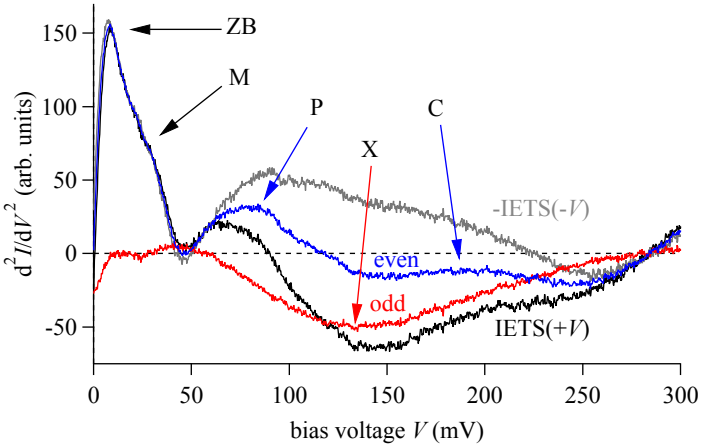

Figure 17: Even and odd IET spectra for sample #1 in the parallel state. The Mg-O phonon (P) peak and the additional peak at 200 mV (C) become more pronounced in the even spectrum. The odd spectrum reveals a broad asymmetric contribution (X).

Ru 30
$Mn_{83}Ir_{17}$ 9
$Co_{70}Fe_{30}$ 6
Ru 0.88
$Co_{40}Fe_{40}B_{20}$ 2.5
MgO 2.1
$Co_{40}Fe_{40}B_{20}$ 2.5
Ta 5
Ru 40
Ta 10
substrate

Table 5: Stack #2. The upper electrode is a pinned artificial ferri magnet.

Pinned artificial ferrimagnet

In stack #2 a pinned artificial ferrimagnet (AFi) forms the upper electrode, while the lower electrode is the free one. The measured junction shows an absolute resistance of 23 kΩ at 13 K.

The spectra in both magnetic states are shown in Figure 18. The look significantly different to those of stack #1. First of all, the general peak-height is much smaller in the parallel state compared to the antiparallel state. In the parallel state the peaks of the zero bias anomaly (ZB) are much smaller than in the sample #1 (for each spectrum in relation to the phonon peaks (P) of the same spectrum). Here, they are not the highest peaks in the spectrum.

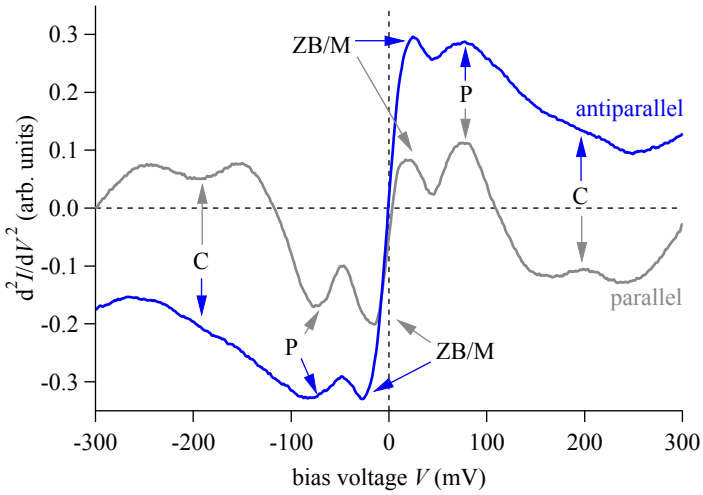

Figure 18: IET spectra of sample #2 in the parallel and antiparallel state. The Magnon (M), and phonon peaks (P, −72 mV and +78 mV) are marked. The additional structure (C, ±200 mV) is found for parallel state. In the antiparallel state there are very slight shoulders at the corresponding position.

Compared to sample #1 the asymmetry of the phonon peaks (P) is smaller and they can also be seen in the antiparallel state. The structure C (about ±200 mV) shows pronounced peaks in the wide dips.

Higher resolved measurements of the low-bias peaks (ZB/M) are shown in Figure 19. In the parallel state the peaks have a substructure with two peaks with separated maxima. The first peaks (ZB) are found at ±8 mV and the other have a maximum at ±28 mV (M). In the antiparallel state the maxima are at ±26 mV (M) as it was the case in sample #1. At the other position (ZB) at around ±8 mV shoulders can hardly be recognized.

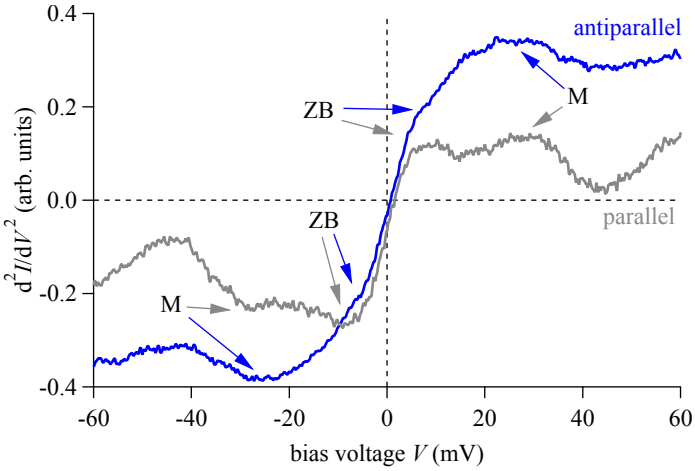

Figure 19: Details of the low-bias peaks for sample #2. In the parallel state the substructure shows two distinct maxima (ZB and M). The antiparallel state shows maxima (M) and shoulders (ZB).

Compared to sample #1 the asymmetry is different in this sample. The even and odd spectra of the sample in the parallel state are shown in Figure 20. They show a shift of the first peaks due to an asymmetric contribution which has its maximum at zero bias. This also leads to a scaling of the height of the spectrum, as IETS($V = 0$) $\neq 0$. After the normal spectra's first crossing with zero (at ± 109 mV for both polarities) the odd spectrum is basically constant. The even phonon peak in the even spectrum is at 76 mV which fits with the value from literature.[78]

[78] P. A. Thiry et al., Phys. Rev. B **29**, 4824 (1984)

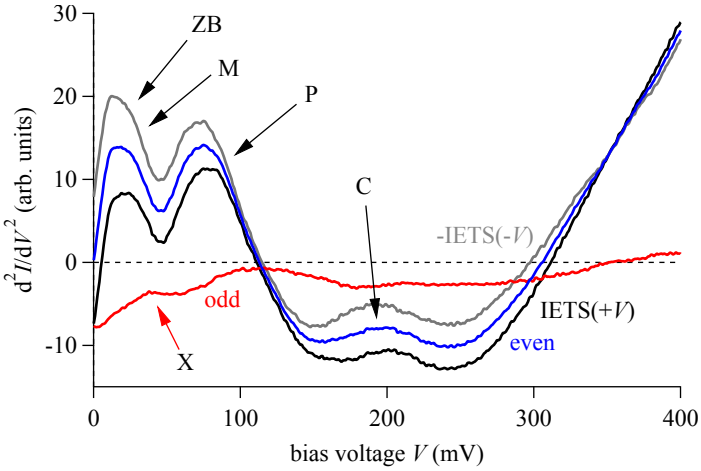

Figure 20: Even and odd IET spectra for the parallel state. The odd spectrum shows an asymmetric contribution (X) at low bias and a constant difference at higher bias.

Ru 30
Ta 5
$Co_{40}Fe_{40}B_{20}$ 1.5
MgO 2.1
$Co_{40}Fe_{40}B_{20}$ 4
Ru 5
Ta 5
Ru 30
Ta 10
substrate

Table 6: Stack #2. The upper electrode is a pinned artificial ferri magnet.

Pseudo spin valve

The pseudo spin valve (sample #3) is investigated now. The MTJs of this sample show an absolute resistance of 4.2 kΩ. Typical spectra are shown in Figure 21. The intensity of the peaks is between the intensities of sample #1 and #2.

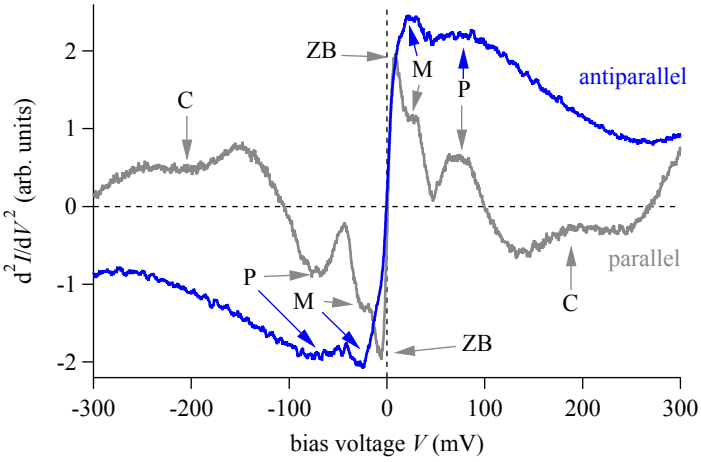

Figure 21: IET spectra of sample #3 in the parallel and antiparallel state. The zero bias (ZB), Magnon (M), and Mg-O phonon peaks (P) are found. The additional peaks (C) are found in the parallel state.

In the parallel state the first peaks (ZB) are smaller than in sample #1 (again compared to the height of the rest of the respective spectra). The shoulders (M) at the first peaks are very pronounced in this sample. The rest of the spectrum, i.e. the phonon peaks (P, ±71 mV) and the structures C around 200 mV, is very similar to that of sample #2. In the antiparallel state the whole spectrum is similar to that of sample #2. Only the relative height (compared to the phonon peaks) of the zero bias (ZB) peaks is a bit larger. At higher bias no further structures are found.

The highly resolved measurements of the low-bias region are shown in Figure 22. In the parallel state only the first peaks (ZB) are strongly different compared to sample #2. The shoulders (M) are very pronounced. In the antiparallel state the positions of the maxima (M) and the shoulders (ZB) are again switched.

Compared to sample #1 and #2 the asymmetry is negligible in this sample (even/odd spectra not shown). There is neither a large asymmetric contribution like in sample #1 nor a constant offset like in sample #2.

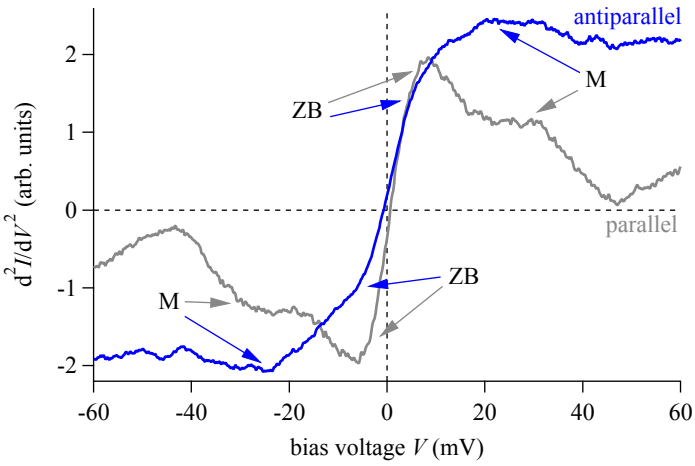

Figure 22: Details of the low-bias peaks for sample #3: in the parallel state the substructure shows a distinct maximum (ZB) and very pronounced shoulders (M). This behavior fits in between sample #1 and #2. In the antiparallel state there are maxima (M) and shoulders (ZB).

Electrodes, zero bias anomaly & magnons

An overview of the findings for the MgO based samples is shown in Table 7. The features found for the samples are summarized schematically. The measurements will now be discussed.

When comparing the spectra of the MgO based samples #1 to #3, the largest difference is found in the distinct peaks at low bias voltages In the parallel state the peaks in sample #1 have very distinct maxima (marked as ZB in Figure 15) which show small shoulders (M). In sample #2 (Figure 19) the initial peaks are much smaller and distinct peaks (M) at the position of the former shoul-

peak		bias (mV)	feature	#1	#2	(#2a)	#3
annealing temperature (°C)				375	350	(400)	400
P	C	190 to 230	*coherence*	+	++	(++)	+
	P	≈ 81	*barrier phonons*	++	++	(++)	++
	M	20 to 35	*magnons*	○	++	(+)	+
	ZB	≤ 15	*zero bias*	++	○	(+)	+
AP	ZB	≤ 15	*zero bias*	○	–		○
	M	20 to 35	*magnons*	+	+		+
	P	≈ 81	*barrier phonons*	–	+		○
	C	190 to 230	*coherence*	–	–		–
TMR ratio at room temperature (%)				210	210	(230)	220

Table 7: The findings for the MgO based samples. The strength of the features is rated (++ strong, + distinct, ○ fair (e.g. shoulder), – not visible). Sample #2 is the most feature rich, especially in the antiparallel state. Samples #3, #1 show sequentially less distinct features, but larger zero bias peaks.

ders can be identified. These spectra are comparable to those presented by MATSUMOTO et al.[79] The spectra of sample #3 (Figure 22) look somewhat in-between. The first peaks are not as high as in sample #1 and the shoulders are clearly seen.

For the different samples the peaks (or shoulders) are located at almost the same positions. They only vary in their relative intensity and width. Therefore, the intrinsic excitation processes responsible for these structures are supposedly the same for the different samples. The first peak (ZB) is roughly comparable in height for the parallel and the antiparallel state in each sample, which means the underlying excitation is not depending on the magnetic configuration or external field.[80] This is different for the shoulders or second peaks (M). The underlying excitation seems more prominent in the antiparallel spectra, where these 'shoulders' indeed form the maxima in the spectra. Thus, what might look like a shift in the position of the peak is indeed a change in the relative height of two different peaks.[81]

With respect to the differences of the samples these peaks are interpreted as follows. The first peak is the zero bias anomaly caused by tunneling through magnetic impurities.[82] It does not depend on the magnetic state of the MTJ. The peaks are most pronounced in sample #1 and much smaller in sample #2. Diffusion of manganese from the antiferromagnet[83] is an explanation for the origin of impurities. It is less distinct in sample #2 because of the lower annealing temperature. The additional layers of ruthenium and Co-Fe between the antiferromagnet and the barrier can also partially prevent[84] the diffusion of Mn. In sample #3 there is no Mn, so the zero bias peaks are smaller than in sample #1. They are not as small as in sample #2. This indicates that other impurities can contribute at the higher annealing temperature of 400 °C.

Different than the zero bias peak the second peak or shoulder (M in Figures 15, 19 and 22) strongly depends on the magnetic state. The $\mathrm{d}I/\mathrm{d}V$-value is roughly twice as high at the maximum in the antiparallel state compared to the parallel state. It is also much broader. This is a major difference compared to the zero bias peak. The most likely magnetically dependent influence is magnon excitation at the ferromagnet-insulator interfaces. It is expected to be much higher in the antiparallel state[85] than in the

[79] R. Matsumoto et al., Solid State Commun. **136**, 611 (2005)

[80] At least the dependence is not strong. The fields of some thousand Oe are low compared to the the some tens of thousands that would be needed to make the ZB anomaly show a change.

[81] This is best seen in sample #1 (Figure 14): the maximum seems just 'shifting' if going from the parallel to the antiparallel state, but in the higher resolved spectra (Figure 15) the peaks and shoulders can be separated.

[82] J. A. Appelbaum, Phys. Rev. **154**, 633 (1967)

[83] P. V. Paluskar et al., J. Appl. Phys. **97**, 10C925 (2005); and J. Hayakawa et al., Appl. Phys. Lett. **89**, 232510 (2006)

[84] A. Thomas, PhD thesis, Bielefeld University, 2003; and J. Hayakawa et al., Appl. Phys. Lett. **89**, 232510 (2006)

[85] R. Matsumoto et al., Solid State Commun. **136**, 611 (2005)

parallel state, because the elastic tunneling contribution is much smaller. Also, possible magnon excitations have been proposed at similar bias voltage by other groups.[86] More precisely, the position of the peak corresponds to the energy where the probability for magnon excitation is maximized.

An additional excitation that should show up is phonons of the electrode. Typically,[87] they should be excited in the range of 20 to 40 meV. Thus, the second peak (M) could be (partially) caused by Co-Fe phonons. However, the excitation of phonons is not dependent on the magnetic state of the junction. But the peak is very different in size in the two magnetic states. The dependence on the magnetic state is expected for magnons. Thus, the second peak must primarily be attributed to the excitation of magnons.

[86] P. V. Paluskar et al., Appl. Phys. Lett. **91**, 222501 (2007); and G.-X. Miao et al., J. Appl. Phys. **99**, 08T305 (2006)

[87] J. Klein et al., Phys. Rev. B **7**, 2336 (1973)

Layer stack & asymmetry

In some of the samples, distinctive asymmetric contributions are found. Sample #2 shows an asymmetry around zero bias (Figure 20). It is an 'offset', i.e. the spectrum value at $V = 0$ is not zero but lower. In a basic model this is the result of an asymmetry in the barrier or the Fermi-energy of the electrodes[88]. In the (non-coherent) tunneling model[89], both lead to a shift of the minimum in the $\mathrm{d}I/\mathrm{d}V$-curve. This leads to a shift in the elastic background of the IET spectra so that $\mathrm{d}^2I/\mathrm{d}V^2(0) \neq 0$.

The asymmetry in sample #1 is very different. There is a large, broad contribution beginning at 50 mV and leading up to 250 mV (Figure 17). The polarity corresponds to electrons tunneling from the bottom to the top electrode. The same contribution is found in the antiparallel state. At low bias the asymmetry is small. In sample #2 the asymmetry must have a different origin compared to sample #2. Sample #3 does not show any asymmetric contribution. From the MgO based samples only in sample #1 is Mn-Ir used in the bottom part of the stack. In sample #2 it is sputtered after the electrode and barrier layers and not used in sample #3. Mn-Ir can induce a columnar growth with tantalum as a buffer, which leads to a higher roughness of the electrodes, the barrier, and the interfaces.[90] Supposedly, this effect is stronger at the lower interface. The barrier is intentionally sputtered at a higher pressure

[88] Compare this to sample #4, where the electrodes are made of two different materials.

[89] W. F. Brinkman et al., J. Appl. Phys. **41**, 1915 (1970)

[90] J. Kanak et al., Phys. Stat. Sol. A **204**, 3942 (2007)

than the other layers to reduce its roughness,[91] which then also reduces the roughness of the upper interface. A rougher lower interface has a different electronic structure. Phonon excitation will also be different. Both should show up as contributions in the spectra.

[91] J. Hayakawa et al., Jap. J. Appl. Phys. **44**, L587 (2005); and W. Shen et al., Appl. Phys. Lett. **88**, 182508 (2006)

Another—speculative—model is, that the coherent injection of tunneling electrons breaks up at relatively low energies, due to the lower symmetry of the interface. The columnar growth could effectively prevent electrons with high $k_{x,y}$ from taking part in the tunneling process. As the upper interface is supposedly less affected by the distortion, the coherent tunneling is possible up to higher energies, from here. This would then lead to an asymmetric effect in the I-V-characteristic.

In sample #2 and #3 the Mn-Ir cannot introduce interface roughness in the same way. This would fit to the absence of asymmetric contributions at higher bias voltage. High resolution TEM pictures[92] show that the barrier is very smooth in sample #2.

[92] G. Eilers et al., TEM pictures of MgO based MTJs, unpublished, 2008

Barrier & coherence

In an effort to identify coherent effects, alumina based MTJs were also investigated. Different to MgO based systems, the alumina junctions have an amorphous barrier, and only incoherent tunneling takes place. Sample #4 has Co-Fe and Ni-Fe electrodes and shows a TMR ratio of 50 % (70 %) at room temperature (13 K), respectively. The spectra are shown in Figure 23.

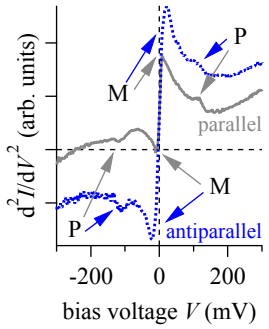

Figure 23: IET spectra of alumina based sample #4.

The first thing to be noticed in the spectra is the very different height for parallel and antiparallel state. The peaks in the parallel spectrum are much smaller than in the antiparallel state. A similar effect was seen for the MgO based sample #2. It was explained with a small zero bias anomaly it the sample. Here, the low annealing temperature and the short annealing time of only a few minutes does not allow diffusion. The small peak size can be expected to be caused by the smaller size of the zero bias anomaly, through less magnetic impurities. The large maximum in the antiparallel state (M) is then mainly caused by the excitation of interface magnons. The antiparallel spectrum also shows shoulders at about 110 mV. These are Al-O phonon peaks which

have energies[93] of 120 meV. There is no further structure at higher bias voltage for this sample. It shows a large asymmetry in the parallel state. This can be explained with the two different electrodes materials, which have different electronic structure.

To get a sample with the same intrinsic structure, an MgO based sample (#1a) was also prepared. It is identical to sample #1 but annealed at only 175°C for 1 hour. At this temperature the recrystallization of Co-Fe-B is not established[94] and no coherence is possible. This preparation process makes it comparable to alumina based sample #4. It shows TMR ratios of 38 % (61 %) at room temperature (13 K). The spectra shown in Figure 24 show the zero bias/magnon peak and phonon shoulders but no further structure. The first peaks are higher for the MgO sample than for the alumina sample. They are not sharp enough to distinguish between what was called zero bias and magnon excitation before.

For higher bias the spectra of the non-coherent MgO sample are comparable to those of the alumina based sample #4.[95] Especially, there is no structure beyond the phonon peak at 81 mV or 120 mV, respectively. The spectra just converge to the roughly linear background. This is very different for the spectra of the MgO based samples #1 to #3, annealed at high temperatures. For these samples additional structures around 200 mV are clearly seen in the parallel state.[96] In this bias region, peaks are embedded in wide dips ($d^2I/dV^2(V) < 0$) for all samples. In the work of Ono et al. similar structures in their IET spectra are visible at 250 mV and are also embedded in a strong dip. This wide dip is found in other publications[97] at bias voltages of 250 to 400 mV. The small peak within is not always visible. Especially this dip structure is seen as evidence for coherent tunneling through the MgO barrier in these publications. The result for the MgO based samples that have been investigated here support this interpretation. If all measurements are compared (schematically done in Table 8) an interesting tendency can be found. The structure C is sharper and more pronounced for junctions with a higher TMR ratio. This makes sense, as a higher coherent tunneling contribution is connected to a higher efficiency of the symmetry filtering and, therefore, an enhanced TMR effect ratio.

[93] E. Wolf, *Principles of Electron Tunneling Spectroscopy*, Int. Ser. Monogr. Phys. No. 71 (Oxford University Press, New York, 1989)

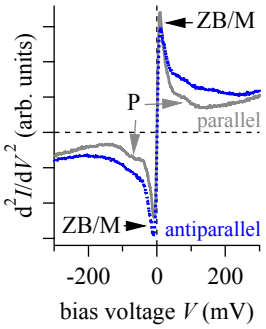

Figure 24: IET spectra of sample #1a with MgO barrier and annealed at low 175 °C.

[94] M. Jimbo et al., J. Magn. Magn. Mater. **165**, 308 (1997)

[95] Also compare e.g.:

X.-F. Han et al., Phys. Rev. B **63**, 224404 (2001)

[96] Structure C, as seen in Figure 14, 18 and 21.

[97] R. Matsumoto et al., Solid State Commun. **136**, 611 (2005); K. Ono et al., J. Appl. Phys. **99**, 08A905 (2006); M. Mizuguchi et al., J. Appl. Phys. **99**, 08T309 (2006); G.-X. Miao et al., J. Appl. Phys. **99**, 08T305 (2006); and W. Wang et al., Phys. Rev. B **81**, 140402 (2010)

peak		bias (mV)	feature	MgO #1	MgO #2	MgO (#2a)	MgO #3	alumina #4	MgO #1a
annealing temperature (°C)				375	350	(400)	400	250	175
P	C	190 to 230	*coherence*	+	++	(++)	+	–	–
	ZB	≤ 15	*zero bias*	++	○	(+)	+	+	+
AP	ZB	≤ 15	*zero bias*	○	-		○	○	+
	C	190 to 230	*coherence*	–	–		–	–	–
TMR ratio at room temperature (%)				210	210	(230)	220	50	38

Table 8: Findings for the samples. The strength of the features is rated (++ strong, + distinct, ○ fair (e.g. shoulder), – not visible). Sample #1 to #3 look similar for C but differ in ZB. MgO based sample #1a is more similar to the alumina based #4.

TMR ratio & conclusion

How does the design of the MTJ affect the TMR ratio and how is that linked to the spectra? The aspect of coherence has been discussed qualitatively. To gain a high TMR ratio, coherent tunneling through a crystalline barrier is indispensable, as it leads to the symmetry-filtering effect. The combination with Co-Fe as a magnetic electrode leads to a low transmission of electrons in the antiparallel state and enhanced transmission in the parallel state. An effective spin-filtering is achieved. The combination of amorphous Co-Fe-B with MgO has been shown to yield flat interfaces. The boron diffuses out of the magnet[98] at annealing temperatures above 300°C and the Co-Fe crystallizes matching the MgO barrier.[99] It was shown, that higher annealing temperatures lead to higher crystallinity. This is where diffusion comes into play as an additional, but negative effect of higher temperatures.[100] Several materials in the stack may diffuse at increasing temperatures, possibly affecting the spin polarization of the ferromagnet (change of the band structure), the properties of the barrier (loss of coherence), and the tunneling process (magnon excitation, impurity scattering).

Here, it was shown that the zero bias peaks are linked with magnetic impurities in the barrier. In the standard MTJ structure (sample #1) the highest zero bias peaks have been found. The annealing temperature is optimal at 375°C, i.e. the TMR ratios of samples annealed at higher temperatures are smaller. This sample is limited by diffusion, which leads to impurities and the zero bias anomaly, and can only be optimized if this diffusion is controlled. This might be possible with a different ferromagnet.

[98] M. Jimbo et al., J. Magn. Magn. Mater. **165**, 308 (1997)

[99] S. S. P. Parkin et al., Nat. Mater. **3**, 862 (2004)

[100] J. Hayakawa et al., Jap. J. Appl. Phys. **44**, L587 (2005)

This is different in sample #2 with the pinned artificial ferrimagnet electrode. The additional layers between the antiferromagnet and the barrier are one way to get less diffusion. The zero bias peaks are very small in this sample. However, the annealing temperature is only 350°C. Here, the limiting factor is the magnetic behavior of the pinned artificial ferrimagnet electrode itself: For a higher annealing temperature of 400°C (sample #2a) its magnetic properties do not allow a fully antiparallel state at low temperature. This is shown in Figure 25.

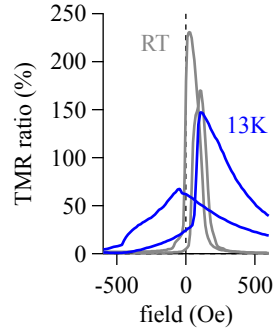

Figure 25: Major loops of sample #2a, annealed at 400°C. At low temperature no stable antiparallel state is found, due to the broad turning of the artificial ferrimagnet.

The full TMR (i.e. not limited by suboptimal magnetic switching) was not measurable. IETS could only be measured for the parallel state, which is shown in Figure 26. The zero bias peak (ZB) for negative bias is bigger for the higher annealed sample. Negative bias corresponds to probing the upper electrode. This fits to the picture of manganese diffusion, as in this sample the Mn-Ir is near the upper electrode. However, the room temperature TMR ratio of sample #2a is 230 %, higher than for sample #2. This means in sample #2 the TMR is not limited by diffusion. But even for sample #2a the zero bias peaks are larger but not as strong as in sample #1. That means the TMR ratio of the sample is still not limited by diffusion. If the magnetic properties of the pinned AFi can be improved there will also be some room for higher TMR in terms of diffusion and impurities.

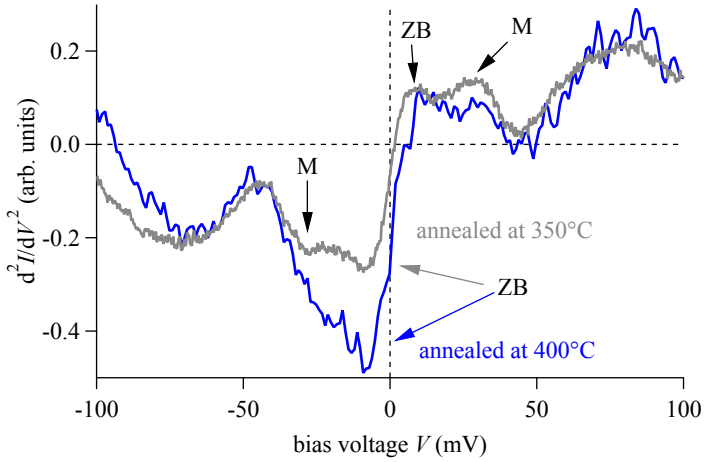

Figure 26: The low-bias peaks in the parallel state of sample #2 and #2a after annealing at 350 °C and 400 °C, respectively.

The pseudo spin valve (sample #3) shows a TMR ratio of up to 220 %, depending on the magnetic separation in an individual junction. This fits with its intermediate position in the strength of the zero bias peak. They are not as high as in sample #1. Yet the TMR ratio is higher. If a stable antiparallel state can still be obtained there will be room for higher TMR ratios.[101]

[101] Indeed there is, as will be shown in later chapters.

SUMMARIZING this chapter, magnetic tunnel junctions were investigated with inelastic electron tunneling spectroscopy. In the parallel and the antiparallel magnetic state of the MTJs several excitations were found. Different ferromagnetic electrode designs were used in order to clarify the origin of the peaks. The zero bias anomaly could be identified, which is caused by magnetic impurities. A second contribution was found, which strongly differs for the parallel and the antiparallel magnetic state. This is attributed to the excitation of magnons. A pronounced additional structure at 200 mV is found in the parallel state which is stronger the higher the TMR ratio. It is attributed to coherent tunneling effects.

Most of the results presented in this chapter have been published[102] *in Physical Review B in 2009.*

[102] V. Drewello et al., Phys. Rev. B **79**, 174417 (2009)

4 Heusler electrodes

In this chapter magnetic tunnel junctions based on magnetic Heusler compound electrodes will be examined. As some Heusler compounds are predicted to have very high spin polarization, the integration in magnetic tunnel junction promises very high TMR ratios. The conductance of the junctions can directly show some interesting features of the Heusler compounds. These will be deeper investigated with the IETS methods, described before. The current model for these effects cannot explain all results and will be altered.

One way to higher effect ratios is using electrodes with high spin polarization. Prominent candidates in this category are the Heusler compounds.[103] Full Heusler compounds are of the composition X_2YZ with X and Y being transition elements and Z an element of the 3rd to 5th main group with an existing $L2_1$ phase. Heusler compounds may be magnetic, even if the constituting elements are not. Some Heusler compounds are predicted to have a gap in the minority density of states (DOS). If this gap is at the fermi level a spin polarization of 100 % can be achieved.[104]

High TMR ratios at room temperature were indeed reported with Heusler based magnetic tunnel junctions: 217 % for Co_2MnSi by Tsunegi et al.[105], 220 % for $Co_2Fe_{0.5}Al_{0.5}Si$ by Inomata et al.[106]. Only recently, high TMR ratios of 330 % have been reported[107] for Co_2FeAl. However, these are MgO based MTJs. The question is, if the Heusler compound or coherent tunneling through the crystalline barrier is responsible for the high TMR values. But, also for MTJs with alumina barrier high TMR ratios were found. It was suggested that the high TMR ratios were caused by the predicted half-metallicity. This explanation was supported by

[103] Recent reviews for further information:

K. Inomata et al., Sci. Technol. Adv. Mater. **9**, 014101 (2008); and B. Balke et al., Sci. Technol. Adv. Mater. **9**, 014102 (2008)

[104] To achieve these interesting features the compounds have to be ordered in the $L2_1$ structure. In some situations features may also be visible for the lower ordered B2 phase.

[105] S. Tsunegi et al., Appl. Phys. Lett. **93**, 112506 (2008)

[106] K. Inomata et al., Sci. Technol. Adv. Mater. **9**, 014101 (2008)

[107] W. Wang et al., Appl. Phys. Lett. **95**, 182502 (2009)

transport measurements. Tunneling spectroscopy (dI/dV, differential conductance) showed a distinctive gap structure. This was found

for Co_2MnSi/Al-O/Co-Fe by SAKURABA et al.,[108]

for $Co_2Fe_xMn_{1-x}Si$/Al-O/Co-Fe by KUBOTA et al.,[109] and

for $Co_2FeAl_{0.5}Si_{0.5}$/($MgAl_2$)-O/Co-Fe by SHAN et al.[110]

[108] Y. Sakuraba et al., Appl. Phys. Lett. **89**, 052508 (2006)

[109] T. Kubota et al., Appl. Phys. Lett. **94**, 122504 (2009)

[110] R. Shan et al., Phys. Rev. Lett. **102**, 246601 (2009)

The gap in the tunneling spectra was interpreted as a signature for vanishing tunneling in the minority channel, due to the gap in the minority DOS of the Heusler compound. Many groups applied tunneling spectroscopy to MgO based magnetic tunnel junctions. The spectra showed some pronounced structures

for Co_2MnSi/MgO/Co-Fe by ISHIKAWA et al.,[111]

for $Co_2FeAl_{0.5}Si_{0.5}$/MgO/$Co_2FeAl_{0.5}Si_{0.5}$ by SUKEGAWA et al.[112] (here the upper electrode was in B2 or $L2_1$-structure).

[111] T. Ishikawa et al., Appl. Phys. Lett. **89**, 192505 (2006)

[112] H. Sukegawa et al., Phys. Rev. B **79**, 184418 (2009)

However, no distinct gap structures but other distinct contributions were found. TSUNEGI et al. compared Co_2MnSi based MTJs with alumina and MgO barrier. They were the first to find a gap structure for the MgO barrier,[113] which was comparable to those of the alumina based junctions.

[113] S. Tsunegi et al., Appl. Phys. Lett. **93**, 112506 (2008)

Recently, WANG et al. reported evidence for coherent tunneling in Co_2FeAl/MgO/Co-Fe junctions.[114] However, the spectra lack the signature of a gap. More insight into the transport process gives the work by SAKURABA et al.[115] who show tunneling spectroscopy for systematically altered Heusler compositions. A systematic behavior is found which will be discussed later.

[114] W. Wang et al., Phys. Rev. B **81**, 140402 (2010)

[115] Y. Sakuraba et al., Phys. Rev. B **81**, 144422 (2010)

Ru 40
$Mn_{87}Ir_{13}$ 10
$Co_{70}Fe_{30}$ 5
MgO 2.1
Heusler 20
MgO 5
substrate

Table 9: MTJ with Heusler compound as an electrode.

THE SAMPLES we investigated are prepared in the LEYBOLD sputter system mentioned before. They have the following layer stack on top of the MgO (001) substrate: MgO 5/Heusler 20/MgO 2.1/$Co_{70}Fe_{30}$ 5/$Mn_{83}Ir_{17}$ 10/Ru 40 (all values in nm). The samples are annealed for 60 minutes. The temperature is chosen to get the optimum TMR ratio at 293 K. Details of the preparation and optimization can be found elsewhere.[116] The usual lithography and ion beam etching techniques are used to get squares of 100 μm^2. These are capped with gold contact pads for bonding.

[116] D. Ebke et al., J. Magn. Magn. Mater. **322**, 996 (2010)

Gap and magnon excitation in Co_2FeAl

Magnetic tunnel junctions based on the compound Co_2FeAl were investigated first. In transport measurements at 13 K the system shows a TMR ratio of 273 % (153 % at RT). The major loop in Figure 27 shows well defined parallel (P) and antiparallel (AP) magnetic states. Figure 28 shows the spectroscopic data obtained in the parallel state at −500 Oe. Here, $\mathrm{d}I/\mathrm{d}V$- as well as IET spectra are investigated. The $\mathrm{d}I/\mathrm{d}V$ data was normalized to its value at a bias voltage of zero, to allow a better comparison. A striking asymmetry in the $\mathrm{d}I/\mathrm{d}V$-data is found with respect to the bias polarity. For negative bias the conductance shows a very weak dependence on the bias voltage down to $V_n = -140$ mV. For positive bias up to 25 mV the conductance sharply increases. For higher bias voltage the slope reduces visibly. The $\mathrm{d}I/\mathrm{d}V$-signal has a local maximum (270 mV), followed by a decrease and a minimum (at 350 mV).

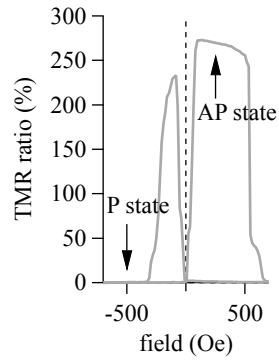

Figure 27: Major loop of a Co_2FeAl MTJ at 13 K. Arrows mark the fields at which spectroscopy is performed.

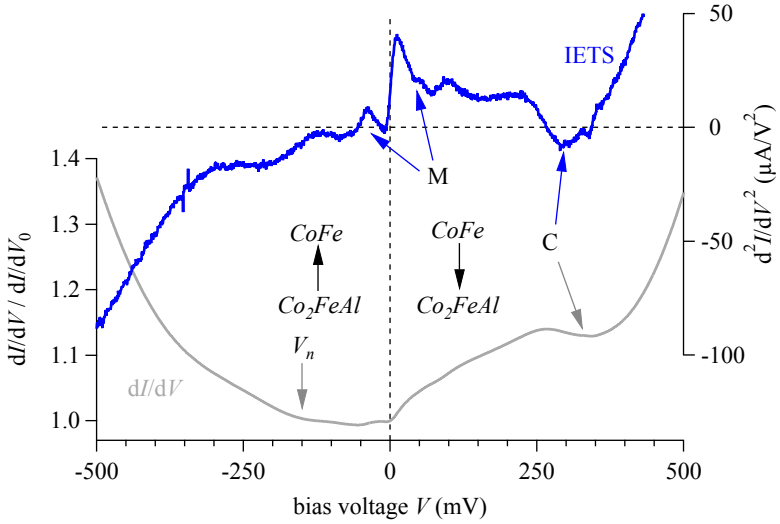

Figure 28: Tunneling and IET spectra of a Co_2FeAl MTJ in the parallel state. A gap down to $-V_n$ is found in $\mathrm{d}I/\mathrm{d}V$, leading to distinct asymmetry in both spectra. The local maximum in $\mathrm{d}I/\mathrm{d}V$ leads to a negative region in IET (C). It is followed by a small feature at 350 mV.

All features can be more clearly seen in the IET spectrum. For small negative bias ($V_n < V < 0$) the spectrum shows small peaks of near-zero height, while for postive bias ($0 < V < 270$ mV) the peaks are larger and always positive. The local minimum in the IET spectrum is negative in value and located at 290 mV.

Ru 40
$Mn_{87}Ir_{13}$ 10
$Co_{70}Fe_{30}$ 5
MgO 2.1
Co_2FeAl 20
MgO 5
substrate

Table 10: Stack #1. Heusler based MTJ with Co_2FeAl as the lower electrode.

The spectroscopic data for the antiparallel state at 250 Oe is shown in Figure 29. There is no obvious asymmetry as in the parallel state. A sharp increase of $\mathrm{d}I/\mathrm{d}V$ is found for both bias polar-

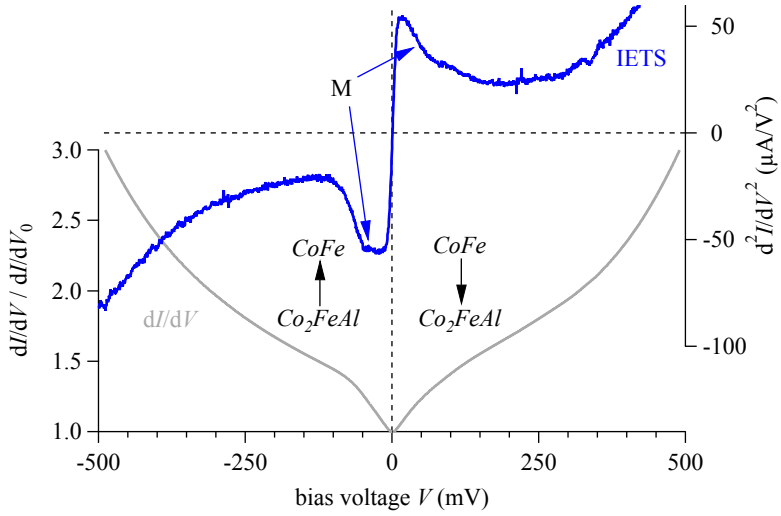

Figure 29: Tunneling and IET spectra of the Co_2FeAl sample in the antiparallel state. They are more symmetric compared to the parallel state. The sharp rise in $\mathrm{d}I/\mathrm{d}V$ for negative bias gives a plateau in IETS. None is seen for positive bias.

ities. However, for negative bias a distinct kink is found (-70 mV), whereas for positive bias the transition to the flatter part is much smoother. Again, the IET spectrum can show these features more clearly. For small negative bias ($-10\,\mathrm{mV} < V < 0$) there is a sharp increase to a broad plateau region (-10 to -50 mV). For higher negative bias voltage the signal rapidly decreases. Then ($V < -100$ mV) it increases monotonically and smoothly. For positive bias the signal also increases rapidly up to a bias voltage of 10 mV. Unlike negative bias there is no plateau and the signal decreases slowly with a small shoulder around 90 mV. After the minimum at about 200 mV it slowly increases.

THE MEASUREMENTS at low bias in both magnetic states will now be discussed. The flat region for $V_n < V < 0$ of the $\mathrm{d}I/\mathrm{d}V$-curve in the parallel state can be understood with the assumption that a gap is present in the minority density of states (DOS) of Co_2FeAl while the majority DOS is not varying much at this energy. Majority electrons can tunnel from the Co_2FeAl into Co-Fe. The constant DOS leads to a constant conductance. Minority electrons

are not available to tunnel into Co-Fe. The gap structure ends at $V_n = -140\,\mathrm{mV}$ where $\mathrm{d}I/\mathrm{d}V$ strongly increases. Here the lower end δ_{VB} of the minority gap is reached ($V = V_n = \delta_{VB}/e$) and electrons can tunnel from the minority valence band of Co_2FeAl in the minority states of Co-Fe. This additional minority tunneling channel increases the conductance for $V < -140\,\mathrm{mV}$. Similar results have been shown by SAKURABA et al.[117] in 2006. They interpreted the immediate rise of $\mathrm{d}I/\mathrm{d}V$ for $V \geq 0$ ([118]) as the upper end of the gap just above the Fermi energy E_F. This would mean that the separation of the Fermi energy and the conductance band is $\delta_{CB} \approx 0$ (in the minority channel).

[117] Y. Sakuraba et al., Appl. Phys. Lett. **89**, 052508 (2006)

[118] Their polarity is switched compared to ours. Here, their findings are translated to our definition of the polarity.

THERE IS A DIFFERENT WAY to look at it. The IET spectrum for the parallel state (Figure 28) is not completely flat but shows some features for negative bias voltage. The first sharp rise is the zero bias anomaly, as discussed before.[119] Next, the magnon peak (M) is of interest. It shows the excitation of magnons by tunneling electrons with excess energies. Compared to the peak for positive bias the peak for negative bias (tunneling out of the Heusler) is not distinguishable or very small.

[119] The zero bias anomaly will not be discussed here. For negative bias the whole spectrum is near zero, for positive bias it is much higher. The magnon peak is a shoulder at 30 to 50 mV (also seen in Figure 31).

In the antiparallel state (Figure 29) this is different. The low-bias peaks have a different shape for the different bias voltage polarity. This is shown in Figure 30. The immediate rise at zero bias is the same for both polarities, but the following magnon shoulder is more distinct for negative bias, i.e. electrons tunneling out of the Heusler. This fits to the assumption of a gap. Virtually all tunneling electrons are majority electrons in the Heusler. Due to the antiparallel orientation of the magnetizations, the tunneling electrons are minority electrons in the Co-Fe. These have a high probability to excite magnons in order to become majority electrons. For tunneling into the Heusler the relative number of majority electrons is lower. Accordingly the magnon shoulder is smaller. This difference leads to an asymmetry (X) in the spectra.

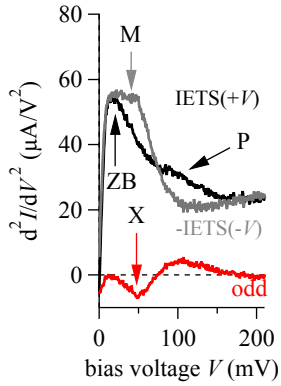

Figure 30: Spectra in the AP state. The magnon peak M is higher for negative than for **positive** bias, where also the broad peak P contributes. P is seen clearer in Figure 31. The resulting asymmetry is seen in the odd spectrum.

Magnon excitation is known[120] to be one of the main reasons for the temperature dependence and low bias behavior of the TMR ratio. This was discussed before. In Table 11 an overview of the first-order magnon excitation (and absorption) processes is given. There are four cases regarding to the magnetic state and the po-

[120] S. Zhang et al., Phys. Rev. Lett. **79**, 3744 (1997)

Table 11: First order magnon processes: E (*e*) is an electron in a Co_2FeAl majority (minority) state, F (f) is an electron in a Co-Fe majority (minority) states and +m (*-m*) is the emission (absorption) of a magnon.

	neg. bias			pos. bias		
	Co_2FeAl	→	Co-Fe	Co-Fe	→	Co_2FeAl
P	E	→	f, *−m*	F	→	*e*, *−m*
	e	→	F, +m	f	→	E, +m
AP	E	→	F, +m	F	→	E, +m
	e	→	f, *−m*	f	→	*e*, *−m*

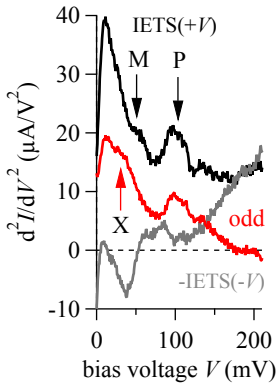

Figure 31: Spectra for **positive** and negative bias and the odd spectrum of the Co_2FeAl based MTJ in the parallel magnetic state.

larity of the bias voltage. With the assumption of a gap in the Co_2FeAl minority states none of the processes involving Co_2FeAl minority electrons are available. Also, the absorption of magnons has a far lower probability at low temperatures than the excitation. These simple assumptions lead to one case where no magnon excitation is possible: for negative bias voltage in the parallel state.

Basically, this is what the IET spectra show. Up to around −100 mV the spectrum has values near zero. The 'forbidden' peak is finite but very small. There is an excess of excitations for the positive bias. The odd spectrum in Figure 31 shows the asymmetry (X) more clearly. The asymmetry leads up to about 200 mV.

The finite size of the features for negative bias can be explained with the assumption of few minority states in Co_2FeAl instead of none. Then only few minority electrons are available to tunnel into the Co-Fe and excite magnons. For positive bias the tunneling essentially is the same as in the case of a distinctive gap. Many minority electrons are available and a tunneling minority electron can excite a magnon, is spin-flip scattered to a majority state of which plenty are available. A small but finite minority DOS could be the result of imperfect ordering. Instead of a gap, some calculations[121] show a finite DOS just below E_F for Co_2FeAl. There, most of the residual minority states originate from Fe d-orbitals. As the tunneling electrons are s-like those states are not accessible through the tunneling process. Most probable is the possibility of interface states that have been predicted[122] and found[123] for other Heusler compounds.

Please note, the presented model gives a reason for the strong increase in conductance that is found for positive bias in the parallel state. It is caused by magnon excitation in Co_2FeAl. Thus, there is no need for the band gap edge to be near E_F. Thus $E_C \approx 0$

[121] M. Sargolzaei et al., Phys. Rev. B **74**, 224410 (2006); and K. Özdoğan et al., J. Appl. Phys. **101**, 073910 (2007)

[122] Y. Miura et al., Phys. Rev. B **78**, 064416 (2008)

[123] T. Ishikawa et al., Appl. Phys. Lett. **94**, 092503 (2009)

cannot be concluded (nor excluded) in this case. This is a major difference to the band model which was used before.

Only recently,[124] SAKURABA et al. have presented[125] more evidence for this model. They systematically alter the composition of their Heusler compound $Co_2MnAl_xSi_{1-x}$ and find a systematic shift of the lower band gap edge in dI/dV. However, the upper band gap edge is not visible—the rise in conductance always begins for very small positive bias voltage.[126] The authors come to the same conclusion, that we have drawn before. For tunneling into the Heusler, interface states can mediate magnon excitation. '*Thus, the no shift [...] may be due to the dominant contribution of inelastic tunneling in the positive bias region.*'

[124] Their work was presented after our publication of the data and model which is presented here.

[125] Y. Sakuraba et al., Phys. Rev. B **81**, 144422 (2010)

[126] Their definition for polarity is the same as in our work.

FURTHER FEATURES will be shortly discussed now. Both the parallel and the antiparallel IET spectrum are shown In Figure 32. The obvious difference for negative bias was discussed before. For positive bias the spectra are comparable. In the antiparallel state

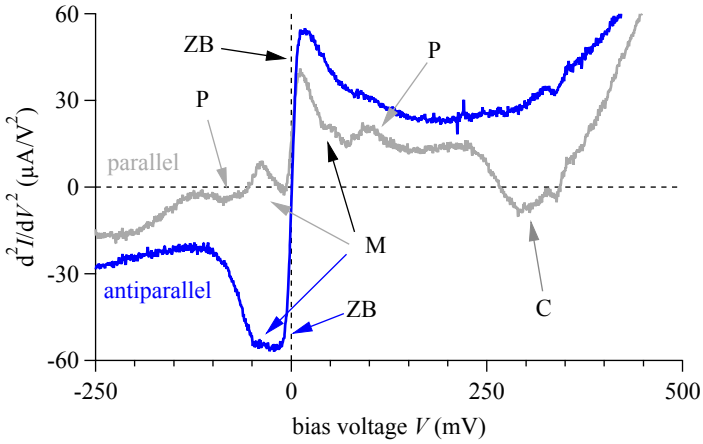

Figure 32: Comparison of the IET spectra of the Co_2FeAl based sample. In the parallel state a pronounced asymmetry is found. In the antiparallel state asymmetric effect are much smaller.

the magnon peak is higher because the magnon excitation only needs majority electrons/states (see Table 11). Also elastic tunneling is less probable and the relative change by magnon excitation is higher. The similarity ends at the large dip at 290 mV in the parallel state. The structure might indicate a signature of coherent tunneling in MTJs with MgO barrier[127] as discussed before. For negative bias it is not visible, supposedly due to the gap in

[127] R. Matsumoto et al., Solid State Commun. **136**, 611 (2005); and G.-X. Miao et al., J. Appl. Phys. **99**, 08T305 (2006)

[128] S. Tsunegi et al., Appl. Phys. Lett. **93**, 112506 (2008)

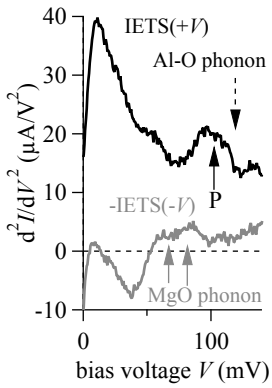

Figure 33: Spectra for **positive bias** with peak at 100 mV and for negative bias with MgO phonon peaks at 66 and 81 mV.

[129] G.-X. Miao et al., J. Appl. Phys. **99**, 08T305 (2006); and J. G. Adler, Solid State Commun. **7**, 1635 (1969)

the minority DOS of Co_2FeAl. This has been seen before for MgO based MTJs.[128]

The other peaks in the IET spectra for the parallel state are shown enlarged in Figure 33. For positive bias the shoulder at $\approx$ 45 mV marks the magnon excitation as described before. A peak around 100 mV is presumably the peak of barrier phonon excitation, which is typical for tunnel junctions and found[129] at 81 mV for Mg-O and 120 mV for Al-O phonons. Here, the position of 100 mV might be related to stress at the Co_2FeAl/MgO interface or a partial oxidation of the Co_2FeAl surface (Al-O). This cannot be clarified here. For negative bias the IETS signal is much flatter. Zero bias anomaly and magnons cannot be divided as discussed before. Additional peaks are found from -60 to -90 mV. This fits to the Mg-O phonon peak positions.

Summarizing this part, magnetic tunnel junctions with the magnetic Heusler compound Co_2FeAl as the bottom electrode were investigated by tunneling spectroscopy. The measurements showed a large asymmetry of the conductance in the parallel state, but only small variations in the antiparallel state. These findings could be explained with the assumption of a gap in the minority DOS of Co_2FeAl. However, for electrons tunneling into the Heusler this model proved to be incomplete. IET spectroscopy revealed magnon excitation, which must be taken into account to explain the behavior. The revised phenomenological model can explain the behavior for both bias polarities. This finding is of fundamental interest, as it means that the presence of a gap in the minority DOS may not be enough to gain high TMR ratios (at room temperature).

[130] O. Schebaum et al., J. Appl. Phys. **107**, 09C717 (2010)

Direct measurements of the spin polarization[130] of this material yielded only 55 %. This does not fit to the assumption of a gap. The measured sample, however, was annealed at only 350°C. It would be interesting to measure MTJs annealed at this temperature and find out if the gap is present or not.

[131] D. Ebke et al., Appl. Phys. Lett. **95**, 232510 (2009)

The results regarding Co_2FeAl based samples have been published[131] in Applied Physics Letters in 2009.

Further effects in Heusler compounds

A variety of Heusler compounds is available for integration in magnetic tunnel junctions. Of special interest are the cobalt based Heusler compounds. It depends on the material if a high degree of crystalline ordering can be achieved. Also, the electronic properties are strongly depending on the ordering. It might not always be possible to prepare a specific compound with the electronic properties that are predicted. It can be more straightforward to optimize a composition, which is more robust in preparation. Different compounds can then be used to optimize the crystalline growth of the whole sample.

The Co_2FeAl based MTJs have been discussed as a model case in the section before. Other compositions will now be investigated.[132] An overview of the samples is given in Table 12.

[132] Like for all Heusler based samples in this work, details about the preparation and optimization can be found in the PhD thesis of DANIEL EBKE, Bielefeld University, 2010.

sample #	lower electrode	barrier & upper stack	T_a (°C)
Co_2FeAl	Co_2FeAl 20	/MgO 2.1/CoFe 5/MnIr 10/Ru 40/	450
$_{[CFA]}Co_2MnSi$	$[Co_2FeAl\ 5/Co_2MnSi\ 5]_{x2}$	/MgO 1.8/CoFe 5/MnIr 10/Ru 40/	425
$_{[CFS]}Co_2MnSi$	$[Co_2FeSi\ 5/Co_2MnSi\ 5]_{x2}$	/MgO 1.8/CoFe 5/MnIr 10/Ru 40/	425
Co_2FeSi	Co_2FeSi 20	/MgO 1.8/CoFe 5/MnIr 10/Ru 40/	375

Table 12: Overview of the different Heusler based samples investigated in this work.

THE FREE ELECTRODE of the next sample consists of four alternating layers of Co_2FeAl and Co_2MnSi. It was difficult to grow a single 20 nm layer of Co_2MnSi on an MgO buffer like for the Co_2FeAl sample described before. The resulting tunnel junctions show TMR ratios below 20 %. To overcome that, the compound is introduced in a multilayer stack with Co_2FeAl. The low ordering temperature[133] of Co_2FeAl is used to introduce ordering in the Co_2MnSi. In the prepared magnetic tunnel junction Co_2MnSi is at the interface, but the bulk consists of alternating materials. The question is, are the transport properties as if the full electrode was Co_2MnSi or do the properties of the multilayer show up?

[133] D. Ebke et al., J. Magn. Magn. Mater. **322**, 996 (2010)

Ru 40
$Mn_{87}Ir_{13}$ 10
$Co_{70}Fe_{30}$ 5
MgO 1.8
Co_2MnSi 5
Co_2FeAl 5
Co_2MnSi 5
Co_2FeAl 5
MgO 5
substrate

Table 13: Stack $_{[CFA]}Co_2MnSi$. A Heusler based MTJ with a multilayer bottom electrode.

The optimized sample is annealed at 425°C and shows a TMR ratio of 107 % at room temperature. At low temperature the TMR ratio is 331 %, which is the highest TMR ratio found for the different Heusler samples in our laboratory. The tunneling spectra for the $_{[CFA]}Co_2MnSi$ sample in the parallel state are shown in Figure

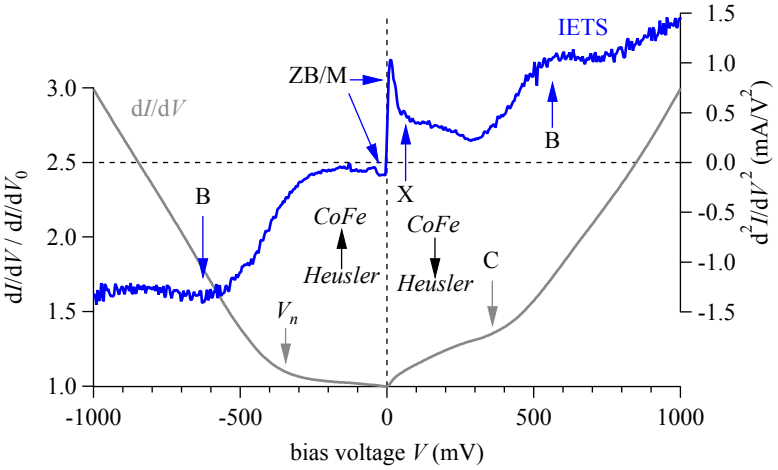

Figure 34: Tunneling and IET spectra of the $_{[CFA]}Co_2MnSi$ sample in the parallel state. The gap-like structure in dI/dV for negative bias is visible as high asymmetry.

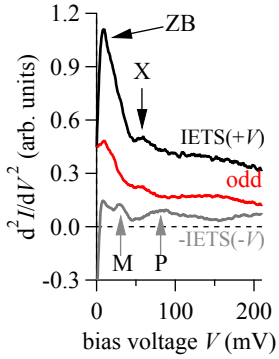

Figure 35: Spectra for **positive** and negative bias and the odd spectrum in the parallel state.

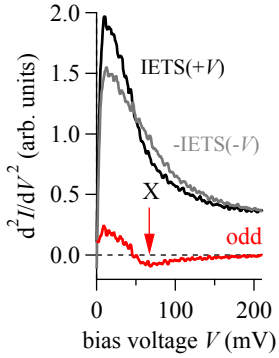

Figure 36: Spectra for **positive** and negative bias and the odd spectrum in the antiparallel magnetic state.

34. A pronounced gap structure is found for negative bias. The voltage where dI/dV begins to rise is $V_n = -350\,\text{mV}$. The gap is much wider than in the Co_2FeAl sample discussed before. For positive bias up to $+25\,\text{mV}$ the conductivity sharply rises. Then it increases slower up to a kink (C, $+350$ to $+400\,\text{mV}$). The Co_2FeAl sample showed a local minimum at this position.

The IET spectrum shows the features more clearly. At higher voltage around 600 mV the IET spectrum has broad, pronounced peaks (B). In dI/dV this contribution is hardly visible. It could be ascribed to band structure effects. For smaller, negative bias the spectrum is flat, with only small low-bias peaks. For positive bias the peaks are much more pronounced. The low-bias peaks are shown enlarged in Figure 35. When tunneling out of the Heusler compound (negative bias) a small magnon peak (M) is found at the typical 25 mV to 30 mV. The accompanying zero bias peak is also very small. The phonon peak (P) is visible at typical 81 mV. For positive bias the zero bias peak (ZB) is very pronounced. It is followed by a peak (X) located at 55 mV. In the Co_2FeAl sample a similar shoulder (M) at 50 mV could be explained by magnon excitation. For the present sample, however, this cannot be concluded, yet. If it was related to magnon excitation it should be visible and more intense in the antiparallel state. But the spectra for low bias (Figure 36) only show the broad peaks (ZB/M) that start at zero bias and have large flanks. The odd spectrum does show some

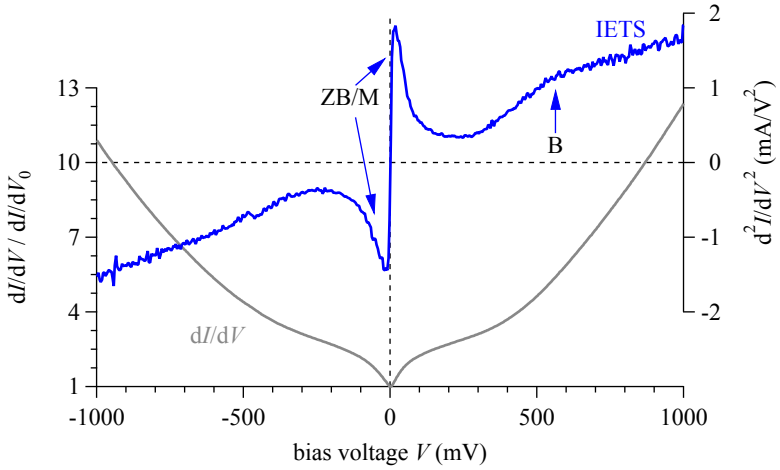

Figure 37: Tunneling and IET spectra of the $_{[CFA]}Co_2MnSi$ sample in the antiparallel state. The spectra are much more symmetric than in the parallel state.

asymmetry (X). The spectrum is higher and sharper for positive bias (tunneling into the Heusler) compared to negative bias.

For higher bias voltages the spectra of the junction in the antiparallel state are shown in Figure 37. The spectra are more symmetric and show less features. In dI/dV the typical V-structure around zero bias and a parabolic shape at higher bias are visible. The IET spectrum is dominated by the large low-bias peaks. Additionally, it shows a small asymmetry. The only distinctive feature is a contribution (B) for positive bias, which is at the same bias voltage of 600 mV as in the parallel state.

THE NEXT SAMPLE has Co_2MnSi on the interface as well. It is buffered with Co_2FeSi a similar multilayer structure that was used before. The TMR ratio at room temperature is 79 % which is far lower than the TMR ratio of the samples investigated so far. However, at 13 K the TMR ratio is 271 %, the same as for the Co_2FeAl sample. This is the largest temperature dependence of the samples investigated in this work.

The spectra for this $_{[CFS]}Co_2MnSi$ sample in the parallel state are shown in Figure 38. The dI/dV spectrum in the parallel state shows no gap, in contrast to the $_{[CFA]}Co_2MnSi$ sample. The kink at about +350 mV is at the same position. The IET spectrum looks much more similar to the former sample. For negative bias it is not near zero, but it shows the same structure. Compared to

Ru 40
$Mn_{87}Ir_{13}$ 10
$Co_{70}Fe_{30}$ 5
MgO 1.8
Co_2MnSi 5
Co_2FeSi 5
Co_2MnSi 5
Co_2FeSi 5
MgO 5
substrate

Table 14: Stack $_{[CFS]}Co_2MnSi$. A Heusler based MTJ with a multilayer bottom electrode.

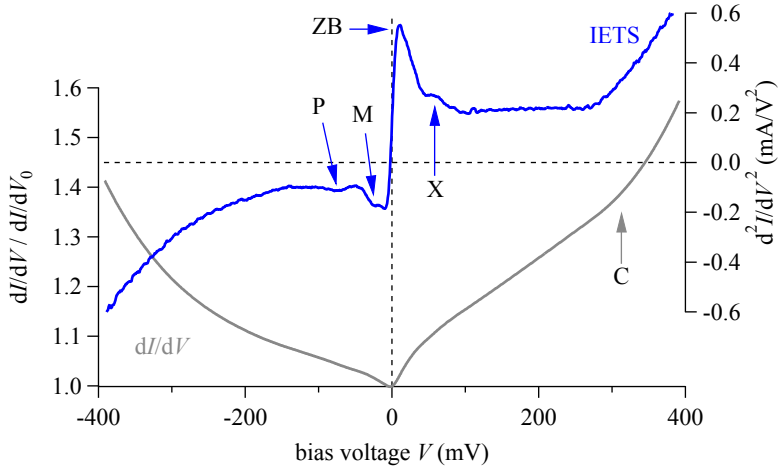

Figure 38: Tunneling and IET spectra of the $_{[CFS]}Co_2MnSi$ sample in the parallel state. No gap structure is visible. For negative bias, IETS is not zero.

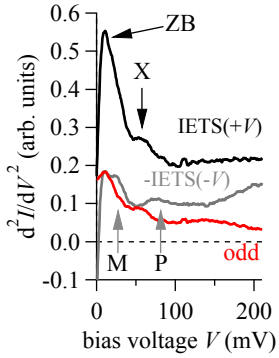

Figure 39: Spectra in the parallel state for $_{[CFS]}Co_2MnSi$.

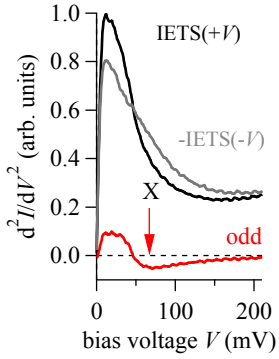

Figure 40: Spectra in the antiparallel state.

Ru 40
$Mn_{87}Ir_{13}$ 10
$Co_{70}Fe_{30}$ 5
MgO 1.8
Co_2FeSi 20
MgO 5
substrate

Table 15: Stack Co_2FeSi. MTJ with Co_2FeSi electrode.

the former sample is shifted by a constant offset. The same low-bias peaks are distinguishable at −10 mV (ZB) and −25 mV (M). At 75 mV the phonon peak (P) is also visible. They are followed by a flatter region down to −150 mV. For positive bias there is a sharp zero bias peak (ZB), with a small but distinct shoulder. It is followed by a flat region, which ends at about +280 mV.

In Figure 39 the low bias part of the spectra is shown in detail. Notably, the odd spectrum is nearly identical to the one found for $_{[CFA]}Co_2MnSi$ although the spectra have a very different height for negative bias. For the antiparallel state (overview spectra not shown) the spectra are more similar for the two samples, especially for low bias (Figure 40). Also here, the characteristically shaped asymmetry is the same for both samples. But again no distinct peaks after the zero bias anomaly are visible, especially the shoulder is not present in the antiparallel state. Voltages higher than 500 mV damaged the junction and could not be measured.

THE LAST SAMPLE that is examined here, uses a single layer of Co_2FeSi as the electrode. It shows a TMR ratio of 75 % at room temperature, comparable to the $_{[CFS]}Co_2MnSi$ sample. The TMR ratio at low temperature of 130 %, however, is much lower than for the other samples. Still, it is interesting to investigate the properties of this material. The properties can be compared to the $_{[CFS]}Co_2MnSi$ sample, where Co_2FeSi is used as a buffer material.

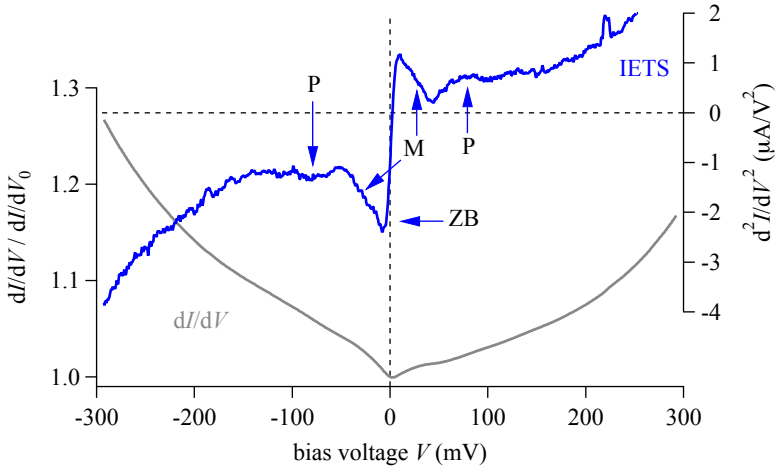

Figure 41: Tunneling and IET spectra of the Co_2FeSi sample in the parallel state. The very high resistance limits the SNR and the quality of the spectra.

The spectra measured in the parallel state are shown in Figure 41. The asymmetry is reversed compared to the samples investigated before. The spectra are flatter for positive bias. Basically, there are also less features in the spectra. This was seen before for the alumina based sample. The spectra of junctions with low TMR ratios also showed fewer, less distinct features. In the other Heusler samples, there were different peaks with regard to position and size for both bias polarities. This is different in the Co_2FeSi sample. For low bias there are the same peaks for both bias polarities, shown in Figure 42. The peaks only differ in height. The zero bias peaks (ZB) have a magnon shoulder (M) and there are additional peaks (P) at 80 mV. This is the energy of the MgO phonon peak.[134] For tunneling into the Heusler compound (positive bias) the phonon excitation was not visible at the correct energy for the other samples.

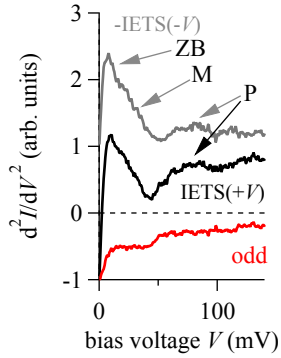

Figure 42: Spectra for negative and for **positive** bias and the odd spectrum.

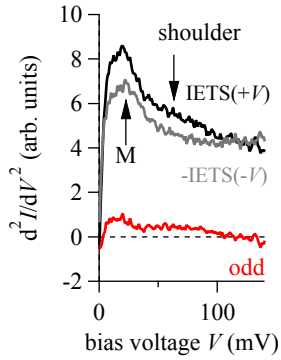

Figure 43: Spectra in the antiparallel state for negative and for **positive** bias and the odd spectrum.

The low bias spectra in the antiparallel state are shown in Figure 43 (overview spectra are not shown). They show a clear substructure, the maximum is between 30 mV and 40 mV. The height is different with regard to the bias polarity and for positive bias a broad shoulder is visible. The asymmetry is different to the other samples. Due to the shoulder for positive bias, there is a higher contribution for positive bias voltage up to more than 100 mV. The peaks are also less sharp and their relative height is smaller, compared to the following minimum.

[134] P. A. Thiry et al., Phys. Rev. B **29**, 4824 (1984)

A QUANTITIVE COMPARISON of different samples has to deal with some difficulties. Different resistances of the actual junctions scale the spectra and different barrier thicknesses lead to different, more complicated backgrounds. To counter these effects the following 'normalized IETS' can be used[135]

[135] Also called 'logarithmic derivative'. See, e.g. W. Plesiewicz et al., Phys. Rev. B **34**, 4583 (1986)

$$\mathrm{IETS}_{norm} = \frac{\mathrm{d}^2 I(V)/\mathrm{d}V^2}{\mathrm{d}I(V)/\mathrm{d}V} \,. \tag{12}$$

It is obvious that this removes the scaling done by different resistances, as $\mathrm{d}I/\mathrm{d}V(0) = \sigma(0) = R(0)^{-1}$. Furthermore, the whole spectrum is rescaled at each point.

This normalization of the IET spectra is now used to compare the different Heusler based samples, that have been discussed in detail before. There are two sets of samples. A single layer sample and the samples where the Heusler compound from the single layer is used as the buffer for Co_2MnSi. Now the spectra of the base compounds Co_2FeAl and Co_2FeSi can be compared to their multilayer counterparts $_{[CFA]}Co_2MnSi$ and $_{[CFS]}Co_2MnSi$. In Figure 44 the normalized spectra in parallel state of the four samples are shown. For negative bias the normalized spectra of the Co_2FeSi sample and the $_{[CFS]}Co_2MnSi$ sample are identical (I). The Co_2FeAl and the $_{[CFA]}Co_2MnSi$ sample also show similarity (II). Both are flat, due to the gap structure seen in $\mathrm{d}I/\mathrm{d}V$. They only differ at $-200\,\mathrm{mV}$ where Co_2FeAl shows a contribution. In both

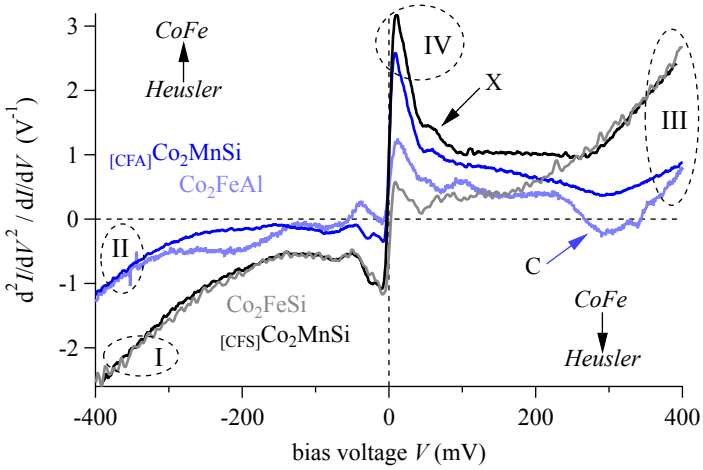

Figure 44: Normalized IET spectra of the different samples in the parallel magnetic state. The single layer samples Co_2FeAl and Co_2FeSi are shown, as well as the multilayer samples $_{[CFA]}Co_2MnSi$ and $_{[CFS]}\mathbf{Co_2MnSi}$.

sets the spectra of the samples are very similar for negative bias. The two sets compared to each other are different. The Co_2FeAl samples show a gap structure, the Co_2FeSi samples do not.

For positive bias the similarities within the sets are not as strong. Only at high bias the accordant samples converge (III). For lower bias voltage this is not the case. Here, the Co_2MnSi samples show similarities. They have a high zero bias peak (IV) (more than a factor of 2 higher than the other samples) with a small shoulder (called X before). This is followed by a flat region, which ends at roughly 300 mV in both samples. The single layer samples are different, with small zero bias peaks. However, also the Co_2FeAl samples show some similarities for positive bias, especially the flat region and the kink at roughly 300 mV.

In the antiparallel state there are the same similarities as for positive bias in the parallel state. The normalized IET spectra are shown in Figure 45. Both Co_2MnSi multilayer samples show very high peaks at low bias (V) with a sharp rise and no shoulder on the decreasing side. In these normalized spectra it becomes clear that possible shoulders may simply be hidden in the large ini-

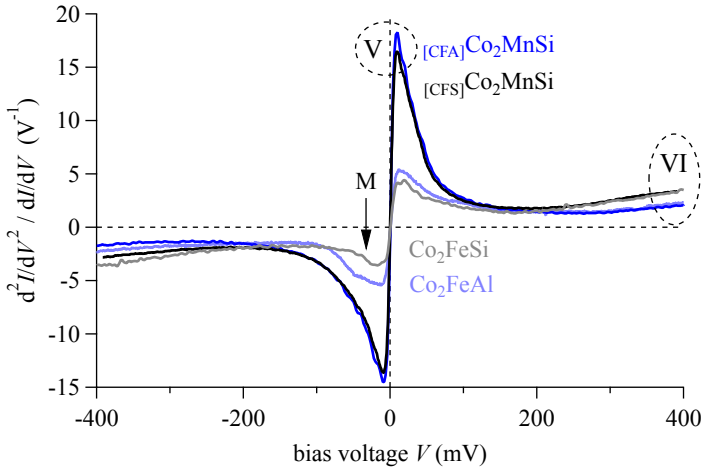

Figure 45: Normalized IET spectra of the different samples in the antiparallel magnetic state. The single layer samples Co_2FeAl and Co_2FeSi are shown, as well as the multilayer samples $_{[CFA]}Co_2MnSi$ and $_{[CFS]}\mathbf{Co_2MnSi}$.

tial peaks. The spectra of Co_2FeAl and $Co_2FeSi$are much smaller and show structure in the low-bias peaks, with distinguishable magnon shoulders. For higher bias voltages, however, the single layer samples converge (VI) to the same values as the multilayer samples with the accordant buffer material.

The findings for the different electrodes are schematically listed in Table 16. Now a phenomenological model is discussed. For

Feature		Co_2FeAl	$_{[CFA]}Co_2MnSi$	$_{[CFS]}Co_2MnSi$	Co_2FeSi
anneal. temp. (°C)		450	425	425	375
P	ZB/M	○ / +	○ / ++	+ / ++	+ / +
	Gap	+	+	–	–
AP	ZB/M	+ / +	++ / ++	++ / ++	+ / +
TMR(RT) (%)		153	107	79	76
TMR(13 K) (%)		273	331	271	133
Γ		1.78	3.08	3.44	1.75

Table 16: Features of the Heusler based samples. The strength of the features is rated (++ strong, + visible, ○ fair (e.g. shoulder), – not present). Γ is a basic measure for the temperature dependence of the TMR ratio with Γ =TMR(13 K)/TMR(RT).

negative bias electrons are emitted from the Heusler electrode and tunnel into the Co-Fe counter electrode. The investigated samples show the MgO phonon peak at the right position in this situation. The magnon peaks are at 20 to 30 mV if they are visible. It is the position known from the chapter before. This shows that the excitations are mainly those present at the target interface, which is MgO/Co-Fe, here. However, there is also a contribution from the band structure of the lower (emitter) electrode. The visible consequence of a gap in the minority DOS of the Heusler electrode is the absence of the according magnon peak and a generally flatter structure in the IET spectra of the Co_2FeAl samples. This was described in detail before. Also the Co_2FeSi sample look identical or negative bias. It can be concluded that in the multilayers the buffer layers play a role in the tunneling process. This means that not only the last 5 nm of the electrode are important. In this case it might be a valid idea to introduce ultra-thin Co-Fe-B interlayers between Heusler compound and barrier[136] to optimize the barrier growth.

[136] S. Tsunegi et al., Appl. Phys. Lett. **94**, 252503 (2009)

For positive bias the situation is different. It was discussed above, that for positive bias magnon excitation is possible, even if a gap is present in the minority DOS of the Heusler electrode. The similarity of the Co_2MnSi based samples shows that the interface is more important than the bulk, here. This makes sense, as the excitation is presumably mediated by interface states.[137] In the antiparallel state, the magnon excitation is even more dominant. So the interface layers dominate the physics of the spectra

[137] Y. Sakuraba et al., Phys. Rev. B **81**, 144422 (2010)

here. Therefore, the Co_2MnSi samples are so similar. As the gap does not affect the magnon excitation in the antiparallel state, the spectra are much more symmetric.

The high contribution at low bias remains to be discussed. It is visible in both Co_2MnSi samples and in both magnetic states. Compared to the other samples, the peaks start at low bias, but have a relatively long flank. The small shoulder in parallel state (X) is presumably hidden in the antiparallel state. Under this assumption it can be ascribed to magnons here, too. It was identified as magnon excitation (M) in the other junctions as well.

However, the strong peaks (ZB) are also very dependent on the magnetic state. Also, the large peaks are correlated with the high temperature dependence Γ of the TMR ratio in these samples.[138] Supposedly, the interfacial Co_2MnSi composition itself has a different magnon spectrum, with a much lower energy for the maximum probability to excite magnons. It also seems to allow far more magnons to be excited. This could explain the strong temperature dependence as well. Additionally, in the pinned junctions in the chapter 'MgO barriers and Co-Fe-B electrodes' the diffusion of manganese was responsible for the large zero bias effects. Here, it could be a similar situation, where the junctions itself has high TMR ratio, but this is to some point reduced by the influence of the manganese (by magnons or zero bias effects). Even if the $_{[CFS]}Co_2MnSi$ sample has the highest TMR ratio of the Heusler samples (at low temperature), the Co-Fe-B based samples are comparable or higher. In the next chapter it will be shown that they reach much higher TMR ratios if annealed at comparably high temperatures of 450°C.

[138] This behavior is seen for other Mn based Heusler compounds as well.

SUMMARIZING this chapter, magnetic tunnel junctions with the Heusler compounds Co_2FeAl, Co_2FeSi and Co_2MnSi were investigated by tunneling spectroscopy. The compound Co_2MnSi was buffered by either Co_2FeAl or Co_2FeSi to induce B2 structure. The spectra show an influence of the buffer material on the tunneling process. This is most clear for negative bias, when electrons are emitted from the Heusler electrode. When electrons tunnel into the Heusler the influence of the interfacial layer is more clearly shown. Here, Co_2MnSi shows much higher magnon excitation,

which is presumably also the reason for the higher temperature dependence of the TMR ratio of these samples. To gain higher TMR ratios at room temperature, this temperature dependence and, therefore, the magnon excitation has to be prevented.

The results presented in this part of the chapter are not yet published.

5 Pseudo spin valves and non-magnetic electrodes

In this chapter nonmagnetic electrodes in tunnel junctions are investigated. The junctions with no ferromagnet provide a simpler case without spin-dependent excitations and can be used as a reference. Junctions with one magnetic electrode show a strong asymmetry which can be used to distinguish magnetic from nonmagnetic excitations. These samples are compared to state of the art magnetic tunnel junctions. These pseudo spin valves with a rather simple, straightforward layer stack can be annealed at high temperatures. They yield very high TMR ratios.

THE SAMPLES which are investigated in this chapter are prepared in a self-made DC-/RF-sputter deposition tool with a base pressure below 1×10^{-9} mbar. The metallic layers are deposited on top of thermally oxidized silicon wafers using argon (7.0) at a pressure of 5×10^{-3} mbar. MgO is deposited at 1×10^{-2} mbar. A list of the layer stacks that will be discussed is given in Table 17. The first sample is a magnetic tunnel junction (MTJ). The other samples are a metal/insulator/metal tunnel junction (M-I-M) and a ferromagnet/insulator/metal junction (FM-I-M). All samples are annealed at 450 °C for 1 hour in a vacuum furnace. Ta and Au are added for protection and to form contact pads. The samples are structured by e-beam or optical lithography and Ar-ion-beam etching.

sample	**lower stack**	**barrier**	**upper stack**
PSV	Ta 20/ $Co_{40}Fe_{40}B_{20}$ 5.3	MgO 2.4	CoFeB 3.2/Ta 20/
M-I-M	W 20	MgO 1.8	W 20/
FM-I-M	W 15/ $Co_{40}Fe_{40}B_{20}$ 6	MgO 1.8	W 20/

Table 17: The layer stacks of the different samples that are investigated in this chapter. Layer thickness in nm.

[139] J. Hayakawa et al., Appl. Phys. Lett. **89**, 232510 (2006)

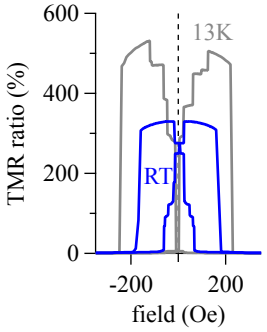

Figure 46: Major Loops of the PSV showing TMR ratios 330 % at RT and 530 % at 13 K.

Ta 20
$Co_{40}Fe_{40}B_{20}$ 3.2
MgO 2.4
$Co_{40}Fe_{40}B_{20}$ 5.3
Ta 22
substrate

Table 18: The stack of the PSV MTJ. A tunnel junction with hard-soft-switching magnetic electrodes.

THE MAGNETIC TUNNEL JUNCTION serves as a reference here and will be characterized first. The antiparallel magnetic state is achieved through different coercive fields of the magnetic layers. Such a layer stack is usually called a pseudo spin valve[139] (PSV). The main advantage of a PSV is the simplicity of the layer stack, which makes is suitable for a very high annealing temperature. This is needed to achieve a good crystallization of the Co-Fe-B electrodes and the MgO barrier. This particular sample exhibits the highest TMR ratio after annealing at 450°C. More on the optimization of this sample can be found in the appendix. Typical major loops of the sample are shown in Figure 46. The sample shows a TMR ratio of 330 % at room temperature and 530 % at 13 K. The measured elements have an elliptical shape with an area of approximately 2.4 µm^2. Due to the thick barrier the MTJs have a relatively high resistance of 485 kΩ at 13 K.

THE SPECTRA in parallel state for the PSV are shown in Figure 47. The tunneling spectrum dI/dV shows a small zero bias anomaly (in comparison to the other features). The conductance decreases for bias voltages higher than 50 mV with pronounced minima at about 350 mV. In the IET spectrum the structures resolve more clearly. The peaks known from the previous samples can be found here. First, there are the zero bias peaks (ZB), at which the magnon shoulders (M) are barely seen in this sample. The phonon peaks (P) are located at the typical position of 80 mV. The minima in conductance translate to the large dips after the phonon peaks, where the second derivative is negative. They are very pronounced and the peak (C) at 200 mV is visible. It is asymmetric with respect to the bias voltage polarity.

These spectra of the PSV are comparable to those of the other MTJs, as described before. The zero bias anomaly is very strong in the spectrum for the parallel state and overlaps the magnon peak. This suggests that the TMR in this sample is limited by the zero bias anomaly and, therefore, diffusion. This is reasonable, as the maximization of the TMR was driven by increasing the annealing temperature.[140] The phonon peaks are sharp and pronounced with only small asymmetry, which can be attributed to the good barrier quality with highly orientated crystalline grains.[141] The

[140] The small magnon peak may partially be attributed to the relatively low resolution of the measurement to some point. It is inevitable due to the sample's high resistance.

[141] This can be seen from the high resolution TEM pictures in the appendix.

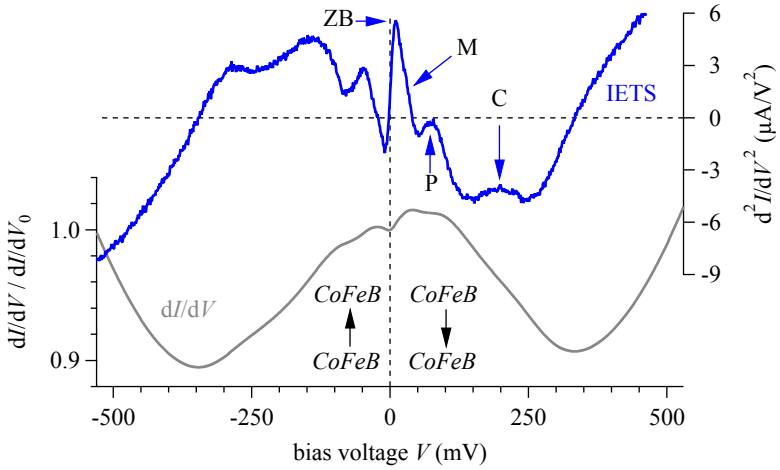

Figure 47: The tunnel spectrum (dI/dV) normalized to its value at $V = 0$ and the IET spectrum (d^2I/dV^2) of the PSV sample in the parallel state. The peaks are only marked at positive bias.

largest feature, however, are the dips around ± 200 mV. They are as deep as the zero bias peaks are high. This indicates a large coherent tunneling contribution, supposedly caused by the good barrier quality. Given the large TMR ratio of more than 530 %, it is reasonable to expect coherent tunneling.

The asymmetry of the dips (and peak C) can be seen clearer in the odd spectrum shown in Figure 48. Two asymmetric contributions can be found. Around zero bias and up to 100 mV a contribution (X) leads to different heights of the zero bias and

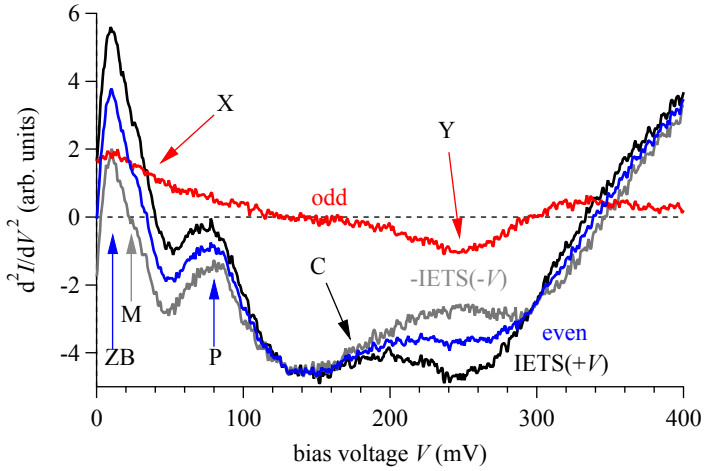

Figure 48: Even and odd IET spectra for the PSV in the parallel state. The odd spectrum reveals asymmetric contributions at low bias (X) and around 250 mV (Y).

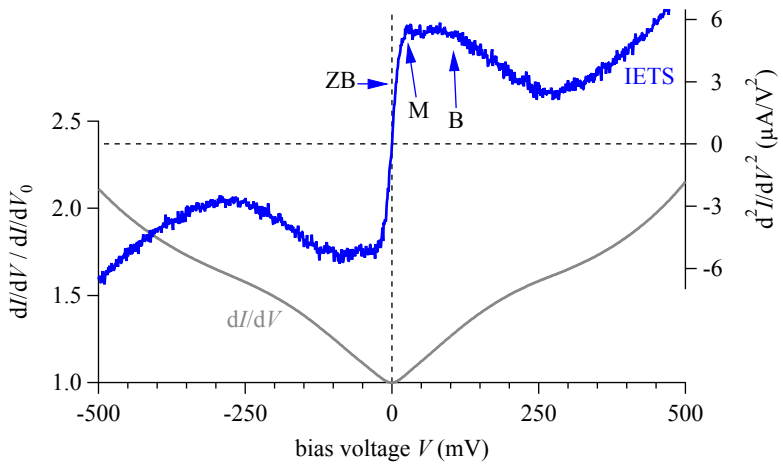

Figure 49: The tunnel spectrum normalized to its value at $V = 0$ and the IET spectrum of the PSV sample in the antiparallel state. The resolution of the measurements is to some point limited by the high resistance (which is six times higher than in the parallel state).

phonon peaks. At 250 mV a sharp contribution (Y) changes the shape of the peak within the large dip.

The spectra in the antiparallel state (Figure 49) show less features, as it was seen for the other MTJs before. The first derivative shows the V-shaped zero bias anomaly and the parabola shape and bias voltages above 250 mV. In the IET spectrum only a broad contribution (B) up to 250 mV can be seen, with a small peak at low bias (M). The rise at zero bias is not as steep as in the parallel state but has a small shoulder (ZB).

W 20
MgO 1.8
W 20
substrate

Table 19: Stack M-I-M. A tunnel junction without magnetic electrodes.

THE NONMAGNETIC METAL that is used in the other stacks instead of a ferromagnetic electrode is tungsten. It is chosen because of its high melting point and the associated low tendency to diffuse into the stack during annealing. While it has similar properties as the often used tantalum,[142] it also has a lower lattice mismatch (6 %) with the MgO barrier (Ta 11 %).

The spectra for the M-I-M junction are shown in Figure 50. The conductance has the predicted parabolic shape[143] with variations at bias voltages up to 100 mV. In the IET spectrum these features can be seen more clearly. First, at 9 mV a negative zero bias anomaly is found, i.e. the conductance decreases at low bias compared to zero bias. This is different compared to the PSV. There, the anomaly has the opposite sign and the magnitude of the effect is also larger. It dominates the spectra, which is typical in MTJs.[144]

[142] M.-A. Nicolet, Thin Solid Films **52**, 415 (1978)

[143] J. G. Simmons, J. Appl. Phys. **35**, 2655 (1964)

[144] J. S. Moodera et al., Phys. Rev. Lett. **80**, 294 (1998); and G.-X. Miao et al., J. Appl. Phys. **99**, 08T305 (2006)

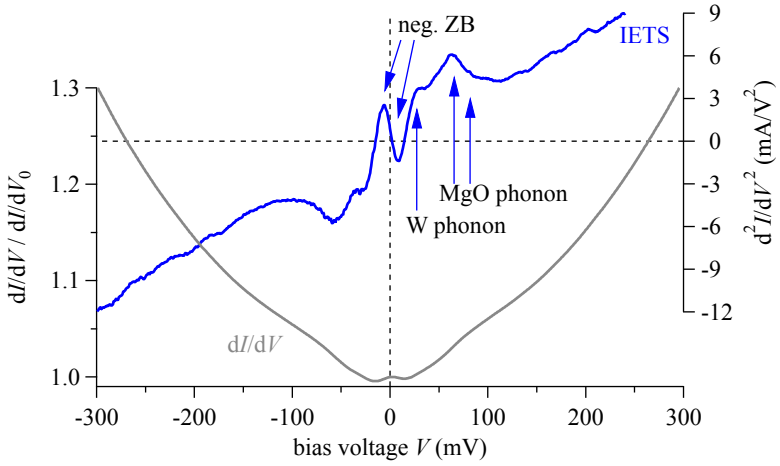

Figure 50: The tunnel spectrum (dI/dV) normalized to its value at $V = 0$ and the IET spectrum (d^2I/dV^2) of the W/ MgO/ W sample.

Second, several broad peaks are found up to 100 mV. As no magnetic materials are used and no magnetic impurities are expected, phonon excitation is an explanation for these peaks. Peaks of the electrode phonons typically have energies[145] around 30 meV while the phonons of oxides have higher energies. Here, the first peak (W) corresponds to the excitation of tungsten phonons with an energy[146] of 26 meV. In the MgO barrier phonons are excited, which leads to peaks[147] at 66 and 81 mV. A strong peak is found at 66 mV but only a shoulder is found at 81 mV. In the MgO based PSV the latter peak is more pronounced. This is typical for MTJs,[148] and was also found before.

[145] J. Klein et al., Phys. Rev. B **7**, 2336 (1973)

[146] W. Olejniczak et al., Appl. Phys. A **66**, 191 (1998)

[147] J. Klein et al., Phys. Rev. B **7**, 2336 (1973)

[148] G.-X. Miao et al., J. Appl. Phys. **99**, 08T305 (2006)

THE FM-I-M JUNCTION shows a strong asymmetry in the slope of the dI/dV-curves (Figure 51). This leads to a different height of the IET spectra for positive compared to negative bias. Nevertheless, a peak structure is visible for both polarities. Most prominent is the sharp rising flank for positive bias. However, this is not the zero bias anomaly. The flank is shifted to higher energy compared to the PSV and leads to a pronounced maximum (M) at 30 mV. This is presumably the magnon peak. The actual excitation may be at lower energy, because of the smearing with the zero bias feature. The latter is still negative for both bias polarities. For negative bias it is found at 10 mV, while it is closer to zero for positive bias. This is also caused by smearing with the flank. The spec-

W 20
MgO 1.8
$Co_{40}Fe_{40}B_{20}$ 6
W 15
substrate

Table 20: Stack FM-I-M. A tunnel junction with one magnetic electrode.

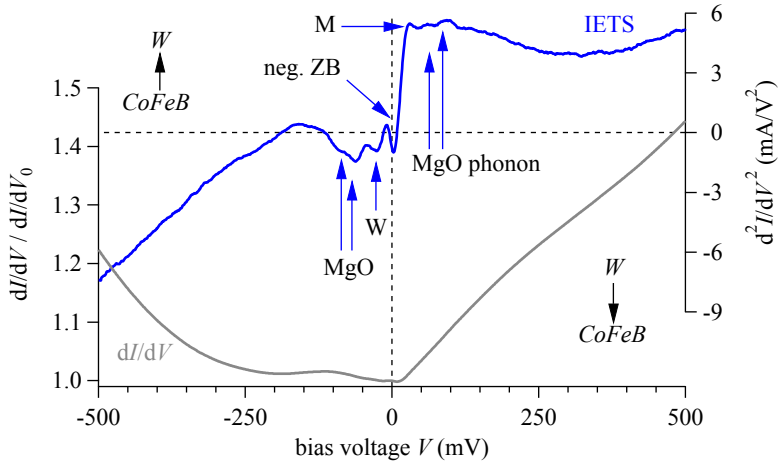

Figure 51: The normalized tunnel spectrum and the IET spectrum of the Co-Fe-B/ MgO/ W sample.

trum for negative bias (tunneling into tungsten) looks similar to the spectrum of the first sample, with the tungsten phonon peak at 26 mV and an MgO phonon peak at 66 mV. The 81 mV shoulder is more pronounced. For positive bias, i.e. tunneling into the ferromagnet, the peaks are higher and less sharp. Here, the second MgO phonon peak is visibly stronger than the first one at 66 mV. However, it is shifted to slightly higher voltage around 100 meV.

A COMPARISON of the IET spectra of the FM-I-M junction with those of the PSV MTJ is twofold. First, the FM-I-M spectrum for tunneling into tungsten (negative bias) is compared to the spectrum for the parallel magnetic state. In this situation no or less magnon excitation is expected. Second, for tunneling into the ferromagnet (positive bias) the spectrum is compared to the PSV in the antiparallel magnetic state. Here, excitation of magnons is supposed to be high.[149] In Figure 52 the spectra have a similar shape in both cases. The striking difference is the zero bias anomaly, which is positive for the PSV and leads to a huge peak in the P state. This effect is also visible in the antiparallel state, but the zero bias peak is only a shoulder. As a result the spectrum immediately rises after zero bias, while for the FM-I-M junction the flank seems shifted to higher bias. The MgO phonon peaks are also similar in both cases. The spectra of the PSV in the parallel state are negative over a wide bias range.

[149] X.-F. Han et al., Phys. Rev. B **63**, 224404 (2001)

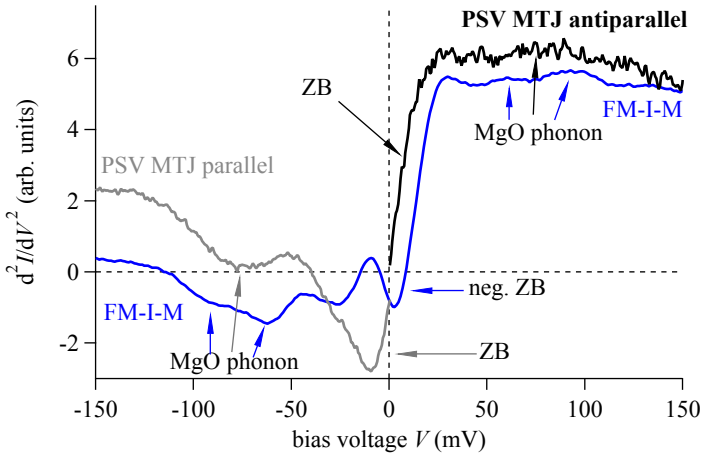

Figure 52: Comparison of the IET spectra of the Co-Fe-B/ MgO/ W sample and those of the PSV sample (scaled). Parallel and **antiparallel** state of the PSV are shown.

NOW THE RESULTS WILL BE DISCUSSED. In the spectra of the samples with nonmagnetic electrodes several peaks can be identified. There are excitations of the phonons of the target electrode and the barrier. Additionally, there is the zero bias anomaly (ZB). Its size and sign is different for the PSV and the (F)M-I-M junctions, and it is not simply a matter of the material of the target electrode. This can be seen from the results of the FM-I-M junction, where the zero bias anomaly is roughly the same for the two different electrode materials. Furthermore, the same ferromagnet shows large positive zero bias peaks in the PSV. The two different results strongly indicate that it is not a excitation of surface magnons which is causing the zero bias anomaly, in none of the junctions. This again leaves tunneling through impurities as an explanation.[150] It is known that the zero bias effect depends on the impurity material,[151] but it is not clear which material could be responsible, here. A simple assumption that would explain impurities in the barrier is implantation of upper electrode atoms during preparation. In this case the material would be tungsten in both samples (in difference to the case of the PSV).

The M-I-M sample shows near ideal symmetry and the expected peaks. The asymmetry in the spectra of the FM-I-M sample, however, rises the question of magnon excitation in the ferromagnet. To get a better idea of the asymmetry, the even and odd spectra are calculated. Some peak structures are indeed en-

[150] J. A. Appelbaum, Phys. Rev. **154**, 633 (1967)

[151] J. R. Cooper et al., J. Phys. F **3**, L120 (1973)

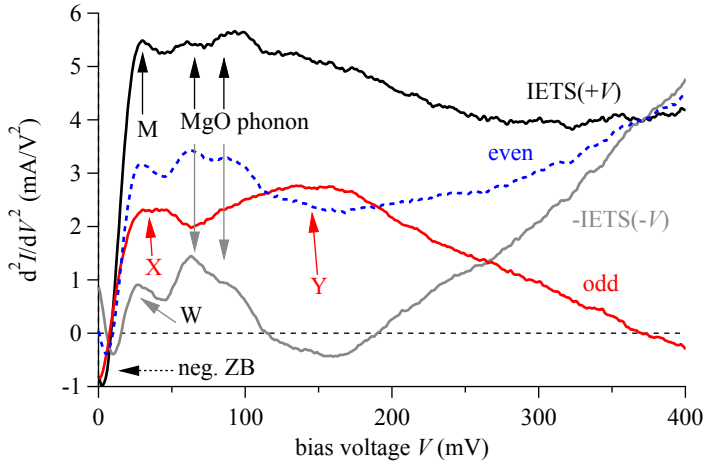

Figure 53: Comparison of IET spectra for **positive**/negative bias and even and odd spectra of the Co-Fe-B/ MgO/ W sample.

hanced in the odd spectrum (Figure 53). The first peak (X) can be attributed to the excitation of magnons. It is at the same energy, where magnons were identified in the previous chapters.

There is, however, a very broad second contribution (Y) around 150 mV, which leads up to some hundred mV. This makes the odd spectrum very different compared to the spectrum found in a similar experiment with aluminum oxide barriers. There, PALUSKAR et al. find a single peak[152] at 10 mV. Of course, in junctions with amorphous alumina barriers only incoherent tunneling takes place. This leaves two possibilities for the origin for the broad feature in the spectra of the presented MgO based junctions. It can be caused by magnons of higher energy (bulk magnons, rather than surface) or it is an effect of coherent tunneling. The energies of some hundred meV are equivalent to temperatures higher than 1000 K and, therefore, the curie-temperature of the ferromagnet. If the whole ferromagnet was at such high temperature there would be no magnetization and, hence, no magnons. However, the high energy of the single hot electron is not equivalent to the total system being at high temperature. The total magnon density of states in a ferromagnet is indeed large at energies up to 300 meV (e.g. iron and nickel[153]). Furthermore bulk magnons are suspected to contribute to the tunneling process at some voltage.[154] So a bulk magnon contribution at these higher voltage is at least not excluded. However, it is not clear if the in-

[152] P. V. Paluskar et al., Appl. Phys. Lett. **91**, 222501 (2007)

[153] S. V. Halilov et al., Europhys. Lett. **39**, 91 (1997)

[154] A. M. Bratkovsky, Appl. Phys. Lett. **72**, 2334 (1998)

teraction potential of electrons and magnons allows the excitation of the corresponding modes.[155]

[155] T. Balashov et al., Phys. Rev. B **78**, 174404 (2008)

Nevertheless, the similarity of the FM-I-M spectra to the state-specific spectra of the MTJ also fits in this model. In the case of electrons tunneling into Co-Fe-B magnons should be the dominant excitation. This is also the case in the antiparallel state of an MTJ where the direct tunneling contribution is smaller due to the inverse spin polarization of the electrodes. As the major difference is caused by the anomaly around zero bias, it can be suspected that the broad contribution, which is not seen in the parallel state, is also the excitation of magnons. Lastly, the broad dip (or gap) in the tunnel spectrum ($\mathrm{d}I/\mathrm{d}V$) of the FM-I-M junction resembles the parallel state spectrum of MTJs that incorporate one half-metallic Heusler compound electrode.[156] In both cases magnon excitation is prohibited for the corresponding bias polarity, while it is allowed for the other one. This is another hint that magnon excitation is the origin of the broader feature (gap in $\mathrm{d}I/\mathrm{d}V$, background in IETS).

[156] Y. Sakuraba et al., Appl. Phys. Lett. **89**, 052508 (2006); and D. Ebke et al., Appl. Phys. Lett. **95**, 232510 (2009)

A minor note regards the PSV spectrum in the parallel state. It is shifted to negative values, which indicates a large coherent tunneling contribution.[157] This can certainly be expected for a sample with a TMR ratio higher than 530 %. However, no such effects are seen in the M-I-M sample. This might be tentatively ascribed to different growth of the MgO barrier depending on the lower electrode material. The different strength of the MgO phonons peaks could then also be an effect of different barrier and interface properties. Also, it is not clear if coherent tunneling should show up in the spectra for a junction with tungsten electrodes.

[157] S. Tsunegi et al., Appl. Phys. Lett. **93**, 112506 (2008)

SUMMARIZING this chapter, magnetic tunnel junctions have been fabricated in a pseudo spin valve design. They yield TMR ratios of more than 530 %, which is the highest value of samples fabricated in Bielefeld. In MTJs with high TMR ratios evidence for coherent tunneling was found. *Nonmagnetic* electrodes have been introduced in tunnel junctions to better understand the excitation processes in the *magnetic* tunnel junctions. A huge asymmetry was found depending on the material that the electrons tunnel into. This asymmetric contribution to the tunneling can be identified

with the excitation of magnons. The origin of additional contribution at higher energies could not finally be clarified. Magnons of higher energy are very probable here. But an effect of the coherent tunneling cannot be fully excluded. However, the features were not seen in the (F)M-I-M-junctions. It remain to be clarified if coherent tunneling should lead to features in the (symmetric) M-I-M or in the (asymmetric) FM-I-M junction.

The results shown in this chapter have been prepared for publication. The preprint can be found in the appendix.

6 Summary and outlook

In this thesis, magnetic tunnel junctions based on MgO barriers have been prepared and investigated. Different aspects were discussed, in order to understand the physical limitations to the TMR ratio of the MTJs and, hence, their performance as a basis of spintronic devices.

In chapter 2, the temperature dependence of the TMR effect has been investigated. The magnon-excitation model by Zhang has been enhanced to incorporate thermal smearing in a phenomenological model. This way a much better agreement of model and experimental data was achieved. This shows that the effect of thermal smearing cannot be neglected for high TMR junctions, because of the very small overall change of the conductance in the parallel state. Furthermore, it becomes evident, that magnon excitation is the basis of the temperature dependence of the TMR ratio. It is indicated that the tailoring of the magnon spectrum is crucial for getting less temperature dependence and, therefore, a higher TMR ratio at room temperature. Our model was published in Physical Review B[158] and adopted by the community, as the citations show.

[158] V. Drewello et al., Phys. Rev. B 77, 014440 (2008)

A method to further investigate the magnon excitation is presented in chapter 3. The bias voltage dependence of the magnetic tunnel junctions was investigated with inelastic electron tunneling spectroscopy. In these measurements peaks show the opening of transport channels due to specific inelastic excitations during the tunneling process. In the parallel and antiparallel magnetic state of the MTJs several excitations were found. Different ferromagnetic electrode designs were used in order to clarify the origin of the peaks. The zero bias anomaly could be identified, which is

caused by magnetic impurities. A second contribution was found, which strongly differs for the parallel and the antiparallel magnetic state. This is attributed to the excitation of magnons. A pronounced additional structure was found in the spectra in parallel state, which is stronger the higher the TMR ratio. It was attributed to coherent tunneling effects. It could be shown, that the increase of the annealing temperature beyond 350°C leads to higher TMR ratio only for the magnetic tunnel junctions in a pseudo spin valve design. For samples that use pinning, ways to minimize diffusion have to be developed. Results of this chapter have been published in Physical Review B.[159]

[159] V. Drewello et al., Phys. Rev. B **79**, 174417 (2009)

Chapter 4 dealt with magnetic tunnel junctions based on Heusler electrodes. The cobalt based compounds Co_2FeAl, Co_2FeSi and Co_2MnSi were investigated by tunneling spectroscopy. The measurements on the Co_2FeAl based sample showed a large asymmetry of the conductance in the parallel state, but only small variations in the antiparallel state. These findings could be explained with the assumption of a gap in the minority DOS of the Co_2FeAl electrode. However, for positive bias voltage this model proved to be incomplete. IET spectroscopy revealed magnon excitation, which must be taken into account. A phenomenological model was shown to explain the behavior for both bias polarities consistently. This is of fundamental interest, as it shows that the presence of a gap in the minority DOS is not automatically enough to gain high TMR ratios (at room temperature). These findings were published in Applied Physics Letter.[160] Shortly thereafter an experiment by another group[161] was published, which can be seen as a prove for our assumed model.

[160] D. Ebke et al., Appl. Phys. Lett. **95**, 232510 (2009)

[161] Y. Sakuraba et al., Phys. Rev. B **81**, 144422 (2010)

The other Heusler based samples showed diverse effects. The compound Co_2MnSi was buffered by either Co_2FeAl or Co_2FeSi to induce B2 structure. The spectra showed an influence of the buffer material on the tunneling spectra. This was most clear for negative bias, where electrons are emitted from the Heusler electrode. For positive bias the interfacial layer played a more crucial role. Here, Co_2MnSi showed much higher magnon excitation, which is presumably also the reason for the larger temperature dependence of the TMR ratio of these samples. This again showed that the magnon excitation weights stronger compared to the band

structure effects. Hence, it must be overcome to benefit from the minority DOS gap and, therefore, the high spin polarization.

In chapter 5, magnetic tunnel junctions have been fabricated in a pseudo spin valve design. TMR ratios of more than 530 % have been reached, which is the highest value of all samples fabricated in our laboratory. In the magnetic tunnel junctions with high TMR ratios evidence for coherent tunneling was found. Nonmagnetic electrodes were used in the tunnel junctions to understand the excitation processes and the contribution of coherent tunneling. An asymmetry was found depending on the material that the electrons tunnel into. This asymmetric contribution to the tunneling could partially be identified with the excitation of magnons. However, at higher energies some features could correspond to magnons of higher energies or an effect of the coherent tunneling. The features were not seen in the junctions with no magnetic electrode. It remains to be clarified if coherent tunneling should lead to features in the spectra of the junctions or not.

INCREASING the room temperature TMR ratio of magnetic tunnel junctions is key to assure higher performance in their spintronic applications. In this work, methods have been shown to determine the limiting factors to the TMR effect. For the Heusler compounds the fingerprint of a gap in the minority DOS is shown by tunneling spectroscopy. It has long been used to identify the materials as half-metallic ferromagnets. Yet again, the understanding of the role of magnons delivers insight into possible physical limitations to the TMR ratio. Also, the temperature driven diffusion has to be minimized while still achieving highly orientated crystalline growth. The magnon excitation is even harder to control. Here, the ferromagnetic materials rather than the tunnel barrier have to be optimized. The effectiveness of one's efforts can best be monitored with IET spectroscopy. It is simple in terms of sample preparation, but delivers insight into the transport characteristics. It is also quite resistant to slight, unavoidable deviations during the preparation of the samples.

The findings for the different samples in this work show some constraints of how sample optimization should be done. The general approach should be like this: Take a stack layout with op-

timized, smooth growth of the electrodes and the interface. Use MgO as the barrier material and optimize its crystallinity. To do so, there are two ways: Using an amorphous electrode and let the MgO determine the crystal growth, or use a highly crystalline electrode and introduce ordering to the MgO. In both cases annealing at high temperatures above 450°C is needed to drive the (re-)crystallization and heal defects. The use of higher annealing temperatures is limited mostly by diffusion. Therefore, antiferromagnets should be used with care, as the typical compounds diffuse at relatively low temperature (about 300°C). In pseudo spin valves no antiferromagnets are needed, but they are hardly usable for application. One has to switch to other antiferromagnetic materials or other methods, like annealing in two steps.

If it is possible to control the magnon excitations in a Heusler compound, i.e. minimizing interface and defects states, its high spin polarization could very well also be used. The results of the multilayered Heusler electrodes indicate, that the use of thin interlayers of other materials might be a way to gain this control. Again, the success of such experiments can effectively be assessed with the IET spectroscopy.

References

A

D. W. Abraham, P. L. Trouilloud, and D. C. Worledge, 'Rapid-turnaround characterization methods for MRAM development', IBM J. Res. & Dev. **50**, 55 (2006).

C. J. Adkins and W. A. Phillips, 'Inelastic electron tunneling spectroscopy', J. Phys. C **18**, 1313 (1985).

J. G. Adler, 'Observation of the phonon spectra of MgO by inelastic electron tunneling in metal-insulator-metal junctions', Solid State Commun. **7**, 1635 (1969).

J. A. Appelbaum, 'Exchange Model of Zero-Bias Tunneling Anomalies', Phys. Rev. **154**, 633 (1967).

J. A. Appelbaum and L. Y. L. Shen, 'Zero-Bias-Conductance-Peak Anomaly of Ta-*I*-Al Tunnel Junctions at 0.3 K and 90 kG', Phys. Rev. B **5**, 544 (1972).

B

T. Balashov, A. F. Takács, M. Däne, A. Ernst, P. Bruno, and W. Wulfhekel, 'Inelastic electron-magnon interaction and spin transfer torque', Phys. Rev. B **78**, 174404 (2008).

B. Balke, S. Wurmehl, G. H. Fecher, C. Felser, and J. Kübler, 'Rational design of new materials for spintronics: Co_2FeZ (Z =Al, Ga, Si, Ge)', Sci. Technol. Adv. Mater. **9**, 014102 (2008).

S. Bermon, D. E. Paraskevopoulos, and P. M. Tedrow, 'Ultra-high magnetic field study of the Kondo-type zero-bias conductance peak in magnetically doped metal-insulator-metal tunnel junctions', Phys. Rev. B **17**, 2110 (1978).

A. M. Bratkovsky, 'Assisted tunneling in ferromagnetic junctions and half-metallic oxides', Appl. Phys. Lett. **72**, 2334 (1998).

W. F. Brinkman, R. C. Dynes, and J. M. Rowell, 'Tunneling Conductance of Asymmetrical Barriers', J. Appl. Phys. **41**, 1915 (1970).

W. H. Butler, X.-G. Zhang, T. C. Schulthess, and J. M. MacLaren, 'Spin-dependant tunneling conductance of Fe/MgO/Fe sandwiches', Phys. Rev. B **63**, 054416 (2001).

C T. T. Chen and J. G. Adler, 'Electron Tunneling In Clean Al-Insulator-Normal Metal Junction', Solid State Commun. **8**, 1965 (1970).

J. R. Cooper and A. F. G. Wyatt, 'Systematic behaviour of tunnel junctions doped with 3d atoms', J. Phys. F **3**, L120 (1973).

D T. Dimopoulos, G. Gieres, J. wecker, Y. Luo, and K. Samwer, 'Analysis of the magnetotransport channels in tunnel junctions with amorphous CoFeB', Europhys. Lett. **68**, 706 (2004).

V. Drewello, Diploma thesis, Bielefeld University, 2006.

V. Drewello, J. Schmalhorst, A. Thomas, and G. Reiss, 'Evidence for strong magnon contribution to the TMR temperature dependence in MgO based tunnel junctions', Phys. Rev. B **77**, 014440 (2008).

V. Drewello, M. Schäfers, O. Schebaum, A. A. Khan, J. Münchenberger, J. Schmalhorst, G. Reiss, and A. Thomas, 'Inelastic electron tunneling spectra of MgO-based magnetic tunnel junctions with different electrode designs', Phys. Rev. B **79**, 174417 (2009).

E D. Ebke, V. Drewello, M. Schäfers, G. Reiss, and A. Thomas, 'Tunneling spectroscopy and magnon excitation in Co_2FeAl/MgO/Co–Fe magnetic tunnel junctions', Appl. Phys. Lett. **95**, 232510 (2009).

D. Ebke, P. Thomas, O. Schebaum, M. Schäfers, D. Nissen, V. Drewello, A. Hütten, and A. Thomas, 'Low B2 crystallization temperature and high tunnel magnetoresistance in Co_2FeAl/MgO/

Co-Fe magnetic tunnel junctions', J. Magn. Magn. Mater. **322**, 996 (2010).

G. Eilers, A. Thomas, and M. Münzenberg, 'TEM pictures of MgO based MTJs', unpublished, 2008.

A. L. Geiger, B. S. Chandrasekhar, and J. G. Adler, 'Inelastic Electron Tunneling in Al-Al-Oxide-Metal Systems', Phys. Rev. **188**, 1130 (1969). **G**

S. V. Halilov, A. Y. Perlov, P. M. Oppeneer, and H. Eschrig, 'Magnon spectrum and related finite-temperature magnetic properties: A first-principle approach', Europhys. Lett. **39**, 91 (1997). **H**

X.-F. Han, A. C. C. Yu, M. Oogane, J. Murai, T. Daibou, and T. Miyazaki, 'Analyses of intrinsic magnetoelectric properties in spin-valve-type tunnel junctions with high magnetoresistance and low resistance', Phys. Rev. B **63**, 224404 (2001).

J. Hayakawa, S. Ikeda, F. Matsukara, H. Takahashi, and H. Ohno, 'Dependence of Giant Tunnel Magnetoresistance of Sputtered CoFeB/MgO/CoFeB Magnetic Tunnel Junctions on MgO Barrier Thickness and Annealing Temperature', Jap. J. Appl. Phys. **44**, 587 (2005).

J. Hayakawa, S. Ikeda, Y. M. Lee, F. Matsukura, and H. Ohno, 'Effect of high annealing temperature on giant tunnel magnetoresistance ratio of CoFeB/MgO/CoFeB magnetic tunnel junctions', Appl. Phys. Lett. **89**, 232510 (2006).

S. Ikeda, J. Hayakawa, Y. Ashizawa, Y. M. Lee, K. Miura, H. Hasegawa, M. Tsunoda, F. Matsukura, and H. Ohno, 'Tunnel magnetoresistance of 604% at 300 K by suppression of Ta diffusion in CoFeB/MgO/CoFeB pseudo-spin-valves annealed at high temperature', Appl. Phys. Lett. **93**, 082508 (2008). **I**

K. Inomata, N. Ikeda, N. Tezuka, R. Goto, S. Sugimoto, and M. W. andEva Jedryka, 'Highly spin-polarized materials and devices for spintronics', Sci. Technol. Adv. Mater. **9**, 014101 (2008).

T. Ishikawa, T. Marukame, H. Kijima, K.-I. Matsuda, T. Uemura, M. Arita, and M. Yamamoto, 'Spin-dependent tunneling characteristics of fully epitaxial magnetic tunneling junctions with

a full-Heusler alloy Co_2MnSi thin film and a MgO tunnel barrier', Appl. Phys. Lett. **89**, 192505 (2006).

T. Ishikawa, N. Itabashi, T. Taira, K. ichi Matsuda, T. Uemura, and M. Yamamoto, 'Critical role of interface states for spin-dependent tunneling in half-metallic Co_2MnSi-based magnetic tunnel junctions investigated by tunneling spectroscopy', Appl. Phys. Lett. **94**, 092503 (2009).

J R. C. Jaklevic and J. Lambe, 'Molecular Vibration Spectra By Electron Tunneling', Phys. Rev. Lett. **17**, 1139 (1966).

M. Jimbo, K. Komiyama, Y. Shirota, Y. Fujiwara, S. Tsunashima, and M. Matsuura, 'Thermal stability of spin valves using amorphous CoFeB', J. Magn. Magn. Mater. **165**, 308 (1997).

M. Jullière, 'Tunneling between ferromagnetic films', Phys. Lett. **54**, 225 (1975).

K J. Kanak, T. Stobiecki, V. Drewello, J. Schmalhorst, and G. Reiss, 'The influence of the texture on properties of IrMn spin valve magnetic tunnel junctions with MgO barrier and CoFeB electrodes', Phys. Stat. Sol. A **204**, 3942 (2007).

A. A. Khan, J. Schmalhorst, A. Thomas, O. Schebaum, and G. Reiss, 'Dielectric breakdown in Co–Fe–B/MgO/Co–Fe–B magnetic tunnel junction', J. Appl. Phys. **103**, 123705 (2008).

J. Klein, A. Léger, M. Belin, D. Défourneau, and M. J. L. Sangster, 'Inelastic-Electron-Tunneling Spectroscopy of Metal-Insulator-Metal Junctions', Phys. Rev. B **7**, 2336 (1973).

T. Kubota, S. Tsunegi, M. Oogane, S. Mizukami, T. Miyazaki, H. Naganuma, and Y. Ando, 'Half-metallicity and Gilbert damping constant in $Co_2Fe_xMn_{1-x}Si$ Heusler alloys depending on the film composition', Appl. Phys. Lett. **94**, 122504 (2009).

L Y. M. Lee, J. Hayakawa, S. Ikeda, F. Matsukura, and H. Ohno, 'Giant tunnel magnetoresistance and high annealing stability in CoFeB/MgO/CoFeB magnetic tunnel junctions with synthetic pinned layer', Appl. Phys. Lett. **89**, 042506 (2006).

J. Mathon and A. Umerski, 'Theory of tunneling magnetoresistance of an epitaxial Fe/MgO/Fe(001) junction', Phys. Rev. B **63**, 220403 (2001). **M**

R. Matsumoto, Y. Hamada, M. Mizuguchi, M. Shiraishi, H. Maehara, K. Tsunekawa, D. D. Djayaprawira, N. Watanabe, Y. Kurosaki, T. Nagahama, A. Fukushima, H. Kubota, S. Yuasa, and Y. Suzuki, 'Tunneling spectra of sputter-deposited CoFeB/MgO/CoFeB magnetic tunnel junctions showing giant tunneling magnetoresistance effect', Solid State Commun. **136**, 611 (2005).

G.-X. Miao, K. B. Chetry, A. Gupta, W. H. Butler, K. Tsunekawa, D. Djayaprawira, and G. Xiao, 'Inelastic tunneling spectroscopy of magnetic tunnel junctions based on CoFeB/MgO/CoFeB with Mg insertion layer', J. Appl. Phys. **99**, 08T305 (2006).

Y. Miura, H. Uchida, Y. Oba, K. Abe, and M. Shirai, 'Half-metallic interface and coherent tunneling in Co_2YZ/MgO/Co_2YZ (YZ = MnSi,CrAl) magnetic tunnel junctions: A first-principles study', Phys. Rev. B **78**, 064416 (2008).

T. Miyazaki and N. Tezuka, 'Giant magnetic tunneling effect in Fe/Al_2O_3/Fe junction', J. Magn. Magn. Mater. **139**, L231 (1995).

M. Mizuguchi, Y. Hamada, R. Matsumoto, S. Nishioka, H. Maehara, K. Tsunekawa, D. D. Djayaprawira, N. Watanabe, T. Nagahama, A. Fukushima, H. Kubota, S. Yuasa, M. Shiraishi, and Y. Suzuki, 'Tunneling spectroscopy of magnetic tunnel junctions: Comparison between CoFeB/MgO/CoFeB and CoFeB/Al–O/CoFeB', J. Appl. Phys. **99**, 08T309 (2006).

J. S. Moodera, L. R. Kinder, T. M. Wong, and R. Meservey, 'Large Magnetoresistance at Room Temperature in Ferromagnetic Thin Film Tunnel Junctions', Phys. Rev. Lett. **74**, 3273 (1995).

J. S. Moodera, J. Nowak, and R. J. M. van de Veerdonk, 'Interface Magnetism and Spin Wave Scattering in Ferromagnet-Insulator-Ferromagnet Tunnel Junctions', Phys. Rev. Lett. **80**, 294 (1998).

J. Murai, Y. Ando, M. Kamijo, H. Kubota, and T. Miyazaki, 'Direct Observation of Magnon Excitation in a Ferromagnetic Tunnel

Junction Using Inelastic-Electron-Tunneling Spectroscopy', Jap. J. Appl. Phys. **38**, L1109 (1999).

N M.-A. Nicolet, 'Diffusion barriers in thin films', Thin Solid Films **52**, 415 (1978).

O K. Özdoğan, B. Aktaş, I. Galanakis, and E. Şaşioğlu, 'Influence of mixing the low-valent transition metal atoms (Y, Y* = Cr, Mn, Fe) on the properties of the quaternary $Co_2[Y_{1-x}Y^*_x]Z$ (Z=Al, Ga, Si, Ge, or Sn) Heusler compounds', J. Appl. Phys. **101**, 073910 (2007).

W. Olejniczak, Z. Klusek, and M. Bieniecki, 'Investigations of the fine structure of I(V) characteristics for highly oriented pyrolitic graphite surface by means of STM/STS at room temperature', Appl. Phys. A **66**, 191 (1998).

K. Ono, T. Daibou, S.-J. Ahn, Y. Sakuraba, T. Miyakoshi, T. Morita, Y. Kikuchi, M. Oogane, Y. Ando, and T. Miyazaki, 'Tunneling spectroscopy in CoFeB/MgO/CoFeB magnetic tunnel junctions', J. Appl. Phys. **99**, 08A905 (2006).

P P. V. Paluskar, C. H. Kant, J. T. Kohlhepp, A. T. Filip, H. J. M. Swagten, B. Koopmans, and W. J. M. de Jonge, 'Mn diffusion and the thermal stability of tunneling spin polarization', J. Appl. Phys. **97**, 10C925 (2005).

P. V. Paluskar, F. L. Bloom, J. T. Kohlhepp, H. J. M. Swagten, B. Koopmans, and E. Snoeck, 'Impact of interface crystallization on inelastic tunneling in $Al/AlO_x/CoFeB$', Appl. Phys. Lett. **91**, 222501 (2007).

S. S. P. Parkin, C. Kaiser, A. Panchula, P. M. Rice, B. Hughes, M. Samant, and S.-H. Yang, 'Giant tunneling magnetoresistance at room temperature with MgO (100) tunnel barriers', Nat. Mater. **3**, 862 (2004).

R. J. Pedersen and J. F. L. Vernon, 'Effect of film resistance on low-impedance tunneling measurements', Appl. Phys. Lett. **10**, 29 (1967).

W. Plesiewicz and J. G. Adler, 'Inelastic electron-tunneling study of MgO barriers', Phys. Rev. B **34**, 4583 (1986).

Y. Sakuraba, T. Miyakoshi, M. Oogane, Y. Ando, A. Sakuma, T. Miyazaki, and H. Kubota, 'Direct observation of half-metallic energy gap in Co_2MnSi by tunneling conductance spectroscopy', Appl. Phys. Lett. **89**, 052508 (2006). **S**

M. Sargolzaei, M. Richter, K. Koepernik, I. Opahle, H. Eschrig, and I. Chaplygin, 'Spin and orbital magnetism in full Heusler alloys: A density functional theory study of Co_2YZ (Y=Mn,Fe; Z=Al,Si,Ga,Ge)', Phys. Rev. B **74**, 224410 (2006).

O. Schebaum, D. Ebke, A. Niemeyer, G. Reiss, J. S. Moodera, and A. Thomas, 'Direct measurement of the spin polarization of Co_2FeAl in combination with MgO tunnel barriers', J. Appl. Phys. **107**, 09C717 (2010).

J. Schmalhorst and G. Reiss, 'Temperature and bias-voltage dependent transport in magnetic tunnel junctions with low energy Ar-ion irradiated barriers', Phys. Rev. B **68**, 224437 (2003).

J. Schmalhorst, A. Thomas, S. Kämmerer, O. Schebaum, D. Ebke, M. D. Sacher, G. Reiss, A. Hütten, A. Turchanin, A. Gölzhäuser, and E. Arenholz, 'Transport properties of magnetic tunnel junctions with Co_2MnSi electrodes: The influence of temperature-dependent interface magnetization and electronic band structure', Phys. Rev. B **75**, 014403 (2007).

R. Shan, H. Sukegawa, W. H. Wang, M. Kodzuka, T. Furubayashi, T. Ohkubo, S. Mitani, K. Inomata, and K. Hono, 'Demonstration of Half-Metallicity in Fermi-Level-Tuned Heusler Alloy $Co_2FeAl_{0.5}Si_{0.5}$ at Room Temperature', Phys. Rev. Lett. **102**, 246601 (2009).

C. H. Shang, J. Nowak, R. Jansen, and J. S. Moodera, 'Temperature dependence of magnetoresistance and surface magnetization in ferromagnetic tunnel junctions', Phys. Rev. B **58**, R2917 (1998).

R. Stratton, 'Volt-current characteristics for tunneling through insulating films', J. Phys. Chem. Solids **23**, 1177 (1962).

H. Sukegawa, W. Wang, R. Shan, T. Nakatani, K. Inomata, and K. Hono, 'Spin-polarized tunneling spectroscopy of fully epi-

taxial magnetic tunnel junctions using $Co_2FeAl_{0.5}Si_{0.5}$ Heusler alloy electrodes', Phys. Rev. B **79**, 184418 (2009).

Y. Sakuraba, K. Takanashi, Y. Kota, T. Kubota, M. Oogane, A. Sakuma, and Y. Ando, 'Evidence of Fermi level control in a half-metallic Heusler compound Co_2MnSi by Al-doping: Comparison of measurements with first-principles calculations', Phys. Rev. B **81**, 144422 (2010).

W. Shen, D. Mazumdar, X. Zou, X. Liu, B. D. Schrag, and G. Xiao, 'Effect of film roughness in MgO-based magnetic tunnel junctions', Appl. Phys. Lett. **88**, 182508 (2006).

J. G. Simmons, 'Generalized Thermal J-V Characteristic for the Electric Tunnel Effect', J. Appl. Phys. **35**, 2655 (1964).

T J. M. Teixeira, J. Ventura, J. P. Araujo, J. B. Sousa, P. Wisniowski, and P. P. Freitas, 'Tunneling processes in thin MgO magnetic junctions', Appl. Phys. Lett. **96**, 262506 (2010).

P. A. Thiry, M. Liehr, J. J. Pireaux, and R. Caudano, 'Infrared optical constants of insulators determined by high-resolution electron-energy-loss spectroscopy', Phys. Rev. B **29**, 4824 (1984).

A. Thomas, 'Preparation and characterisation of magnetic single and double barrier junctions'PhD thesis, Bielefeld University (2003)

A. Thomas, V. Drewello, M. Schäfers, A. Weddemann, G. Reiss, G. Eilers, M. Münzenberg, K. Thiel, and M. Seibt, 'Direct imaging of the structural change generated by dielectric breakdown in MgO based magnetic tunnel junctions', Appl. Phys. Lett. **93**, 152508 (2008).

S. Tsunegi, Y. Sakuraba, M. Oogane, K. Takanashi, and Y. Ando, 'Large tunnel magnetoresistance in magnetic tunnel junctions using a Co_2MnSi Heusler alloy electrode and a MgO barrier', Appl. Phys. Lett. **93**, 112506 (2008).

S. Tsunegi, Y. Sakuraba, M. Oogane, H. Naganuma, K. Takanashi, and Y. Ando, 'Enhancement in tunnel magnetoresistance effect by inserting CoFeB to the tunneling barrier interface in

Co_2MnSi/MgO/CoFe magnetic tunnel junctions', Appl. Phys. Lett. **94**, 252503 (2009).

D. C. Tsui, R. E. Dietz, and L. R. Walker, 'Multiple Magnon Excitation in NiO by Electron Tunneling', Phys. Rev. Lett. **27**, 1729 (1971).

R. H. Wallis and A. F. G. Wyatt, 'Exchange scattering in Ti-doped Al/Al oxide/Ag tunnel junctions: II. Magnetic field', J. Phys. C **7**, 1293 (1974). **W**

W. Wang, H. Sukegawa, R. Shan, S. Mitani, and K. Inomata, 'Giant tunneling magnetoresistance up to 330% at room temperature in sputter deposited Co_2FeAl/MgO/CoFe magnetic tunnel junctions', Appl. Phys. Lett. **95**, 182502 (2009).

W. Wang, E. Liu, M. Kodzuka, H. Sukegawa, M. Wojcik, E. Jedryka, G. H. Wu, K. Inomata, S. Mitani, and K. Hono, 'Coherent tunneling and giant tunneling magnetoresistance in Co_2FeAl/MgO/CoFe magnetic tunneling junctions', Phys. Rev. B **81**, 140402 (2010).

R. C. Whited, C. J. Flaten, and W. C. Walker, 'Exciton thermoreflectance of MgO and CaO', Solid State Commun. **13**, 1903 (1973).

E. Wolf, 'Principles of Electron Tunneling Spectroscopy', Int. Ser. Monogr. Phys. No. **71** (Oxford University Press, New York, 1989).

D. C. Worledge and P. L. Trouilloud, 'Magnetoresistance measurement of unpatterned magnetic tunnel junction wafers by current-in-plane tunneling', Appl. Phys. Lett. **83**, 84 (2003).

A. F. G. Wyatt, 'Anomalous Densities of States in Normal Tantalum and Niobium', Phys. Rev. Lett. **13**, 401 (1964).

L. Yuan, S. H. Liou, and D. Wang, 'Temperature dependence of magnetoresistance in magnetic tunnel junctions with different free layer structures', Phys. Rev. B **73**, 134403 (2006). **Y**

S. Yuasa, T. Nagahama, A. Fukushima, Y. Suzuki, and K. Ando, 'Giant room- temperature magnetoresistance in single-crystal

Fe/MgO/Fe magnetic tunnel junctions', Nat. Mater. **3**, 868 (2004).

S. Yuasa, A. Fukushima, H. Kubota, Y. Suzuki, and K. Ando, 'Giant tunneling magnetoresistance up to 410% at room temperature in fully epitaxial Co/MgO/Co magnetic tunnel junctions with bcc Co(001) electrodes', Appl. Phys. Lett. **89**, 042505 (2006).

Z S. Zhang, P. M. Levy, A. C. Marley, and S. S. P. Parkin, 'Quenching of Magnetoresistance by Hot Electrons in Magnetic Tunnel Junctions', Phys. Rev. Lett. **79**, 3744 (1997).

85 References in total.

Appendix: Optimization and characterization of pseudo spin valves

This chapter deals with the fabrication of MgO based magnetic tunnel junctions, specifically pseudo spin valves. A short, topical summary of the optimization of the TMR ratio is given and the resulting samples are characterized. They yield the highest TMR ratios achieved in our laboratory.

In magnetic tunnel junctions the antiparallel alignment of the electrodes can be achieved by different switching fields of the electrodes. Then no antiferromagnet is needed for a pinning of one of the electrodes. Such a layer stack is usually called a pseudo spin valve[162] (PSV). The main advantage of a PSV is the simplicity of the layer stack, which consist of very few different materials. This makes it easier to find a suitable layer stack for a very high annealing temperature. The high temperatures are needed to achieve a good crystallization of the Co-Fe-B electrodes, the MgO barrier, and especially the interface between them.

[162] J. Hayakawa et al., Appl. Phys. Lett. **89**, 232510 (2006)

THE PSEUDO SPIN VALVES which are investigated in this chapter are prepared in a self-made sputter deposition tool with a base pressure below 1×10^{-9} mbar. The metallic layers are deposited on top of thermally oxidized silicon wafers using clean argon (7.0) at a pressure of 5×10^{-3} mbar. MgO is deposited at 1×10^{-2} mbar. The samples are post annealed for 1 hour in a high vacuum furnace with temperatures of up to 550°C. Then a capping of Ta and Au is added for protection and to form contact pads. The layer stacks are structured by e-beam or optical lithography and Ar-ion-beam etching.

Ta 20
$Co_{40}Fe_{40}B_{20}$ 3.2
MgO 2.4
$Co_{40}Fe_{40}B_{20}$ 5.3
Ta 22
substrate

Table 21: The stack of a pseudo spin valve MTJ.

The layer stack that has been optimized, is Ta 20/ CoFeB 5.3/ MgO 2.4/ CoFeB 3.2/ Ta 20 (all values in nm). It has been annealed at temperatures from 375 to 500°C. The lowest temperature was chosen, because it it the optimum for the bottom pinned standard stack (see chapter 'MgO barrier and Co-Fe-B electrodes'). The PSV is supposed to have higher optimal annealing temperature, because no manganese diffusion is possible.[163]

[163] Y. M. Lee et al., Appl. Phys. Lett. **89**, 042506 (2006); and J. Hayakawa et al., Appl. Phys. Lett. **89**, 232510 (2006)

The area resistance and the TMR ratio for different annealing temperatures are shown in Figure 54. The samples were patterned by optical lithography with square elements of 90 µm^2. Two values for the TMR are given. The first one is gained from a major loop (TMR min). The second one is the maximum TMR ratio that was measured with a 'virgin'-curve, i.e. beginning from zero magnetic field. In this state the magnetic layers are magnetized antiparallel. The curves show the same steps in the virgin loop and the major loop. The effect and the similarity of the switching is shown in Figure 55. The magnetic behavior (switching of domains) is the same in both measurements. It can be assumed that the switching fields of the magnetic layers are not different enough (i.e. the difference is smaller than the width of the switching of the soft layer). The softer electrode is not switching sharply but seems to have many domains.

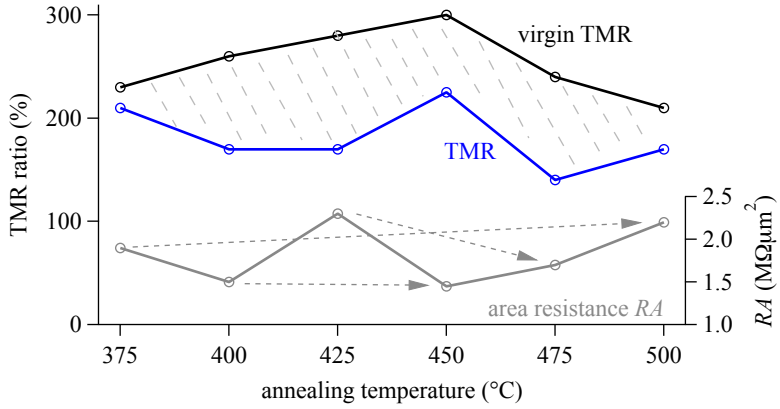

Figure 54: Area resistance product in parallel state and TMR ratio in dependence of the annealing temperature. The **virgin TMR ratio** (see text) is also given. Arrows indicate the order of step-by-step annealing.

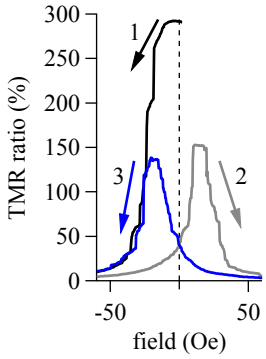

Figure 55: Major loop (forth and back) and **virgin curve** after antiparallel alignment by contact stress. Arrows indicate the direction of the measurement.

These virgin TMR values were used as the base for the optimization. The optimum temperature is 450°C. It shows the highest TMR ratio, from the major loop as well as the virgin measure-

ment. The area resistance product shows a strong variation for the different, subsequently annealed samples (the order of the subsequent annealing is indicated by arrows in the Figure). However, for both 450°C and 475°C the resistance drops, compared to the value before. This indicates crystallization of the MgO barrier, as the coherent effects allow for higher transmission compared to an amorphous barrier.[164]

After 450°C was chosen as annealing temperature, smaller elements were formed by e-beam lithography to achieve a better separation of the switching of the electrodes. The elements were ellipses, sized 6×2 and $3 \times 1\,\mu m^2$ and squares, sized $3 \times 3\,\mu m^2$. The elliptic shape is chosen to exploit the shape anisotropy. Stray field coupling can also be expected to be present, due to the small size of the elements. The squares showed no improvement of the switching behavior. The highest switching fields (about 160 Oe) of the harder magnetic layer were gained with the small ellipses.

Figure 56 shows the results of these changes. The major loop at room temperature shows a defined antiparallel state, with switching fields of the harder electrode of nearly 200 Oe. A high TMR ratio of 330 % is achieved. It is comparable to the virgin value found with larger elements. In zero field, however, the parallel magnetic state is not stable. The sample shows an antiparallel coupling, supposedly cause by the stray field. At low temperature of 13 K the major loop at 10 mV shows many steps in the switching of the soft electrode. Nevertheless, the TMR ratio is as high as 535 %. In Figure 57 the bias voltage dependence of the TMR ratio is shown. At zero bias the TMR ratio is in excess of 550 %. It rapidly decreases with higher bias voltage. At 500 mV the TMR ratio is decreased to about 200 %.

The temperature dependence of the TMR ratio and the resistance of the sample is shown in Figure 58. The change of the resistance in the parallel state is relatively small compared to the change in the antiparallel state (here, 5.7 % vs. 56 %), which is typical for MgO based magnetic tunnel junctions. The TMR ratio changes by a factor of 1.62 from RT to 13 K.

The sample was also investigated with high resolution TEM by Michael Seibt's group in Göttingen. The TEM specimen was prepared from a previously measured element by using a FIB tech-

[164] J. Mathon et al., Phys. Rev. B **63**, 220403 (2001); and W. H. Butler et al., Phys. Rev. B **63**, 054416 (2001)

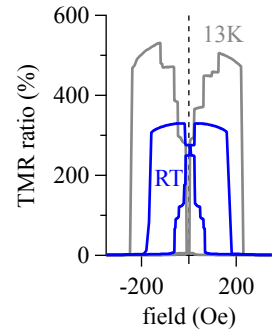

Figure 56: Major loop of the optimized PSV, at room temperature and 13 K.

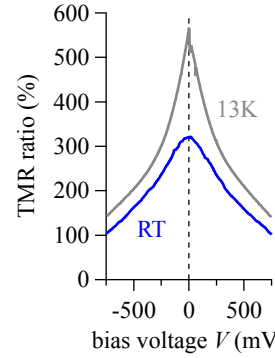

Figure 57: TMR ratio in dependence of bias voltage at room temperature and at 13 K.

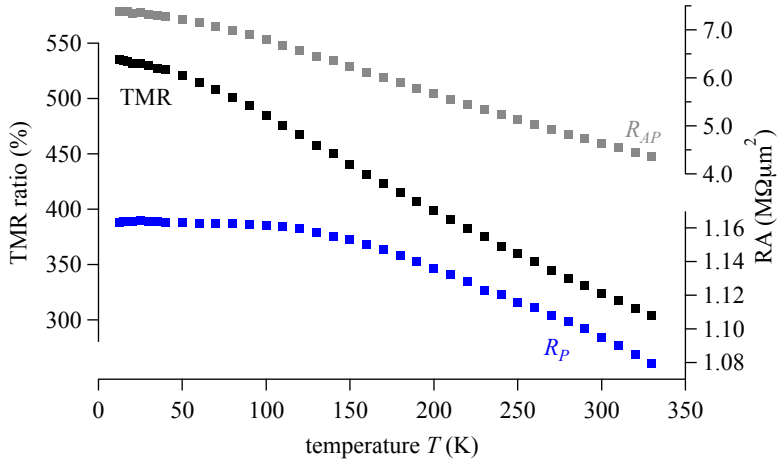

Figure 58: Temperature dependence of the **TMR ratio** and the resistance in the parallel and the antiparallel state of the PSV sample measured at 10 mV.

nique. The MTJ showed a TMR ratio of 330 % at room temperature. In Figure 59 the crystalline barrier, grains of crystalline Co-Fe (crystallized Co-Fe-B) and very smooth interfaces are seen. The tantalum shows no structure. The boron is diffused into tantalum layers which makes them amorphous.[165]

[165] S. Ikeda et al., Appl. Phys. Lett. **93**, 082508 (2008)

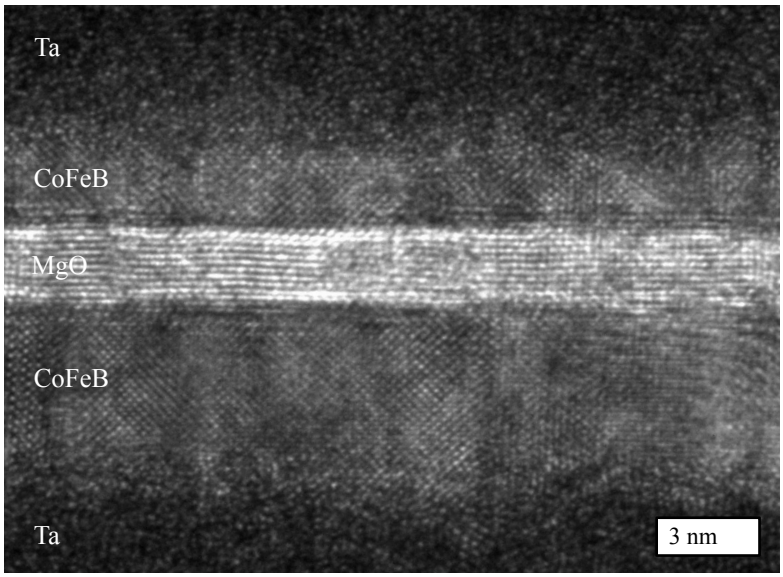

Figure 59: High resolution TEM picture of the PSV sample. Barrier and electrodes are clearly visible.

Appendix: Publications and manuscripts

Main author publications

1. V. Drewello, J. Schmalhorst, A. Thomas, G. Reiss, 'Evidence for strong magnon contribution to the TMR temperature dependence in MgO based tunnel junctions', Phys. Rev. B **77**, 014440 (2008)

2. V. Drewello, M. Schäfers, O. Schebaum, A. A. Khan, J. Münchenberger, J. Schmalhorst, A. Thomas, G. Reiss, 'Inelastic electron tunneling spectra of MgO based magnetic tunnel junctions with different electrode designs', Phys. Rev. B **79**, 174417 (2009)

3. D. Ebke, V. Drewello, M. Schäfers, G. Reiss, A. Thomas, 'Tunneling spectroscopy and magnon excitation in Co_2FeAl/ MgO/ Co-Fe magnetic tunnel junctions', Appl. Phys. Lett. **95**, 232510 (2009)

Unpublished manuscripts

4. V. Drewello, Z. Kugler, G. Reiss, A. Thomas, 'Tunneling spectroscopy probing magnetic and nonmagnetic electrodes in tunnel junctions', arXiv:1008.0326 (2010)

Coauthor publications

5. J. Kanak, T. Stobiecki, V. Drewello, J. Schmalhorst, G. Reiss, 'The influence of the texture on properties of IrMn spin valve magnetic tunnel junctions with MgO barrier and CoFeB electrodes', Phys. Stat. Sol. A **204**, 3942 (2007)

6. A. Thomas, V. Drewello, M. Schäfers, A. Weddemann, G. Reiss, G. Eilers, M. Münzenberg, K. Thiel, M. Seibt, 'Direct imaging of the structural change generated by dielectric breakdown in MgO based magnetic tunnel junctions', Appl. Phys. Lett. **93**, 152508 (2008)

7. M. Seibt, G. Eilers, M. Walter, K. Ubben, K. Thiel, V. Drewello, A. Thomas, G. Reiss, M. Münzenberg, 'Transmission Electron Microscopy Analysis of Tunnel Magneto Resistance Elements with Amorphous CoFeB Electrodes and MgO Barrier', EMC 2008 Ed.: S. Richter, A. Schwedt, 107 (2008) Springer

8. A. A. Khan, J. Schmalhorst, A. Thomas, V. Drewello, G. Reiss, 'Dielectric breakdown and inelastic electron tunneling spectroscopy of top and bottom pinned Co-Fe-B/MgO/Co-Fe-B magnetic tunnel junctions', J. Appl. Phys. **105**, 083723 (2009)

9. M. Schäfers, V. Drewello, G. Reiss, A. Thomas, K. Thiel, G. Eilers, M. Münzenberg, H. Schuhmann, M. Seibt, 'Electric breakdown in ultrathin MgO tunnel barrier junctions for spin-transfer torque switching', Appl. Phys. Lett. **95**, 232119 (2009)

10. D. Ebke, P. Thomas, O. Schebaum, M. Schäfers, D. Nissen, V. Drewello, A. Hütten, A. Thomas, 'Low B2 crystallization temperature and high tunnel magnetoresistance in Co_2FeAl/MgO/Co-Fe magnetic tunnel junctions', J. Magn. Magn. Mater. **322**, 996 (2010)

Unpublished manuscripts

11. Z. Kugler, V. Drewello, M. Schäfers, G. Reiss, A. Thomas, 'Temperature and bias voltage dependence of Co/Pd multilayer-based magnetic tunnel junctions with perpendicular magnetic anisotropy', arXiv:1008.0341 (2010)

12. O. Schebaum, V. Drewello, A. Auge, G. Reiss, A. Thomas, 'Tunnel magnetoresistance in alumina, magnesia and composite tunnel barrier magnetic tunnel junctions', arXiv:1008.0761 (2010)

Presentations

- 'Investigation of magnetic tunnel junctions with MgO barriers' (talk), DPG Spring Meeting 2006, Dresden
- 'Temperature dependence of resistance and TMR in MgO based tunnel junctions' (talk), DPG Spring Meeting 2007, Regensburg
- 'Inelastic electron tunneling spectra of MgO based magnetic tunnel junctions with various soft electrode materials' (talk), DPG Spring Meeting 2008, Berlin
- 'Inelastic electron tunneling spectroscopy of magnetic tunnel junctions with different electrode designs and barrier materials' (poster), DPG Spring Meeting 2009, Dresden
- 'Tunneling spectroscopy and magnon excitation in Co_2FeAl/ MgO/ Co-Fe magnetic tunnel junctions' (talk), DPG Spring Meeting 2010, Regensburg

PHYSICAL REVIEW B **77**, 014440 (2008)

Evidence for strong magnon contribution to the TMR temperature dependence in MgO based tunnel junctions

V. Drewello,* J. Schmalhorst, A. Thomas, and G. Reiss
Bielefeld University, Thin Films and Physics of Nanostructures, 33615 Bielefeld, Germany
(Received 2 March 2007; revised manuscript received 26 November 2007; published 31 January 2008)

We have prepared MgO based magnetic tunnel junctions which show up to 143% tunneling magnetoresistance (TMR) ratio at room temperature and 205% at 12 K. This TMR temperature dependence is mainly caused by a strong temperature dependence in the antiparallel magnetic state, while in the parallel state the change of conductance is small. We found that a modified version of the magnon excitation model may be applied to these MgO magnetic tunnel junctions. If the thermal smearing of the tunneling electron's energy is included it is possible to fit the temperature dependence. We will show the results for our data and we have also tested our model successfully on data from other publications.

DOI: 10.1103/PhysRevB.77.014440 PACS number(s): 75.47.−m

I. INTRODUCTION

Since the discovery of the tunneling magnetoresistance (TMR) effect[1] its amplitude has strongly increased. While early experiments showed significant TMR only at low temperature,[2] the effect was later also shown at room temperature,[3,4] leading to ratios as high as 472% (Ref. 5) to date. Yet, the TMR still increases significantly if the junctions are cooled to low temperatures.[6]

While the changing TMR ratio in magnetic tunnel junctions (MTJs) with alumina barriers goes along with comparable conductance changes in both magnetic states,[7,8] this is not the case in newer junctions with MgO barriers and high TMR ratios.[5,9,10] Even in systems with very different electrodes[11] the decrease of TMR with rising temperature is mostly carried by a change in the antiparallel conductance. The parallel conductance changes so little that it seems roughly constant, if compared to the antiparallel conductance.

Different models are at hand for the mechanism of this temperature dependence. One is the model by Shang and Moodera[8,12] which is based on Jullière's model with a directly temperature dependent spin polarization of the ferromagnetic electrodes.

The other model by Zhang *et al.*[7] is based on two-dimensional spin waves excited by tunneling electrons at the insulator ferromagnet interface. In this model a lower energy cutoff E_c was introduced to get a finite number of excited magnons at a nonzero temperature. The physical representation of this cutoff can be, e.g., a maximum coherence length in the magnetic structure or an anisotropy for the spins present at the interfaces.

For incoherent tunneling this model gives a TMR-voltage-dependence at zero temperature $T=0$ and low bias V of

$$TMR(0,V) = TMR(0,0) - Q\frac{SeV}{E_m}\frac{R_{AP}(0,0)}{R_P(0,0)}\left(\frac{1}{\xi} - \xi\right), \quad (1)$$

where $TMR(0,0)$, $R_P(0,0)$, and $R_{AP}(0,0)$ are the TMR ratio and the resistance in the parallel and antiparallel state, with $TMR=(R_{AP}-R_P)/R_P$. The parameter Q describes the probability of a magnon to be involved in the tunneling process and will be used as a fitting parameter. S is the spin parameter, while E_m is related to the Curie temperature $E_m = 3k_BT_C/(S+1)$ of the ferromagnetic electrodes. It should be noted that in both Eq. (1) and the following temperature dependence Q is scaled by S/E_m. Therefore their actual values do not change the temperature dependence but only the numerical value of Q. The parameter ξ is the ratio of the products of density of states in parallel and antiparallel configuration: $\xi = 2\rho_M\rho_m/(\rho_M^2+\rho_m^2)$. In our case this is the same as the ratio of current or resistance in both states $\xi = j_{AP}(0,0)/j_P(0,0) = R_P(0,0)/R_AP(0,0)$.

Then the temperature dependence of the resistance in parallel $R_P(T,V=0)$ and antiparallel $R_{AP}(T,V=0)$ state at zero bias V can be expressed as

$$R_P(T,0) = R_P(0,0)\left[1 + Q\xi\frac{2S}{E_m}k_BT\ln\left(\frac{k_BT}{E_c}\right)\right]^{-1}, \quad (2)$$

$$R_{AP}(T,0) = R_{AP}(0,0)\left[1 + Q\frac{1}{\xi}\frac{2S}{E_m}k_BT\ln\left(\frac{k_BT}{E_c}\right)\right]^{-1}. \quad (3)$$

Here, E_c is the magnon energy cutoff energy. Further details can be found elsewhere.[7,13]

Until now another fundamental intrinsic mechanism has been disregarded as very small: In a free electron, incoherent tunneling model the thermal smearing of the electron energies decreases the effective barrier height with increasing temperature.[14] This effect could be ignored when the changes in conductivity were substantially higher due to other (extrinsic) effects; but this is not the case for newer systems with higher TMR, especially in the parallel magnetic state where the overall change in conductance is very small. Also for coherent tunneling a change of the conductance is expected because additional conductance channels above and below the Fermi energy E_F can be opened.

No theoretical description of coherent tunneling including thermal smearing has been done so far. In this paper we will show that the extension of the magnon-assisted tunneling model by thermal smearing can also be successfully applied as a phenomenological model to MgO based MTJs.

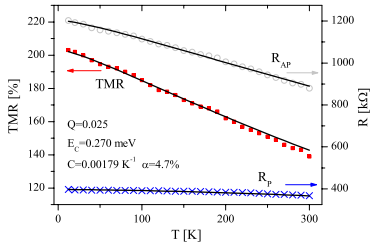

FIG. 1. (Color online) Resulting fit for the TMR temperature dependence of our MgO MTJ using the magnon excitation model and thermal smearing.

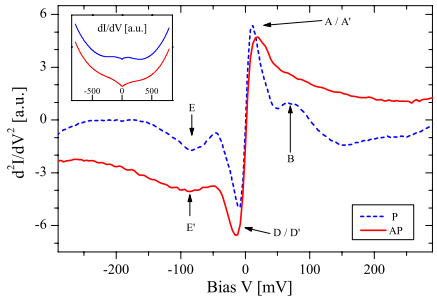

FIG. 2. (Color online) IET spectra of a MgO MTJ in a parallel (dashed line) and antiparallel (solid line) state at 12 K. Typical magnon (A, D) and phonon (B, E) peaks can be identified in parallel and antiparallel (e.g., A′) configuration.

II. PREPARATION

The magnetic tunnel junctions are prepared in a magnetron sputter system with a base pressure of 1×10^{-7} mbar. The layer stack is Ta 10/Cu 30/Ta 10/Cu 5/$Mn_{83}Ir_{17}$ 10/$Co_{40}Fe_{40}B_{20}$ 2.5/MgO 1.5/$Co_{40}Fe_{40}B_{20}$ 4/Ta 10/Cu 30/Ru 10 (all values in nm) on top of a thermally oxidized (50 nm) silicon (100) wafer. To activate the exchange biasing and for the crystallization of the MgO barrier, the layer stack is annealed after sputtering at 623 K for 60 min in a magnetic field of 6500 Oe. The stack is patterned by *e*-beam lithography and ion beam etching. The resulting patterns are ellipses with an aspect ratio of 3 and long axes of 6, 1.5, and 0.75 μm. These structures are capped with gold pads.

All measurements are done by a conventional two probe technique in a closed cycle helium cryostat (Oxford Cryodrive 1.5) with a temperature range of 12–330 K. We have also performed inelastic electron tunneling spectroscopy (IETS) measurements at 12 K utilizing a lock-in technique with a bias modulation of 2 mV at 500 Hz.

III. RESULTS AND DISCUSSION

The measurement of a typical junction's resistance is shown in Fig. 1. The element shows a TMR of 143% at RT, increasing to 205% if cooled to 12 K. This is a relative increase of 43%, while at the same time the junctions resistance changes 36% and 8% in the antiparallel and parallel state, respectively.

Compared to our CeFeB/Al-O/CeFeB junctions[15] this change in resistance in the parallel case is smaller. This suggests that also smaller effects like thermal smearing become more important here.

The thermally induced change of the resistance is different for alumina and MgO based MTJs, but IETS shows very similar properties. IET spectra of a MgO MTJ in a parallel and antiparallel state are shown in Fig. 2 whereas spectra of our alumina junctions can be found elsewhere.[16]

The zero bias anomaly which is related to magnons[13,16] and the typical phonon peaks—at around ±81 mV for the Mg-O (Ref. 17) and ±120 mV for the Al-O phonon—can easily be identified. This gives strong evidence that magnons are also involved in the tunneling process for MgO. Moreover, the spectra look similar, both lacking substantial features hinting to a macroscopic effect of coherent tunneling.

A. First model: No convergence for high TMR

The basic assumption of the model by Shang[8] is a temperature dependence of the ferromagnets spin polarization which is proportional to the magnetization. Using Julliere's formula leads to a resistance in antiparallel state which strongly decreases with rising temperature. In the parallel case the resistance is rising with temperature. As the opposite behavior—a small decrease of the resistance in parallel state with rising temperature—is found in many magnetic tunnel junctions[5,8,9,18–20] an additional term has to be introduced. This term must be spin-independent and have a temperature dependence which shows a strong decrease in resistance in order to compensate the basic $dR_P/dT>0$ behavior. Shang *et al.* proposed that this could be hopping through localized states[8] because it can fit the observed power law with an exponent of about 4/3.

However, this model cannot hold for junctions with higher TMR. If one investigates junctions with higher TMR the model describes a stronger temperature dependence of the resistance in both magnetic states. Therefore the spin-independent term in this model must also increase in order to compensate the stronger basic $dR/dT>0$ tendency. One would assume that a higher TMR is linked to a MTJ of better quality with regard to barrier structure and magnetism. A spin independent term has the tendency of lowering the TMR and is a sign for a barrier of inferior quality. Then it would be very unlikely that a spin independent term can be higher in a MTJ with higher TMR. Yet, it is unlikely but not impossible.

What counts more is that in every single case the two independent contributions to the tunneling current would have to be "fine tuned" to exactly cancel each other out to give a small dependence with $dR_P/dT<0$. For a given set of samples this could be possible by incident, but it would be physically unreasonable to expect this in general for all MTJs. To the best of our knowledge there is not a single

publication which states a tendency of R_P to rise with rising temperature. On the contrary the size of the dependence is nearly the same in all publications. The chance that the spin-independent and spin-dependent term cancel each other out in every sample prepared by different groups and different methods and with different materials is too small to be a reasonable explanation. Therefore we think this model is not able to give a physical explanation of the T-dependence in high TMR junctions.

B. Magnon model expanded by thermal smearing

In the magnon model, a surface magnon can be emitted or absorbed by a tunneling electron, opening additional conductance channels. Because of angular momentum conversation the spin of this electron has to be flipped and it contributes to another spin-channel. Therefore the overall conductance is always a mixed state of both parallel and antiparallel state if magnons are excited. If only incoherent tunneling is considered the electronic band structure of the ferromagnetic electrodes can be simply described as the density of spin-up and spin-down states. Moreover, if only the states at the Fermi energy are taken into account a spin polarization of the electrodes can be defined.

The most notable result is the simultaneous modeling of the low temperature dependence of the conductivity in the parallel state and the large dependence in the antiparallel state for high TMR junctions without introduction of additional contributions to the conductance.

In principle, the proposed magnon assisted tunneling model by Zhang *et al.*[7] is also able to theoretically describe coherent effects. The barrier Hamiltonian H_B is a function of the annihilation operators for electrons and magnons as well as the transition matrix. The latter depends on the wave vectors $\mathbf{k}$ and $\mathbf{k}'$ of the initial and final state. In this situation coherent tunneling can mathematically be described where $\mathbf{k}=\mathbf{k}'$ or $\mathbf{k}=\mathbf{k}'\pm\mathbf{q}$ if magnons are involved; but the Hamiltonian in this form is not applicable to any experimental data. The full band structure and all the energy- and wave-vector-dependent transmission matrix elements would have to be calculated to get an exact description.

In the former case of incoherent tunneling two simplifications were made, namely the introduction of an effective spin polarization and the nonenergy dependent transmission matrix. In our case, two simplifications have also to be made to do quantitative analysis of the presented measurements.

(i) The spin polarization P in alumina based MTJs is often interpreted as the difference of the itinerant spin-up and spin-down electrons at the Fermi energy. This is certainly incorrect for our case. Here, the parameter P specifies the difference between the number of spin-up and spin-down electrons tunneling from one ferromagnet through the barrier into the other ferromagnet and is an effective value averaged over the total tunneling current.

(ii) The probability for electrons of different energy and spin tunneling from their initial to their final state (i.e., the transmission matrix elements) is also taken as an effective, averaged value. We think that these effective values can describe real MTJs that show no sign of sharp features indicating coherent tunneling in, e.g., IETS curves, as shown before.

In addition to the basic model by Zhang *et al.* the intrinsic effect of thermal smearing has to be considered. With the above-mentioned assumptions an increasing temperature and the accordingly wider Fermi edge leads to a smaller effective barrier height not only for alumina but also for MgO based MTJs and, therefore, an additional increase in conductance. For nonmagnetic Al/Al-O/Al tunnel junctions this change is only a few percent depending on the barrier properties.[14] Thus it could be neglected for alumina MTJs with strong temperature dependence caused by other (extrinsic) effects. However, this is not true for MTJs with higher TMR ratios, as the conductance change in the parallel state becomes very small.

We will see shortly that the magnon model alone cannot be used to fit the temperature dependence in both magnetic states correctly. Adding the thermal smearing can improve the fit quality and give a self-contained explanation for the characteristics of the temperature dependence.

We can estimate the influence of the thermal smearing using

$$\frac{G(T)}{G(0)} = \frac{CT}{\sin(CT)}, \tag{4}$$

with $C=1.387\times10^{-4}d/\sqrt{\phi}$ where d is the barrier thickness (in Å) and ϕ the barrier height (in eV).[14]

For our junction we have a thickness of $d=1.5$ nm. Using a barrier height of $\phi=3.5$ eV, which is half of the MgO band gap,[21] results in $C=1.222\times10^{-3}$. To get a better idea of the size of the thermal smearing contribution we define $\alpha=1-\frac{\sin(C\times300\ \mathrm{K})}{C\times300\ \mathrm{K}}$, thus the change in resistance from 0 to 300 K. The value for C then corresponds to $\alpha=1.8\%$. This is in the same order as the overall temperature dependence in the parallel case and should not be neglected.

As a first order approximation we can, therefore, multiply the additional term from Eq. (4) and use C as an additional fitting parameter:

$$R_\gamma(T,0) = R_\gamma(0,0)\frac{\sin(CT)}{CT}\left[1+Q\beta_\gamma \ln\left(\frac{k_BT}{E_c}\right)\right]^{-1}. \tag{5}$$

Here $\gamma=(P,AP)$ denotes parallel and antiparallel state, respectively, with $\beta_P=Sk_BT\xi/E_m$ and $\beta_{AP}=Sk_BT/(\xi E_m)$.

The first step to apply this model is to get the parameter Q from the TMR(V)-curve at 0 K using Eq. (1). We approximate this with our measurements at 12 K. The MTJs parameters are $R_P(0,0)=397\ \mathrm{k\Omega}$, $R_{AP}(0,0)=1203\ \mathrm{k\Omega}$, $TMR(0,0)=205\%$, and $\xi=3.279$. The other parameters used are $S=3/2$, $E_m=121$ meV. The fit results in $Q=0.0242$.

With these values, we can fit the overall temperature dependence with Eq. (5) and get $E_c=0.270$ meV and $C=1.79\times10^{-3}\ \mathrm{K}^{-1}$ or $\alpha=4.7\%$. The fit shows very good agreement with the measured data and is shown in Fig. 1. The size of the thermal smearing is also in good agreement with the theoretical expectation.

A comparison between the pure magnon model and our enhanced model is shown in Fig. 3. Clearly, the simple magnon model underestimates the temperature dependence in the

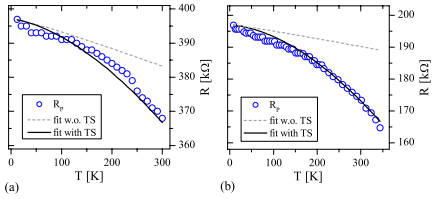

FIG. 3. (Color online) Fit results for the magnon excitation model without and with the thermal smearing extension for (a) our data and (b) the data of Parkin *et al.* (Ref. 9). (While in both cases R_P and R_{AP} are fitted, only the resistance in parallel state is shown—the improvement is largest here.)

parallel state. As the overall change of the resistance with temperature is very small in high TMR junctions, the change due to other small (nonmagnon) effects cannot be neglected here. Not only the improvement to the fit provided by our model but also the good agreement of theoretical expectations and the gained fit value for the thermal smearing suggest that thermal smearing is a reasonable explanation. Furthermore, both magnon-excitation and thermal smearing are intrinsic effects which are present in every magnetic tunnel junction. Together a simple self-consistent explanation for the temperature dependence in high TMR MTJs can be provided.

IV. OTHER DATA

We applied this model to other data available. First, the work by Parkin *et al.*[9] was investigated.[22] As the barrier used has a much higher thickness of 2.9 nm we would expect a stronger temperature dependence of the thermal smearing according to Eq. (4). The calculation gives an α of 7% (ϕ=3.5 eV).

As we have no TMR(V)-data available we assume that the parameter Q is the same as in our junctions. For a general test of our model this seems adequate due to the similar layer stack. The result of the fit is shown in Fig. 4. The cutoff energy of E_C=0.116 meV corresponds to 1.35 K and is in the same range as for our junctions. The thermal smearing has a constant of C=0.002 56 K^{-1} or α=9.5% in very good agreement with the expectation. The parallel conductance change is again almost entirely caused by thermal smearing which is, therefore, even less ignorable.

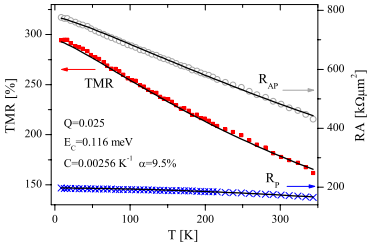

FIG. 4. (Color online) Resulting fit using our model including thermal smearing on the data of Parkin *et al.* (Ref. 9).

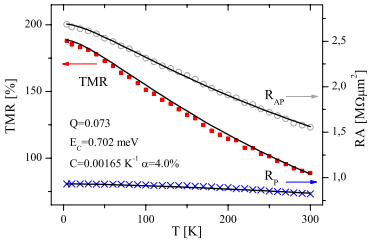

FIG. 5. (Color online) TMR temperature dependence of junctions by Ishikawa *et al.* (Ref. 11) fitted using our enhanced model.

We also tested our model on data by Ishikawa *et al.*[11] They used a tunnel junction with two different electrodes, one is a Heusler alloy and the other one CoFe resulting in a TMR of 90% at room temperature. While it is likely that the parameters Q and E_c are different for these different magnetic materials, the amount of thermal smearing should not depend on the magnetic properties. A barrier thickness of 2.4 nm and a height of 3.5 eV lead to α=4.9%.

Again the data for Q is not available. As the magnon spectrum is expected to be different for a Heusler alloy compared to Co-Fe-B we use Q as another free parameter. The result of the fit can be seen in Fig. 5. Here, the fit reproduces the change from a concave to a convex shape of the TMR curve. The parameters are Q=0.073, E_C=0.702 meV corresponding to 8.1 K and C=0.001 65 K^{-1} or α=4.0%. This is again in good agreement with the expected value. While the thermal smearing is nearly the same size as in our junction, the other parameters differ stronger, which is an expression of the overall stronger temperature dependence. Please note that also for Co_2MnSi/Al-O/CoFe a considerably stronger bias voltage dependence and accordingly higher Q has been found.[15]

V. SUMMARY

We have prepared MgO based magnetic tunnel junctions which show up to 143% TMR at room temperature and 205% TMR at 12 K. This TMR temperature dependence is mainly based on the strong temperature dependence in the antiparallel magnetic state, while the change of conductance is only small in the parallel state. This is the case for all MTJs with high TMR we investigated and can basically be understood by the model of magnon assisted tunneling.

For quantitative agreement with the experiment, however, it is not sufficient. Additionally taking the thermal smearing into account in a phenomenological model, we obtained a very good agreement of model and experimental data. Thus

this effect cannot be neglected for high TMR junctions because of the very small overall change of conductance in the parallel state. Our effective, averaged values seem justified, as there is no evidence for macroscopic coherent effects, e.g., in IET spectra. We have also tested our model on data from other groups for magnetic tunnel junctions with high TMR ratios. The change in the fit parameters can be attributed to the differences in the junctions used but the agreement of the fits with the experimental data remains very good.

We suggest that the tailoring of the magnon spectrum is crucial for getting less temperature dependence and, therefore, a higher TMR ratio at room temperature.

ACKNOWLEDGMENTS

We gratefully acknowledge D. Brinkmann for experimental help and the DFG (Grant No. RE 1052/13-1) for financial support.

*drewello@physik.uni-bielefeld.de

[1] M. Julliere, Phys. Lett. **54A**, 225 (1975).
[2] S. Maekawa and U. Gäfvert, IEEE Trans. Magn. **18**, 707 (1982).
[3] T. Miyazaki, T. Yoai, and S. Ishio, J. Magn. Magn. Mater. **98**, L7 (1991).
[4] J. S. Moodera, L. R. Kinder, T. M. Wong, and R. Meservey, Phys. Rev. Lett. **74**, 3273 (1995).
[5] J. Hayakawa, S. Ikeda, Y. M. Lee, F. Matsukura, and H. Ohno, Appl. Phys. Lett. **89**, 232510 (2006).
[6] Y. M. Lee, J. Hayakawa, S. Ikeda, F. Matsukura, and H. Ohno, Appl. Phys. Lett. **90**, 212507 (2007).
[7] S. Zhang, P. M. Levy, A. C. Marley, and S. S. P. Parkin, Phys. Rev. Lett. **79**, 3744 (1997).
[8] C. H. Shang, J. Nowak, R. Jansen, and J. S. Moodera, Phys. Rev. B **58**, R2917 (1998).
[9] S. S. P. Parkin, C. Kaiser, A. Panchula, P. M. Rice, B. Hughes, M. Samant, and S.-H. Yang, Nat. Mater. **3**, 862 (2004).
[10] S. Yuasa, A. Fukushima, H. Kubota, Y. Suzuki, and K. Ando, Appl. Phys. Lett. **89**, 042505 (2006).
[11] T. Ishikawa, T. Marukame, H. Kijima, K.-I. Matsuda, T. Uemura, M. Arita, and M. Yamamoto, Appl. Phys. Lett. **89**, 192505 (2006).
[12] J. S. Moodera and G. Mathon, J. Magn. Magn. Mater. **200**, 248 (1999).
[13] X.-F. Han, A. C. C. Yu, M. Oogane, J. Murai, T. Daibou, and T. Miyazaki, Phys. Rev. B **63**, 224404 (2001).
[14] R. Stratton, J. Phys. Chem. Solids **23**, 1177 (1962).
[15] J. Schmalhorst *et al.*, Phys. Rev. B **75**, 014403 (2007).
[16] J. Schmalhorst, S. Kämmerer, G. Reiss, and A. Hütten, Appl. Phys. Lett. **86**, 052501 (2005).
[17] P. A. Thiry, M. Liehr, J. J. Pireaux, and R. Caudano, Phys. Rev. B **29**, 4824 (1984).
[18] J. Schmalhorst and G. Reiss, Phys. Rev. B **68**, 224437 (2003).
[19] T. Dimopoulos, G. Gieres, J. Wecker, Y. Luo, and K. Samwer, Europhys. Lett. **68**, 706 (2004).
[20] L. Yuan, S. H. Liou, and D. Wang, Phys. Rev. B **73**, 134403 (2006).
[21] R. Whited, C. J. Flaten, and W. Walker, Solid State Commun. **13**, 1903 (1973).
[22] The data of Fig. 4(a).

PHYSICAL REVIEW B **79**, 174417 (2009)

Inelastic electron tunneling spectra of MgO-based magnetic tunnel junctions with different electrode designs

Volker Drewello,* Markus Schäfers, Oliver Schebaum, Ayaz Arif Khan, Jana Münchenberger, Jan Schmalhorst, Günter Reiss, and Andy Thomas

Thin Films and Physics of Nanostructures, Bielefeld University, 33615 Bielefeld, Germany

(Received 14 August 2008; published 12 May 2009)

MgO-based magnetic tunnel junctions with up to 230% tunnel magnetoresistance ratio at room temperature and up to 345% at 13 K are prepared. The lower electrode is either exchange-biased or free, while the top electrode is free or an exchanged-biased artificial ferrimagnet, respectively. Additionally, a pseudo-spin-valve (hard-soft switching) design with two unpinned electrodes is used. Inelastic electron-tunneling spectra for each of these systems show a strong variation in the zero-bias anomaly with a reduced peak for some of the junctions. At voltages around 200 mV additional structures are found, which are not known from junctions with lower magneto resistance, such as alumina-based junctions. We discuss the spectra for the different electrode types and compare our findings with respect to barrier material and magnetoresistance ratio.

DOI: 10.1103/PhysRevB.79.174417 PACS number(s): 73.40.Gk, 73.43.Qt, 75.47.−m, 75.70.Cn

I. MOTIVATION

Magnetic tunnel junctions (MTJs) with MgO as a crystalline barrier have been predicted to show very large tunnel magnetoresistance (TMR) ratios.[1,2] Recently, TMR ratios larger than 1000% at low temperature have been shown by Lee *et al.*[3] Nevertheless, the TMR ratio still significantly decreases if higher temperatures or voltages are applied; the room-temperature TMR ratio of the above system is about 500%, limiting the applicability of those systems. One reason for the decreasing TMR values is intrinsic excitations within the junctions which can be studied by inelastic electron-tunneling spetroscopy (IETS).

IETS is a well-established method to characterize nonmagnetic-tunnel junctions[4–6] and was applied to MTJs as well.[7–9] This technique has not only a resolution that is limited only by the intrinsic temperature driven energy broadening of the spectra. The bias-voltage range of the spectra is also only limited by the breakdown voltage of the junctions (typically in the range of a few volts).[10] It is much simpler than laterally resolved methods in terms of sample preparation. Furthermore, it is also closer to applications as it provides information about MTJs that could be used as the base for reconfigurable magnetic logic,[11] magnetic sensors, or magnetic random-access memory.[12]

As indicated by the name, IETS can in principle reveal all inelastic processes in which electrons take part in the tunneling process. An overview can be found in Ref. 13. It is especially possible to excite and identify phonons of the barrier[14] and the electrodes[15] as well as magnons in ferromagnetic materials.[16] Another prominent feature in IET spectra is the zero-bias anomaly. In the dI/dV characteristics a sharp dip at zero bias (up to a few mV) is usually found which results in large peaks in the IET spectrum. In nonmagnetic-tunnel junctions this effect was discovered by Wyatt[17] and has been attributed to single-magnetic impurities.[18,19] A qualitative study of scattering at such impurities, however, has proven to be difficult.[20,21] In MTJs the zero-bias anomaly has always been found since IETS was first applied to MTJs by Moodera *et al.*[7] Recently, also structures at bias voltages higher than 200 mV have been discussed.[22,23] They are of interest because they are presumably connected to the coherent tunneling process which is the base of the high TMR ratios of crystalline MgO barriers.

Here, we measured IET spectra of several tunnel junctions, including MgO-based MTJs and alumina-based systems. We will show differences and similarities of these systems, especially with respect to different electrode types in MgO systems and the different barrier materials. Since the growth of the tunnel barrier is crucial in preparing high TMR MTJs we will describe the layer stacks of the different samples. We will compare our findings to results found in literature and discuss the similarities and specific differences.

II. PREPARATION

The magnetic tunnel junctions are prepared in a magnetron sputter system with a base pressure better than 1×10^{-7} mbar. We used different layer stacks—an overview is given in Table I. The stacks are sputtered on top of a thermally oxidized (50 nm SiO_2) silicon (100) wafer. Stack 1 is a typical system with MgO barrier and Co-Fe-B electrodes. Stack 2 incorporates a pinned artificial ferrimagnet (AFi) as the top electrode. Hard-soft-switching is used to get an antiparallel state in stack 3 (usually called pseudo-spin-valve).

Layer stacks 1—3 are annealed after sputtering for 60 min in a magnetic field of 6500 Oe. This activates the exchange bias and initiates the crystallization of the MgO barrier. Layer stack 1 is annealed at 648 K, stack 2 at 623 K, and stack 3 at 673 K. The different annealing temperatures are chosen to get highest TMR ratios at room temperature (RT) and good magnetic separation in the antiparallel state of the two electrodes at low temperatures. Spectra for the different samples are taken and evaluated. The strength of different inelastic contributions may depend on the annealing temperature. The described approach gives the opportunity to compare the limiting factors for each of the layer stacks. Alternatively, the annealing temperature could haven been identical for all samples. Then the different evolution of in-

TABLE I. The different layer stacks and the corresponding annealing temperatures T_a. Numbers represent the layer thickness in nm. The compositions are Co-Fe-B 40/40/20 at. %, Ni-Fe 81/19 (Permalloy), Co-Fe 70/30, and Mn-Ir 83/17, respectively.

Sample	Lower stack	Barrier	Upper stack	T_a [°C]
1	Ta 10/Ru 30/Ta 5/Ru 5/MnIr 10/CoFeB 2.5	MgO 1.8	CoFeB 2.5/Ta 5/Ru 30/	375
1a	Ta 10/Ru 30/Ta 5/Ru 5/MnIr 10/CoFeB 2.5	MgO 1.8	CoFeB 2.5/Ta 5/Ru 30/	175
2	Ta 5/Ru 40/Ta 5/CoFeB 2.5	MgO 2.1	CoFeB 2.5/Ru 0.88/CoFe 6/MnIr 9/Ru 40/	350
3	Ta 5/Ru 30/Ta 10/Ru 5/CoFeB 4	MgO 2.1	CoFeB 1.5/Ta 5/Ru 30/	400
4	1 Cu 30/NiFe 4/MnIr 15/CoFe 3	AlO_x 1.4[a]	NiFe 4/Ta 3/Cu 55/	250[c]
5	Ta 5/Cu 20/Ta 5/Cu 5/Ta 5/MnIr 12/CoFeB 4	AlO_x 1.2[b]	/CoFeB 4/NiFe 3/Ta 5/Cu 20/	275[c]

[a]1.4 nm aluminum+oxidation. See Ref. 24 for details.
[b]1.2 nm aluminum+oxidation.
[c]for 5 min.

elastic contributions could be compared, but one could not be sure if contribution limits the TMR.

Sample 1a is annealed at only 448 K to get a low TMR comparable to alumina-based junctions such as sample 4. The samples are patterned by e-beam lithography and ion-beam etching. The resulting patterns are squares of 25 μm^2. These structures are capped with gold contact pads.

The measurements at 13 K are done in a closed-cycle Helium cryostat (OXFORD Cryodrive 1.5) with a temperature range of 13–330 K by conventional two-probe technique. The bias voltage is always defined with respect to the lower electrode. Thus, negative bias results in electrons tunneling into the upper soft electrode. We use a lock-in technique (STANDFORD SR830 DSP digital two channel Lock-In) with a modulation frequency of 7 kHz and an amplitude of 2 mV (effective, 5.66 mV peak to peak). The resulting measurement is a dI/dV curve which is differentiated numerically to get the d^2I/dV^2 spectra. The thermal smearing of a sharp peak is $5.4k_BT$ [full width at half maximum (FWHM)]. The broadening introduced by the modulation is $1.7\times V_{ac,eff}$ (effective voltage) or $0.6\times V_{ac,p\text{-}p}$ (peak-to-peak value). To see peaks that are limited by the thermal smearing we need $e\times V_{ac,eff} \ll 3.2\times k_BT = 0.28\ \text{meV}\times T\ [\text{K}]$. With our values we have $e\times V_{ac,eff}=2<3\ \text{meV}=5.4k_BT$. For more details see Refs. 6 and 25.

III. RESULTS

A. Bottom pinned Co-Fe-B

Stack 1 is a standard MTJ design with a pinned lower electrode. Our sample exhibits a TMR ratio of over 200% at RT and up to 345% at 13 K. The measured junction has an absolute resistance of 8 kΩ at 13 K. The high resistance of the tunneling barrier ensures that neither line resistances nor inhomogeneous current injection influence the measurement. The absolute resistance of lines and electrodes can be extracted from an MTJ that suffered dielectrical breakdown. It is typically smaller than 50 Ohms. The spectra for parallel- and antiparallel-magnetic states (P state and AP state) are shown in Fig. 1. The zero-bias (ZB) anomaly is clearly visible in both states (peaks are marked ZB in the figure), as well as broader peaks around 85 mV (P) and a smaller peak (in P state) at about 200 mV (C), while at −200 mV a shoulder is visible.

The peaks of the ZB anomaly are located at $(\pm 8\pm 2)$ mV in P state. In the AP state the highest peaks are located at slightly higher bias of (-15 ± 3) mV and $(+19\pm 3)$ mV. This shift to higher energies is commonly observed in other MTJ.[9,22,26] The zero-bias peaks also have shoulders that will be discussed later. The next peaks appear at (-86 ± 5) mV (P) and $(+68\pm 5)$ mV in the P state, thus having a significant asymmetry. In the AP state the peak corresponding to peak P appears at a higher bias voltage of (-100 ± 5) mV. At positive bias no peak is visible. The excitation of MgO phonons at the barrier-electrode interface—which is typical for tunnel junctions[25]—can be identified as the origin of these peaks. The Mg-O-surface phonon has an energy of 80.7 meV (Ref. 27) which corresponds to the peaks we observed. A similar behavior is also found in Refs. 22 and 28

The zero-bias peaks are very symmetric for the P state. In the AP state there is a small asymmetry. More details of these peaks are shown in Fig. 2 for both magnetic states. There, a substructure in the zero-bias peaks is found. In the P state the maxima are at $(\pm 8\pm 1)$ mV (ZB) and shoulders (M) at $(+30\pm 5)$ mV and (-25 ± 5) mV. In the AP state these positions are nearly switched—the maxima are located (M) at

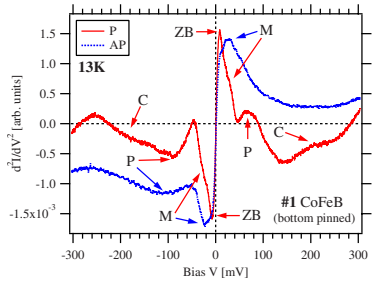

FIG. 1. (Color online) IET spectra of a Co-Fe-B/MgO/Co-Fe-B MTJ (sample 1) in the P state (solid line) and the AP state (dashed line) at 13 K. The ZB and Mg-O phonon peaks (P) are marked. Please note the additional structure (C).

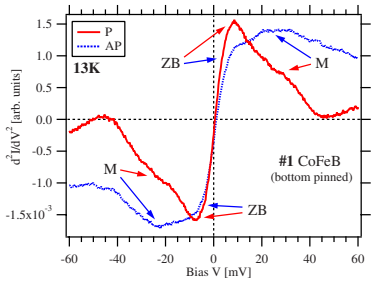

FIG. 2. (Color online) Details of the zero-bias peaks in the P state (solid line) and the AP state (dashed line) at 13 K. Peaks show substructure with maxima (ZB for P state, and *M* for AP state) and shoulders (vice versa).

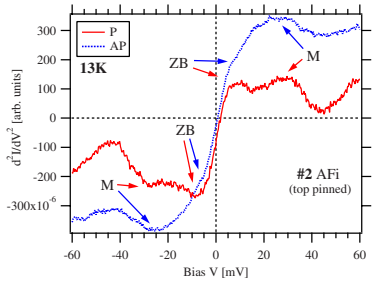

FIG. 4. (Color online) Details of the zero-bias peaks for the AFi sample (stack 2) in the P state (solid line) and the AP state (dashed line) at 13 K. In P state the substructure shows two distinct maxima (ZB and *M*). In AP state there are maxima (*M*) and shoulders (ZB).

$(+27 \pm 5)$ mV and (-24 ± 5) mV while at the other positions (ZB) shoulders appear (more pronounced at negative bias).

B. Top pinned artificial ferrimagnet

In stack 2 a pinned artificial ferrimagnet (AFi) forms the upper electrode, while the lower electrode is the free one. The measured junction shows an absolute resistance of 23 kΩ at 13 K. The spectra in both magnetic states shown in Fig. 3 look significantly different to those of stack 1. First of all the peak heights are much smaller in P state compared to AP state. In both states the peaks of the ZB anomaly (ZB) are much smaller as in the sample 1 [relative to the corresponding phonon peaks (*P*) in the same state].

Details of the zero-bias peaks are shown in Fig. 4. In P state the substructure is visible in form of two peaks with clearly separated maxima. The first peaks (ZB) are at $(\pm 8 \pm 1)$ mV and the other at $(\pm 28 \pm 3)$ mV (*M*). In the AP state the maxima are at $(\pm 26 \pm 5)$ mV (*M*) as it was the case in sample 1. At the other position (ZB) at around ± 8 mV shoulders can be recognized.

C. Co-Fe-B pseudo-spin-valve

Sample 3 is a pseudo-spin-valve, i.e., the AP state is possible due to different switching fields of the upper and lower electrode. The investigated MTJ showed an absolute resistance of 4.2 kΩ. The spectra are shown in Fig. 5. They look like an intermediate piece between samples 1 and 2. In the P state the peaks (ZB) (at -6 ± 1 and $+8 \pm 1$ mV) are smaller than in sample 1 which makes the shoulders (*M*) very pronounced. The phonon peaks (*P*) at $(\pm 71 \pm 2)$ mV and the structures *C* around 200 mV are very similar to those in sample 2. Moreover, everything except the innermost peaks looks nearly identical to sample 2. In comparison to sample 1 (Fig. 1) structure *C* is very different. In the AP state the spectrum looks very much like that of sample 2. Only the relative height of the ZB peaks is a bit larger. Also, the struc-

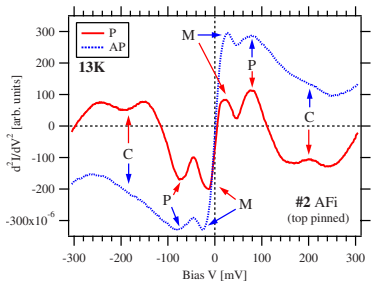

FIG. 3. (Color online) IET spectra of sample 2 (AFi as pinned electrode) in the P state (solid line) and the AP state (dashed line) at 13 K. The same peaks as in sample 1 are found: the ZB, magnon (*M*), and Mg-O phonon peaks (*P*) are marked. An additional feature (*C*) is found for both magnetic states and polarities.

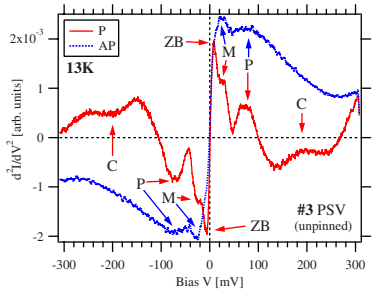

FIG. 5. (Color online) IET spectra of sample 3 (hard-soft switching) in the P state (solid line) and the AP state (dashed line) at 13 K. The same peaks as in samples 1 and 2 are found: ZB, magnon (*M*), and Mg-O phonon peaks (*P*) are marked. The additional peaks are found in P state (*C*).

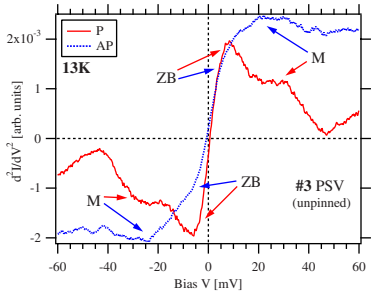

FIG. 6. (Color online) Details of the zero-bias peaks for the pseudo-spin-valve sample (stack 3) in the P state (solid line) and the AP state (dashed line) at 13 K. In P state the substructure shows a distinct maximum (ZB) and very pronounced shoulders (*M*). This behavior fits in between samples 1 and 2. In AP state there are maxima (*M*) and shoulders (ZB).

tures at 200 mV (*C*) are not distinguishable in AP state.

A closer look at the lower bias region (Fig. 6) reveals that only the first peaks in P state (ZB) are strongly different compared to sample 2. The AP spectrum is very similar to the one of sample 2.

IV. DISCUSSION

In Table II the different features of the spectra of all samples are summarized. We will now discuss the different aspects of our measurements.

A. Low bias peaks in the spectra of MgO based samples

When comparing the spectra of the MgO-based samples, in which the electrode design was varied (1–3), we find the largest difference in the distinct peaks at low-bias voltage. In the P state the peaks in sample 1 have very distinct maxima (ZB, Fig. 2) which show small shoulders (*M*). These shoulders can be overlooked if insufficient resolution or zoom is used. In sample 2 (Fig. 4) the initial peaks are much smaller and distinct peaks at the position of the former shoulders can be identified. These spectra are very comparable to those presented by Matsumoto *et al.*[29] Sample 3 (Fig. 6) shows an intermediate state, where the first peaks are not as high as in sample 1 and the shoulders are very clearly seen. For the different samples the peaks (or shoulders) are located at the same positions within small range of error. They only vary in their relative intensity and width. Therefore the intrinsic excitation processes responsible for these structures are supposedly the same for the different samples. The first peak (ZB) is comparable in height for the P and the AP state in each sample, which means the underlying excitation is not depending on the magnetic configuration or external field. This is different for the shoulders or second peaks (*M*). The underlying excitation seems much more prominent in the AP spectra, where these "shoulders" indeed form the maxima in the spectra. Thus, what might look like a shift in the position of the peak could be a change in the relative height of two different peaks. This is most clearly seen in sample 2 (Fig. 3). The maximum seems just "shifting" if going from the P to the AP state but in the higher resolved spectra (Fig. 4) the peaks and shoulders can be separated.

The very first peak is the zero-bias anomaly caused by magnetic impurities. There is no dependence on the magnetic state of the junction. The peaks are most pronounced in sample 1, presumably because of diffusion of Manganese from the antiferromagnet.[30,31] The zero-bias peak in sample 2 is smaller than in sample 1 because of the additional layers of Ruthenium and Co-Fe between the antiferromagnet and the barrier, which partially prevents the diffusion of manganese.[31] In sample 3 no Mn is present, so the ZB peaks are also smaller than in sample 1. They are not as small as in

TABLE II. An overview of our findings for the different samples. The visibility of the listed features is evaluated [++ strong, + distinct, ∘ fair (e.g., shoulder), and − not visible]. The upper half shows the parallel magnetic state, the lower half shows the antiparallel magnetic state. Please note that the order of samples has been changed in order to emphasize similarities and differences, respectively. We find that sample 2 is the most feature rich, especially in the AP state. Samples 3, 1, and 5 show sequentially less distinct features, but at the same time larger (and broader) low-bias peaks. We also find that the MgO-based samples look similar, with the exception of sample 1a. This sample—annealed at lower temperature—is more similar to the alumina-based sample 4.

	Feature			MgO			Alumina		MgO
State	Peak	Bias [mV]	Suggested origin	2	3	1	5	4	1a
P	*C*	190–230	"high TMR feature"	++	++	+	+	−	−
	P	≈81/120	barrier phonons	++	++	++	∘	+	∘
	M	20–35	interface magnons	++	+	∘	∘	−	−
	ZB	≤15	zero bias/impurities	∘	+	++	+	+	+
AP	ZB	≤15	zero bias/impurities	∘	∘	∘	∘	∘	+
	M	20–35	interface magnons	+	+	+	+	+	−
	P	≈81/120	barrier phonons	+	−	∘	∘	+	−
	C	190–230	"high TMR feature"	∘	−	−	−	−	−
	TMR ratio at room temperature [%]			210	220	210	72	50	38

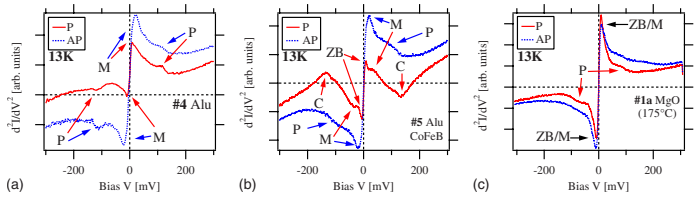

FIG. 7. (Color online) IET spectra of sample 4 (a), 5 (b), and 1a (c) in the P state (solid line) and the AP state (dashed line) at 13 K. Basically, the same peaks are found: the ZB, magnon (M), and phonon peaks (P) are marked, the latter are less pronounced in the spectra of sample 1a. At higher voltage no structure is found for samples 1a and 4, but for sample 5 large dips can be found around 130 mV (C) in parallel state, which also reduce peaks M to smaller shoulders.

sample 2—other impurities may contribute at higher annealing temperatures.

More impurities should lower the TMR ratio of a junction, which is the case for our samples at room temperature. We always observe higher zero-bias peaks with lower TMR ratios which supports our interpretation. The TMR ratios of sample 1 and sample 2 are as high as 210%. However, if sample 2 is annealed at higher temperature of 400 °C a TMR ratio of over 230% is achieved. We can conclude that for sample 2 the TMR ratio is not limited by diffusion but subtotal recrystallization.[32] The pseudo-spin-valve (sample 3) shows up to 220% depending on the magnetic separation in an individual junction, which fits with its intermediate position in the strength of the zero-bias peak.

The second peak (or shoulder) (M in Figs. 2, 4, and 6) strongly depends on the magnetic state: it is roughly twice as high in the AP state compared to the P state. This is a major difference compared to the zero-bias peak. We suggest that this peak corresponds to the maximum probability for magnon excitation at the ferromagnet-insulator interfaces, which is proposed to be higher in the AP state.[29,33] Also, possible magnon excitations have been identified at similar bias voltage by other groups.[29,34]

B. Spectra of MgO and alumina based junctions—Can we see coherence?

We also investigated alumina-based MTJs in order to compare the results to our MgO-based systems. Alumina-based junctions have an amorphous barrier and only incoherent tunneling takes place. Sample 4 has Co-Fe and Ni-Fe electrodes and a TMR ratio of 50% and 70% at room temperature and 13 K, respectively. The spectra are shown in Fig. 7(a). Sample 5 has two Co-Fe-B electrodes and shows a TMR ratio of 72% and 110% at room temperature and 13 K, respectively. The corresponding spectra can be found in Fig. 7(b).

The first thing to be noticed in the spectra is the small zero-bias anomaly in these two samples. The zero-bias anomaly is previously explained by the diffusion of magnetic impurities. Therefore, the small peaks can be explained by the low annealing temperature and the short annealing time of only a few minutes. The large maximum in the AP state is mainly caused by the second peak, identified as excitation of interface magnons before. The spectra also show peaks around 120 mV. These were identified as Al-O phonon peaks before.[25] For sample 4 there is no further structure at higher bias voltage.

We prepared an MgO-based sample [1a] identical to sample 1 but was annealed at only 175 °C for 1 h. At this temperature the recrystallization of Co-Fe-B is not established[35] and therefore no coherence is possible. This preparation process makes it comparable to alumina-based sample 4. It shows TMR ratios of 38% and 61% at room temperature and 13 K. The spectra presented in Fig. 7(c) show magnon and phonon peaks but no further structure. The first peaks are higher for the MgO sample, but they are not sharp enough to distinguish between what we called zero bias and magnon excitation before. Nevertheless, the spectra are very similar to those of sample 4 (also compare, e.g., Ref. 9). Especially, there is no structure beyond the phonon peak at 81 or 120 mV, respectively.

This is different for the spectra of the MgO-based samples 1 to 3. For these samples additional structures around 200 mV are clearly seen in P state (Figs. 1, 3, and 5). In this bias region, peaks are embedded in wide dips (IETS signal <0) for all samples. In the work of Ono *et al.*[28] similar structures in their IET spectra are visible at 250 mV and are also embedded in a strong dip. It should be noted that only the wide dip is found in most other publications[23,28,29] at bias voltages of 250–400 mV. The small peak within is not always visible, while in this work it is always found in the P state and for sample 2 also in the AP state.

This structure is discussed as evidence for coherent tunneling through MgO.[22,23,28] However, we cannot conclude that the dip structure found in the MgO-based MTJs with high TMR ratio is caused by coherent tunneling. The spectra of the alumina-based sample 5 also show deep dips in the P state [Fig. 7(c)]. The d^2I/dV^2 signal becomes negative as it is the case for the MgO-based junctions. However, these dips are located at lower voltages of around 130 mV. This also leads to a reduction in the phonon peaks in the P state.

If all measurements are compared an interesting tendency can be found—the dip gets more pronounced with a higher TMR ratio of the junction. However, no samples were available with TMR ratios between the 72% of sample 5 and 200%. We suggest that a highly spin-polarized electrode material without a crystalline barrier should be investigated to get higher TMR ratios while maintaining incoherent tunnel-

ing. A possible candidate would be a Heusler compound electrode and an alumina barrier. It would be possible to judge whether the dip structure is related to the barrier material, a high TMR ratio, or even coherent tunneling, if, e.g., junctions with TMR ratios around 150% and alumina as well as MgO barriers could be prepared.

V. SUMMARY

In summary, we prepared MgO-based magnetic tunnel junctions which show up to 230% TMR at room temperature and 345% TMR at 13 K. We measured IET spectra of those systems in parallel and antiparallel magnetic state. Several ferromagnetic electrode designs were used in order to clarify the origin of the peaks. The zero-bias anomaly could be identified, which is caused by magnetic impurities. A second peak was found, which strongly differs for parallel and antiparallel magnetic state. This is attributed to the excitation of magnons.

A pronounced additional structure at 200 mV is found in parallel state which is stronger the higher the TMR. This cannot be attributed to coherent tunneling (or the MgO barrier) as it is also found in alumina-based junctions.

ACKNOWLEDGMENTS

We gratefully acknowledge Catherine A. Jenkins for helpful discussions and the DFG (Grant No. RE 1052/13-1) for financial support.

*drewello@physik.uni-bielefeld.de

[1] W. H. Butler, X.-G. Zhang, T. C. Schulthess, and J. M. MacLaren, Phys. Rev. B **63**, 054416 (2001).
[2] J. Mathon and A. Umerski, Phys. Rev. B **63**, 220403(R) (2001).
[3] Y. M. Lee, J. Hayakawa, S. Ikeda, F. Matsukura, and H. Ohno, Appl. Phys. Lett. **90**, 212507 (2007).
[4] R. C. Jaklevic and J. Lambe, Phys. Rev. Lett. **17**, 1139 (1966).
[5] A. Geiger, B. Chandras, and J. Adler, Phys. Rev. **188**, 1130 (1969).
[6] J. Klein, A. Léger, M. Belin, D. Défourneau, and M. J. L. Sangster,Phys. Rev. B **7**, 2336 (1973).
[7] J. S. Moodera, J. Nowak, and R. J. M. van de Veerdonk, Phys. Rev. Lett. **80**, 2941 (1998).
[8] R. J. M. van de Veerdonk, J. S. Moodera, and W. J. M. de Jonge, J. Magn. Magn. Mater. **198-199**, 152 (1999).
[9] X.-F. Han, A. C. C. Yu, M. Oogane, J. Murai, T. Daibou, and T. Miyazaki, Phys. Rev. B **63**, 224404 (2001).
[10] A. A. Khan, J. Schmalhorst, A. Thomas, O. Schebaum, and G. Reiss, J. Appl. Phys. **103**, 123705 (2008).
[11] A. Thomas, D. Meyners, D. Ebke, N.-N. Liu, M. D. Sacher, J. Schmalhorst, G. Reiss, H. Ebert, and A. Hütten, Appl. Phys. Lett. **89**, 012502 (2006).
[12] S. A. Wolf, D. D. Awschalom, R. A. Buhrman, J. M. Daughton, S. von Molnar, M. L. Roukes, A. Y. Chtchelkanova, and D. M. Treger, Science **294**, 1488 (2001).
[13] C. J. Adkins and W. A. Phillips, J. Phys. C **18**, 1313 (1985).
[14] J. G. Adler, Solid State Commun. **7**, 1635 (1969).
[15] T. T. Chen and J. G. Adler, Solid State Commun. **8**, 1965 (1970).
[16] D. C. Tsui, R. E. Dietz, and L. R. Walker, Phys. Rev. Lett. **27**, 1729 (1971).
[17] A. F. G. Wyatt, Phys. Rev. Lett. **13**, 401 (1964).
[18] J. A. Appelbaum, Phys. Rev. **154**, 633 (1967).
[19] J. A. Appelbaum and L. Y. L. Shen, Phys. Rev. B **5**, 544 (1972).
[20] R. H. Wallis and A. F. G. Wyatt, J. Phys. C **7**, 1293 (1974).
[21] S. Bermon, D. E. Paraskevopoulos, and P. M. Tedrow, Phys. Rev. B **17**, 2110 (1978).
[22] G.-X. Miao, K. B. Chetry, A. Gupta, W. H. Butler, K. Tsunekawa, D. Djayaprawira, and G. Xiao, J. Appl. Phys. **99**, 08T305 (2006).
[23] M. Mizuguchi, *et al.*, J. Appl. Phys. **99**, 08T309 (2006).
[24] J. Schmalhorst and G. Reiss, Phys. Rev. B **68**, 224437 (2003).
[25] E. Wolf, in *Principles of Electron Tunneling Spectroskopy*, International Series of Monographs on Physics No. 71 edited by R. Elliot, J. Krumhansl, W. Marshall, and D. Wilkinson (Oxford University Press, New York, 1989).
[26] J. Murai, Y. Ando, M. Kamijo, H. Kubota, and T. Miyazaki, Jpn. J. Appl. Phys., Part 2 **38**, L1106 (1999).
[27] P. A. Thiry, M. Liehr, J. J. Pireaux, and R. Caudano, Phys. Rev. B **29**, 4824 (1984).
[28] K. Ono, T. Daibou, S.-J. Ahn, Y. Sakuraba, T. Miyakoshi, T. Morita, Y. Kikuchi, M. Oogane, Y. Ando, and T. Miyazaki, J. Appl. Phys. **99**, 08A905 (2006).
[29] R. Matsumoto, *et al.*, Solid State Commun. **136**, 611 (2005).
[30] P. V. Paluskar, C. H. Kant, J. T. Kohlhepp, A. T. Filip, H. J. M. Swagten, B. Koopmans, and W. J. M. de Jonge, J. Appl. Phys. **97**, 10C925 (2005).
[31] J. Hayakawa, S. Ikeda, Y. M. Lee, F. Matsukura, and H. Ohno, Appl. Phys. Lett. **89**, 232510 (2006).
[32] At low temperatures the sample with over 230% at RT-TMR ratio showed no sufficient magnetic separation for TMR measurements or IETS of a defined magnetic state.
[33] V. Drewello, J. Schmalhorst, A. Thomas, and G. Reiss, Phys. Rev. B **77**, 014440 (2008).
[34] P. V. Paluskar, F. L. Bloom, J. T. Kohlhepp, H. J. M. Swagten, B. Koopmans, and E. Snoeck, Appl. Phys. Lett. **91**, 222501 (2007).
[35] M. Jimbo, K. Komiyama, Y. Shirota, Y. Fujiwara, S. Tsunashima, and M. Matsuura, J. Magn. Magn. Mater. **165**, 308 (1997).

APPLIED PHYSICS LETTERS **95**, 232510 (2009)

Tunneling spectroscopy and magnon excitation in $Co_2FeAl/MgO/Co–Fe$ magnetic tunnel junctions

Daniel Ebke, Volker Drewello,[a] Markus Schäfers, Günter Reiss, and Andy Thomas
Thin Films and Physics of Nanostructures, Bielefeld University, 33615 Bielefeld, Germany

(Received 3 November 2009; accepted 16 November 2009; published online 10 December 2009)

Magnetic tunnel junctions with the Heusler compound Co_2FeAl as the soft electrode are prepared. Pinned Co–Fe is used as the hard reference electrode. The junctions show a high tunnel magnetoresistance ratio of 273% at 13 K. The electronic transport characteristics are investigated by tunneling spectroscopy—dI/dV and d^2I/dV^2 are discussed. In the parallel magnetic state the tunneling spectra are asymmetric with respect to the bias voltage, with a pronounced bias-independent region. In the antiparallel state the dependence on bias voltage is much stronger and the curves are symmetric. The findings can be explained with a gap in the minority density of states of Co_2FeAl. © *2009 American Institute of Physics*. [doi:10.1063/1.3272947]

In the recent years spintronic devices have been highly anticipated. It is essential to improve such systems' performance to make them become a commercial reality. In spintronic devices like magnetic sensors, reconfigurable logic, and magnetic random access memory cells[1] it is of crucial interest to increase the tunneling magnetoresistance (TMR) effect of the underlying magnetic tunnel junctions (MTJs). One way to gain this higher effect is by using electrodes with high spinpolarization. Prominent candidates in this category are the Heusler compounds. Recently high TMR ratios were reported with Heusler based MTJs; 217% for Co_2MnSi (Ref. 2) and 220% for $Co_2Fe_{0.5}Al_{0.5}Si$.[3] The high TMR ratios for Heusler based MTJs were explained by the predicted half-metallic behavior of the used Heusler compounds. This explanation was supported by tunneling spectroscopy measurements, which showed a pronounced gap structure.[4–7] The highest reported TMR ratio for Co_2FeAl is 54%[3,9] so far. In this letter we present tunneling spectroscopy measurements (dI/dV and d^2I/dV^2 are discussed) of Co_2FeAl based tunnel junctions with MgO barrier. These junctions show up to 153% and 273% TMR ratio at room and low temperature, respectively.

The MTJs are prepared in a magnetron sputter system with a base pressure of 1×10^{-7} mbar and a Argon working pressure of approximately 1.5×10^{-3} mbar. The layer stack used in this work is MgO (001) substrate/MgO 5/Co_2FeAl (CFA) 20/MgO 2.1/Co–Fe 5/MnIr 10/Ru 40 (all values in nm). The samples are annealed in a vacuum furnace for 60 min at a optimized temperature of 723 K. Details of the preparation and optimization of the samples will be published elsewhere.[8] The samples are patterned by laser lithography and ion beam etching. The resulting patterns are squares of 100 μm^2. These structures are capped with gold contact pads.

The low temperature measurements are done at 13 K in a closed cycle Helium cryostat by a standard two probe technique. The bias voltage is always defined with respect to the upper electrode. Thus, negative bias results in electrons tunneling into the upper electrode. A lock-in technique is used to derive the dI/dV curves which are differentiated numerically to get the inelastic electron tunneling (IET) spectra (d^2I/dV^2). Details of the measurement setup and procedure can be found elsewhere.[10]

Figure 1 shows a major loop of the CFA MTJ at 13 K. The sample exhibits a TMR ratio of 273% with well defined parallel (P) and antiparallel (AP) states. Figure 2(a) shows spectroscopic data obtained in the P state at −500 Oe. The dI/dV data was normalized to $dI/dV(V=0)$ to allow a better comparison. A striking asymmetry in the dI/dV-data is found with respect to the bias polarity. For negative bias the conductance shows a very weak dependence on the bias voltage up to −140 mV. For positive bias up to $V=25$ mV the conductance sharply increases. For $V>25$ mV the slope reduces visibly. At 270 mV the dI/dV-signal has a local maximum, followed by a decrease and a pronounced minimum at 350 mV. These features can more clearly be seen in the IET spectrum. For $-140\ \text{mV}<V<0$ mV the spectrum shows only small peaks around zero height, while for $0<V<270$ mV the peaks are larger and always positive. The local minimum in the IET spectrum is located at 290 mV with an additional small feature at 350 mV. Figure 2(b) shows the spectroscopic data for the AP state at 250 Oe. The asymmetry is much smaller here. A sharp increase of dI/dV is found for both bias polarities. However, for negative bias a distinct kink is found at −70 mV, whereas for positive bias the transition to the flatter part is much smoother. Again, the IET spectrum can show these features more clearly. For

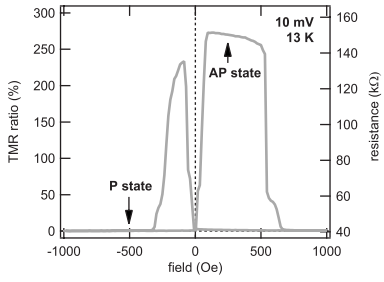

FIG. 1. Major loop of a CFA MTJ. Arrows mark the field and resistance values at which spectroscopy is performed.

[a]Electronic mail: drewello@physik.uni-bielefeld.de.

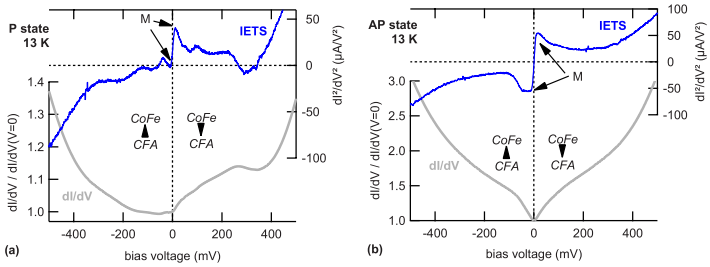

FIG. 2. (Color online) Tunneling and IET spectra of a CFA MTJ in (a) P state and (b) AP state.

-10 mV$<V<0$ mV there is a sharp increase to a broad plateau region up to -50 mV. For $V<-50$ mV the signal rapidly decreases. For positive bias the signal also increases rapidly up to $V=10$ mV. Unlike negative bias there is no plateau and for $V>10$ mV the signal slowly decreases with a small shoulder around 90 mV. For $V<-100$ mV the IETS signal increases monotonically and smoothly. For positive bias $V>200$ mV this is also the case, except for a small feature located at 350 mV as in the P state.

The measurements at small bias in both magnetic states will now be discussed. The flat region for -140 mV$<V<0$ of the dI/dV-curve in the P state can be understood with the assumption that a gap is present in the minority density of states (DOS) of CFA while the majority DOS is not varying much in this region. Majority electrons can tunnel from the CFA into Co–Fe. The constant DOS leads to a constant conductance. Minority electrons are not available to tunnel into Co–Fe. The gap structure ends at approximately -140 mV where dI/dV strongly increases. Here the lower end E_V of the minority gap is reached and electrons can tunnel from the minority "valence band" of CFA in the minority states of Co–Fe. This additional minority tunneling channel increases the conductance for $V<-140$ mV. Similar results have been shown for $Co_2MnSi/Al-O/Co-Fe$,[4,5] for $Co_2Fe_xMn_{1-x}Si/Al-O/Co-Fe$,[6] and for $Co_2FeAl_{0.5}Si_{0.5}/(MgAl_2)-O/Co-Fe$.[7] The immediate rise of dI/dV for $V\geq 0$ can be interpreted as the upper end of the gap just above the Fermi energy E_F. This would mean that the separation of the Fermi energy and the conductance band (in the minority channel) is $E_C\approx 0$.

But there is a different way to look at it. The IET spectrum for the P state [Fig. 2(a)] is not completely flat but shows some features for $V<0$. Especially the first peak (M) is interesting as it shows the excitation of magnons by tunneling electrons with excess energies. Compared to the peak for $V>0$ this peak is very small. In the AP state [Fig. 2(b)] the peaks (M) are of the same size for both bias polarities. Magnon excitation is known to be one of the main reasons for the temperature dependence and low bias behavior of the TMR ratio.[11,12] In Table I an overview of the first-order magnon excitation processes is given. There are four cases regarding to magnetic state and bias voltage polarity. With the assumption of a gap in the CFA minority states none of the processes involving CFA minority electrons are available (marked red/italic). Also, absorption of magnons has a far lower probability at low temperatures than the excitation.

These simple assumptions lead to one case where no magnon excitation is possible: for negative bias voltage in the P state.

Basically, this is what the IET spectra show. The 'forbidden' peak is finite but very small. This can be explained with the assumption of very few minority states in CFA instead of none. Then only very few minority electrons are available to tunnel into the Co–Fe and excite magnons. For positive bias the tunneling essentially is the same as in the case of a distinctive gap. Many minority electrons are available and a tunneling minority electron can excite a magnon, is spin-flip scattered to a majority state of which plenty are available. A small but finite minority DOS could be the result of imperfect ordering. On the other hand, a finite DOS has been predicted below E_F for CFA by some calculations.[13,14] There, most of the residual minority states originate from Fe d-orbitals. As the tunneling electrons are s-like those states are not accessible through the tunneling process. There is also the possibility of interface states that have been predicted[15] and found[16] for other Heusler compounds.

Please note, the presented model gives a reason for the strong increase in conductance, at least for $0<V<25$ mV (in the P state). It can simply be caused by magnons excited only in Co–Fe. Thus, there is no need for a band gap edge near E_F and $E_C\approx 0$ cannot be concluded (nor excluded) in this case.

In Fig. 3 both IET spectra are shown for comparison. The difference for negative bias is obvious, but for positive bias the spectra are comparable. In the AP state the magnon peak is stronger because the magnon excitation only needs majority electrons/states (see Table I). Also the direct tunneling processes are less probable and the relative change

TABLE I. Overview of first order magnon excitation/absorption in the tunneling process. Here, E(e) is an electron in a CFA majority (minority) state, F(f) is an electron in a Co–Fe majority (minority) states and +m(−m) is the emission (absorption) of a magnon. A small DOS or a less probable absorption is marked italic.

	Negative bias	Positive bias
	CFA→Co–Fe	Co–Fe→CFA
P	E→f, *−m*	F→*e*, *−m*
	e→F, +m	f→E, +m
AP	E→F, +m	F→E, +m
	e→f, *−m*	f→*e*, *−m*

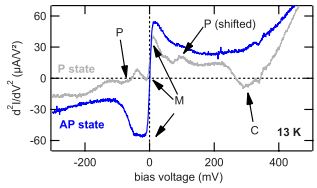

FIG. 3. (Color online) Comparison of IET spectra for both magnetic states.

through magnon excitation is higher. The similarity ends at the large dip at 290 mV in P state. The structure is assumed to be a signature of coherent tunneling in MTJs with MgO barrier.[2,17,18] For negative bias it is not visible, supposedly because of the structure of the minority DOS of CFA.

On a minor note, additional peaks are visible in the IET spectra. They are all much smaller that the magnon peaks around $V=0$. For $V>0$ a shoulder at $\approx$45 mV and a peak around 100 mV are visible. The shoulder might be related to magnons of higher order. The peak around 100 mV is presumably the peak of barrier phonon excitation, which is typical for tunnel junctions[19] and found at 81 mV[18,20] for Mg–O and 120 mV for Al–O phonons. Here, the position of 100 mV might be related to stress at the CFA/MgO interface or a partial oxidation of the CFA surface (Al–O). This cannot be clarified here. For $V<0$ the IETS signal is much flatter. Additional peaks can only be estimated around -80 to -90 mV. This would fit to the known Mg–O phonon peak position.

In summary, we prepared MTJs with Co_2FeAl bottom electrodes, which show up to 273 and 153% TMR ratio at 13 K and room temperature, respectively. Tunneling spectroscopy measurements showed a large asymmetry of the conductance in the P state, but only small variations in the AP state. These findings can be explained with a gap in the minority DOS of CFA.

We gratefully acknowledge Jan Schmalhorst and Andreas Hütten for helpful discussions and the DFG (Grant No. RE 1052/13-1) and BMBF (Heuspin) for financial support.

[1]G. A. Prinz, Science **282**, 1660 (1998).
[2]S. Tsunegi, Y. Sakuraba, M. Oogane, K. Takanashi, and Y. Ando, Appl. Phys. Lett. **93**, 112506 (2008).
[3]K. Inomata, N. Ikeda, N. Tezuka, R. Goto, S. Sugimoto, M. Wojcik, and E. Jedryka, Sci. Technol. Adv. Mater. **9**, 014101 (2008).
[4]Y. Sakuraba, T. Miyakoshi, M. Oogane, Y. Ando, A. Sakuma, T. Miyazaki, and H. Kubota, Appl. Phys. Lett. **89**, 052508 (2006).
[5]T. Ishikawa, T. Marukame, H. Kijima, K.-I. Matsuda, T. Uemura, M. Arita, and M. Yamamoto, Appl. Phys. Lett. **89**, 192505 (2006).
[6]T. Kubota, S. Tsunegi, M. Oogane, S. Mizukami, T. Miyazaki, H. Naganuma, and Y. Ando, Appl. Phys. Lett. **94**, 122504 (2009).
[7]R. Shan, H. Sukegawa, W. H. Wang, M. Kodzuka, T. Furubayashi, T. Ohkubo, S. Mitani, K. Inomata, and K. Hono, Phys. Rev. Lett. **102**, 246601 (2009).
[8]D. Ebke, P. Thomas, V. Drewello, O. Schebaum, M. Schäfers, D. Nissen, A. Hütten, and A. Thomas (accepted).
[9]N. Tezuka, N. Ikeda, A. Miyazaki, S. Sugimoto, M. Kikuchi, and K. Inomata, Appl. Phys. Lett. **89**, 112514 (2006).
[10]V. Drewello, M. Schäfers, O. Schebaum, A. A. Khan, J. Münchenberger, J. Schmalhorst, G. Reiss, and A. Thomas, Phys. Rev. B **79**, 174417 (2009).
[11]S. Zhang, P. M. Levy, A. C. Marley, and S. S. P. Parkin, Phys. Rev. Lett. **79**, 3744 (1997).
[12]V. Drewello, J. Schmalhorst, A. Thomas, and G. Reiss, Phys. Rev. B **77**, 014440 (2008).
[13]M. Sargolzaei, M. Richter, K. Koepernik, I. Opahle, H. Eschrig, and I. Chaplygin, Phys. Rev. B **74**, 224410 (2006).
[14]K. Özdoğan, B. Aktaş, I. Galanakis, and E. Şaşioğlu, J. Appl. Phys. **101**, 073910 (2007).
[15]Y. Miura, H. Uchida, Y. Oba, K. Abe, and M. Shirai, Phys. Rev. B **78**, 064416 (2008).
[16]T. Ishikawa, N. Itabashi, and T. Taira, K. Matsuda, T. Uemura, and M. Yamamoto, Appl. Phys. Lett. **94**, 092503 (2009).
[17]R. Matsumoto, Y. Hamada, M. Mizuguchi, M. Shiraishi, H. Maehara, K. Tsunekawa, D. D. Djayaprawira, N. Watanabe, Y. Kurosaki, T. Nagahama, A. Fukushima, H. Kubota, S. Yuasa, and Y. Suzuki, Solid State Commun. **136**, 611 (2005).
[18]G.-X. Miao, K. B. Chetry, A. Gupta, W. H. Butler, K. Tsunekawa, D. Djayaprawira, and G. Xiao, J. Appl. Phys. **99**, 08T305 (2006).
[19]E. Wolf, in *Principles of Electron Tunneling Spectroskopy, International Series of Monographs on Physics No. 71*, edited by R. Elliot, J. Krumhansl, W. Marshall, and D. Wilkinson (Oxford University Press, New York, 1989).
[20]J. G. Adler, Solid State Commun. **7**, 1635 (1969).

Tunneling spectroscopy probing magnetic and nonmagnetic electrodes in tunnel junctions

Volker Drewello,* Zoë Kugler, Günter Reiss, and Andy Thomas
Bielefeld University, Thin Films and Physics of Nanostructures, 33615 Bielefeld, Germany
(Dated: August 3, 2010)

Tunneling spectroscopy is applied to tunnel junctions with only one or no ferromagnetic electrode to study the excitation of quasi particles in magnetic tunnel junctions. The bias dependence is investigated with high accuracy by inelastic electron tunneling spectroscopy. Both types of junctions show a zero bias anomaly that is different in size and sign compared to magnetic tunnel junctions, i.e. junctions with two ferromagnetic electrodes. A pronounced difference is also found depending on the material that is probed by the tunneling electrons, which might be attributed to the excitation of magnons.

PACS numbers: 73.40.Gk, 73.43.Qt, 75.47.-m,75.70.Cn

Magnetic tunnel junctions (MTJs) with MgO as a crystalline barrier show large tunnel magnetoresistance (TMR) ratios of up to 1000 % at low temperature[1,2]. Nevertheless, the TMR ratio at room temperature is still by a factor of 2 to 3 smaller. Decreasing this temperature dependence is one way to gain higher TMR ratios at room temperature and increase the applicability of MTJ based spintronic devices. The main reason for the decreasing TMR values are intrinsic excitations within the junctions[3–5] which can be studied by means of inelastic electron tunneling spectroscopy (IETS). In this paper, the different excitations in magnetic and nonmagnetic electrodes are investigated. Tungsten is chosen as the nonmagnetic metal electrode because of its high melting point. It also has a lower lattice mismatch with the MgO barrier than e.g. Tantalum (6 % vs. 11 %).

The samples are prepared in a self-made sputter deposition tool with a base pressure below 10^{-9} mbar. The layers are deposited on top of thermally oxidized silicon wafers at an Ar pressure of 5×10^{-3} mbar (MgO at 10^{-2} mbar). The first sample is a metal/ insulator/ metal tunnel junction (M-I-M) with the layer stacking W 20/ MgO 1.8/ W 20 (all values in nm). The second sample has a ferromagnet as the lower electrode (FM-I-M). The layer stack is W 15/ $Co_{40}Fe_{40}B_{20}$ 6/ MgO 1.8/ W 20. Both stacks are annealed at 723 K for 1 hour in a high vacuum furnace. A capping of Ta and Au is added for protection and to form contact pads. The samples are structured by optical lithography and Ar ion beam etching.

The low temperature measurements are done at 13 K in a closed cycle Helium cryostat by a standard two-probe technique. The bias voltage is defined with respect to the upper electrode. Thus, negative bias results in electrons tunneling into the upper electrode. A Lock-In technique is used to obtain the dI/dV curves which are differentiated numerically to get the IET spectra (d^2I/dV^2). Details of the measurement setup and procedure can be found elsewhere[6].

The spectra for the M-I-M junction are shown in Figure 1. The conductance has the predicted parabolic shape[7] with variations at bias voltages up to 100 mV. In the IET spectrum these features can be seen much clearer. First, at approximately 9 mV a negative zero bias anomaly is found, i.e. the conductance decreases at low bias compared to zero bias. In typical full MTJs (i.e. with two magnetic electrodes) the zero bias anomaly shows the opposite sign. Often the magnitude of the effect is larger and dominates the spectra[6,8,9]. Second, several broad peaks are found up to 100 mV. Figure 2 shows these features in more detail. As no magnetic materials are used and no magnetic impurities are expected, phonon excitation is an explanation for these peaks. Peaks of the electrode phonons typically have energies around 30 meV[10] while the phonons of barrier oxides have higher energies. Here, the first peaks correspond to an excitation of tungsten phonons with an energy of 26 meV[11]. The MgO tunneling barrier leads to phonon peaks at 66 and 81 mV[10]. A strong peak is indeed found at 66 mV but only a shoulder is found at 81 mV. In MgO based full MTJs this peak is typically more pronounced[6,9].

The spectra of the FM-I-M junction show a strong asymmetry in the slope of the dI/dV-curves (Figure 3). This leads to a different height of the IET spectra for

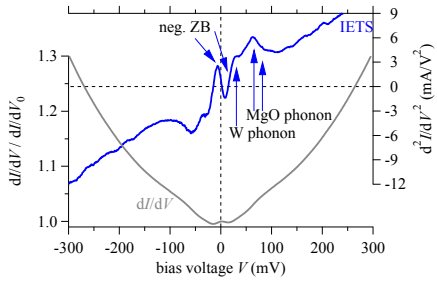

FIG. 1. The tunnel spectrum (dI/dV) normalized to its value at $V = 0$ and the IET spectrum (d^2I/dV^2) of the W/ MgO/ W sample.

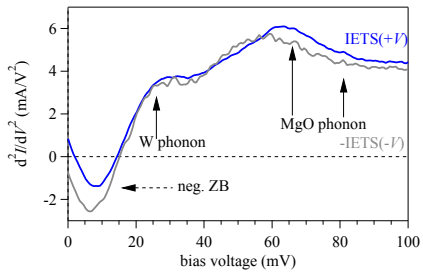

FIG. 2. The IET spectrum of the W/ MgO/ W junction. The low bias region is shown for both polarities. The arrows mark energies of known excitations.

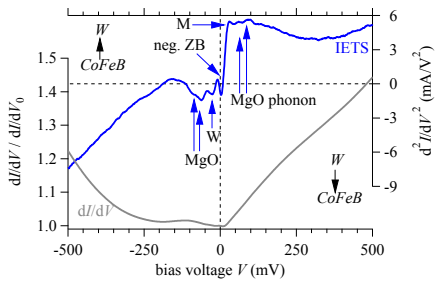

FIG. 3. The normalized tunnel spectrum and the IET spectrum of the Co-Fe-B/ MgO/ W sample.

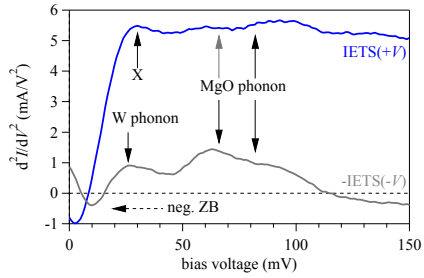

FIG. 4. Comparison of the IET spectra for positive (electrons tunnel into Co-Fe-B) and negative (into W) bias voltage for the Co-Fe-B/ MgO/ W sample.

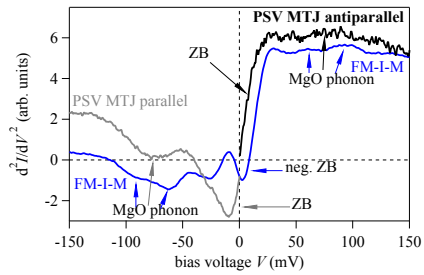

FIG. 5. Comparison of the IET spectra of the Co-Fe-B/ MgO/ W sample and those of a typical MTJ (scaled). Arrows mark the ZBA.

positive compared to negative bias, nevertheless the peak structure is visible. Magnified spectra for negative (electrons tunnel into W) and positive bias (electrons tunnel into Co-Fe-B) can be compared in Figure 4. Most prominent is the zero bias feature which is still negative for both bias polarities. For negative bias it is found at approximately 10 mV, while it is closer to zero for positive bias. This is presumably caused by smearing with the following peaks, which have a much higher intensity (X). For both polarities several features are found. The spectrum for negative bias looks similar to the spectrum of the first sample, with the tungsten phonon peak at 26 mV and a MgO phonon peak at 66 mV. The 81 mV shoulder is more pronounced. For positive bias, i.e. tunneling into the ferromagnet, the peaks are higher and less sharp. After the neagtive ZBA the spectrum rises strongly to the first peak. This must be the excitation of magnons (X). Also, the MgO phonon peak at 81 mV peak is more pronounced than the one at 66 mV.

In Figure 5 the IET spectra are compared to those of a typical MTJ[12].The FM-I-M spectrum for tunneling into W (negative bias) is compared to the spectrum for the parallel (P) magnetic state. For tunneling into the FM (pos. bias) the spectrum is compared to the MTJ in antiparallel (AP) magnetic state. In both cases the spectra have a similar shape. The striking difference is the zero bias anomaly, which is positive for the MTJ and leads to a huge peak in the P state. This effect is also visible in the AP state, but the zero bias peak is only a shoulder. As a result the spectrum immediately rises after zero bias, while for the FM-I-M junction the flank seems shifted to higher bias. The MgO phonon peaks are also similar in both cases. The spectra of the full MTJ in the P state are negative over a wide bias range. In the AP state, the spectra are much lower compared to the FM-I-M-spectra in the same bias region.

Now the results will be discussed. In the presented spectra most peaks can be identified as belonging to the target electrode and the barrier with the exception of the zero bias anomaly (ZBA). Its size and sign is obviously not simply a matter of the material of the target elec-

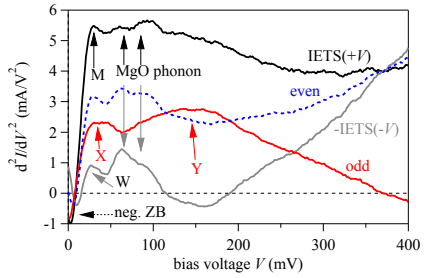

FIG. 6. Comparison of IET spectra for positive/negative bias and even and odd spectra of the Co-Fe-B/ MgO/ W sample.

trode. This can be seen from the results of the FM-I-M junction, where the ZBA is roughly the same for the two different electrode materials. Furthermore, the same ferromagnet shows large positive ZBA peaks in the MTJ. The two different results suggest that it is not a excitation of surface magnons which is causing the ZBA. This leaves tunneling through impurities as an explanation. It is known that the zero bias effect depends on the impurity material[13]. A model that would explain impurities in the barrier is implantation of upper electrode atoms during preparation. In this case the material would be tungsten in both samples (in difference to the MTJ case).

The M-I-M sample shows near ideal symmetry and the anticipated peaks. The asymmetry in the spectra of the FM-I-M sample, however, rises the question of magnon excitation in the ferromagnet. If even/odd spectra[14] are calculated, peak structures are indeed found in the odd spectrum (Figure 6). The first peak must be the excitation of magnons, as observed before. However, the origin of the second, much broader peak is not clear. It's maximum is at high bias voltage around 150 mV and leads up to some hundred mV. This result is different compared to the peak at 10 mV that Paluskar et al. find for incoherent Alumina based junctions[15]. The high energies we find would be equivalent to temperatures higher than 1000 K and, therefore, T_C. The total magnon density of states in a ferromagnet is large at these energies[16] and bulk magnons are suspected to contribute to the tunneling process at some voltage[3]. However, it is not clear if the interaction potential allows these modes to be excited[17].

Nevertheless, the similarity of the FM-I-M spectra to the state-specific spectra of the MTJ also fits in this model. In the case of electrons tunneling into Co-Fe-B magnons should be the dominant excitation. This is also the case in the AP state of a MTJ where the direct tunneling contribution is smaller due to the inverse spin-polarization of the electrodes. As the major difference is caused by the anomaly around zero bias, it can be suspected that the broad contribution, which is not seen in the P state, is also the excitation of magnons. Lastly, the broad dip (or gap) in the tunnel spectrum ($\mathrm{d}I/\mathrm{d}V$) of the FM-I-M junction resembles the P state spectrum of MTJs that incorporate one half-metallic Heusler compound electrode[18,19]. In both cases magnon excitation is prohibited for the corresponding bias polarity, while it is allowed for the other one. This is another hint that the magnon excitation is the origin of the broader feature (gap in $\mathrm{d}I/\mathrm{d}V$, background in IETS).

A minor note regards the MTJ spectrum in the P state. It is shifted to negative values, which might indicate a large coherent tunneling contribution[20]. This is not seen in the M-I-M sample, which might be tentatively ascribed to different growth of the MgO barrier depending on the lower electrode material. The different strength of the MgO phonons peaks could then also be a effect of different barrier and interface properties.

In summary, tunnel junctions with only one or no ferromagnetic electrode have been investigated by inelastic electron tunneling spectroscopy. The excitations of electrode and barrier phonons are observed in all junctions. For the junction with one ferromagnetic electrode the excitation spectra show a strong asymmetry, which is attributed to magnon excitation. In contrast to full magnetic tunnel junction, the presented junctions show a negative zero bias anomaly.

ACKNOWLEDGMENTS

We gratefully acknowledge Jan Schmalhorst for helpful discussions, Patryk Krzysteczko and Markus Schäfers for technical assistance, and the DFG (Grant RE 1052/13-1) for financial support.

* drewello@physik.uni-bielefeld.de

[1] S. Ikeda, J. Hayakawa, Y. Ashizawa, Y. M. Lee, K. Miura, H. Hasegawa, M. Tsunoda, F. Matsukura, and H. Ohno, Applied Physics Letters, **93**, 082508 (2008).
[2] N. Tezuka, N. Ikeda, F. Mitsuhashi, and S. Sugimoto, Applied Physics Letters, **94**, 162504 (2009).
[3] A. M. Bratkovsky, Applied Physics Letters, **72**, 2334 (1998).
[4] X.-F. Han, A. C. C. Yu, M. Oogane, J. Murai, T. Daibou, and T. Miyazaki, Physical Review B, **63**, 224404 (2001).
[5] V. Drewello, J. Schmalhorst, A. Thomas, and G. Reiss, Physical Review B (Condensed Matter and Materials Physics), **77**, 014440 (2008).
[6] V. Drewello, M. Schäfers, O. Schebaum, A. A. Khan, J. Münchenberger, J. Schmalhorst, G. Reiss, and A. Thomas, Physical Review B (Condensed Matter and Materials Physics), **79**, 174417 (2009).
[7] J. G. Simmons, Journal of Applied Physics, **35**, 2655

(1964).
[8] J. S. Moodera, J. Nowak, and R. J. M. van de Veerdonk, Physical Review Letters, **80**, 2941 (1998).
[9] G.-X. Miao, K. B. Chetry, A. Gupta, W. H. Butler, K. Tsunekawa, D. Djayaprawira, and G. Xiao, Journal of Applied Physics, **99**, 08T305 (2006).
[10] J. Klein, A. Léger, M. Belin, D. Défourneau, and M. J. L. Sangster, Phys. Rev. B, **7**, 2336 (1973).
[11] W. Olejniczak, Z. Klusek, and M. Bieniecki, Applied Physics A, **66**, 191 (1998).
[12] The full MTJ is a pseudo spin valve with a similar layer stack: Ta 20 / Co-Fe-B 5.4/ MgO 2.4/ Co-Fe-B 2.4/ Ta 20. It is annealed at 723 K for 1 hour.
[13] J. R. Cooper and A. F. G. Wyatt, J. Phys. F: Metal Phys., **3**, L120 (1973).
[14] The even (odd) spectrum is the average (difference) of the spectra for positive and negative bias.
[15] P. V. Paluskar, F. L. Bloom, J. T. Kohlhepp, H. J. M. Swagten, B. Koopmans, and E. Snoeck, Applied Physics Letters, **91**, 222501 (2007).
[16] S. V. Halilov, A. Y. Perlov, P. M. Oppeneer, and H. Eschrig, Europhys. Lett., **39**, 91 (1997).
[17] T. Balashov, A. F. Takács, M. Däne, A. Ernst, P. Bruno, and W. Wulfhekel, Phys. Rev. B, **78**, 174404 (2008).
[18] Y. Sakuraba, T. Miyakoshi, M. Oogane, Y. Ando, A. Sakuma, T. Miyazaki, and H. Kubota, Applied Physics Letters, **89**, 052508 (2006).
[19] D. Ebke, V. Drewello, M. Schäfers, G. Reiss, and A. Thomas, Applied Physics Letters, **95**, 232510 (2009).
[20] S. Tsunegi, Y. Sakuraba, M. Oogane, K. Takanashi, and Y. Ando, Applied Physics Letters, **93**, 112506 (2008).